Mechanical Spectroscopy of Zr-based bulk glass forming alloys

Von der Gemeinsamen Naturwissenschaftlichen Fakultät
der Technischen Universität Carolo-Wilhelmina
zu Braunschweig
zur Erlangung des Grades eines
Doktors der Naturwissenschaften
(Dr.rer.nat.)
genehmigte
Dissertation

von
Roberto Scarfone
aus Mailand

1. Referent: Apl. Prof. Dr. H.-R. Sinning
2. Referent: Prof. Dr. H. Neuhäuser
eingereicht am: 20.12.2001
mündliche Prüfung (Disputation) am: 25.03.2002
2002 (Druckjahr)

Vorabveröffentlichungen der Dissertation

Teilergebnisse aus dieser Arbeit wurden mit Genehmigung der Gemeinsamen Naturwissenschaftlichen Fakultät, vertreten durch den Mentor der Arbeit, in folgenden Beiträgen vorab veröffentlicht:

Publikationen

Sinning, H.-R., Steckler, G. and Scarfone, R.: Mechanical damping by hydrogen diffusion in intermetallic compounds. Adv. Eng. Mat. 3(9): 706-711 (2001)

Scarfone, R. and Sinning, H.-R.: A mechanical spectroscopy study of the $Zr_{69,5}Cu_{12}Ni_{11}Al_{7,5}$ alloy. J. Alloys Compnd. 310: 229-232 (2000).

Sinning, H.-R., and Scarfone, R.: Local structure of amorphous and metastable alloys as seen by mechanical hydrogen relaxation. Mat. Sci. Forum 343-346: 738-743 (2000).

Scarfone, R. and Sinning, H.-R.: A mechanical spectroscopy study of Zr-based bulk metallic glasses. Materials Development and Processing (Euromat - Vol. 8), eds. J.V. Wood, L. Schultz and D.M. Herlach, Wiley-VCH, Weinheim: 34-39 (2000).

Sinning, H.-R., Steckler, G. and Scarfone, R.: Some current aspects of anelastic relaxation by hydrogen diffusion in metals. Def. Diff. Forum 167-168: 1-15 (1999).

Tagungsbeiträge

Scarfone, R. and Sinning, H.-R.: Mechanical spectroscopy of Zr-based bulk metallic glasses. (Vortrag). DPG Frühjahrstagung, Hamburg (2001).

Sinning, H.-R., Scarfone, R. and Steckler, G.: Mechanical spectroscopy of hydrogen effects in bulk amorphous alloys and intermetallic compounds. (Eingeladener Vortrag). THERMEC 2000, Las Vegas.

Scarfone, R. and Sinning, H.-R.: Mechanical hydrogen relaxation spectra in amorphous, quasicrystalline and crystalline phases of the Zr-Cu-Ni-Al system. (Poster). DPG Frühjahrstagung, Münster (1999).

Scarfone, R. and Sinning, H.-R.: Phase transformations of Zr-based bulk metallic glasses studied by means of mechanical spectroscopy. (Poster). DPG Frühjahrstagung, Regensburg (1998).

Acknowledgements

Several people have helped and encouraged me during the preparation of this work and I wish to thank them, now that my efforts have come to an end.

Among the ones belonging to the Technical University of Braunschweig, my first thought goes to apl. Prof. Dr. H.-R. Sinning, who has not only been the referent for scientific questions, but also supported me in most of the formalities concerning my stay in Germany and with whom it was possible to establish a friendly climate of work and communication.

Guido Steckler and Frank Winter were very helpful, especially at the beginning, for all what regards the experimental setup. They helped me not only to understand the principle of the vibrating reed technique but also made several useful measurements for me.

Without Frank Scholz it would have been very problematic to make the necessary experiments with the differential scanning calorimeter and for the sputtering of my samples with Palladium; also to him goes my gratitude.

My thanks to Frank Klose, Ulrich Harms, Tilo Eggeling and Rüdiger Lippok (formerly at the Technical University of München) for some useful discussions and friendly suggestions.

I wish also to thank all my colleagues of the Institut für Werkstoffe for the nice working atmosphere.

Among the technical staff I feel particularly obliged to Mrs. Grusewsky for the time spent finding quasicrystalline structures with the electron microscope, to Mr. Scholz for the measurements of the hydrogen concentration and for the many useful hints given on experimental problems, to Mr. Michael, Abt and Calberlah for the construction of several parts of the experimental setup and for carrying so often the heavy liquid nitrogen container.

The materials investigated in this work were kindly prepared at the Universities of Augsburg, Dortmund and at Caltech, Pasadena, by Dr. Moske, Dr Rüdiger and Dr. Geyer respectively.

My family and in particular my girlfriend Catia have been an important source of support, especially when my motivation was low; in such moments their words and encouragement have stimulated me to go on. To them goes all my thankfulness for all their comprehension and patience and to them I wish to dedicate this work.

Finally, this project has been financed by the Deutsche Forschungsgemeinschaft in the frame of the scientific program *Unterkühlte Metallschmelzen: Phasenselektion und Glasbildung*. This support is gratefully acknowledged.

Abstract

Mechanical spectroscopy combined with the use of hydrogen as a probe has been chosen to investigate firstly the phase transformations, then the structural affinities and differences in various Zr-Ti-Cu-Ni-Be and Zr-Cu-(Ni)-Al bulk glass forming alloys. The change of eigenfrequency of a clamped-free vibrating reed as function of temperature showed peculiar features, before crystallization of the glasses, characterizing e.g. the phase separation of $Zr_{41}Ti_{14}Cu_{12,5}Ni_{10}Be_{22,5}$ or the formation of metastable quasicrystalline $Zr_{69,5}Cu_{12}Ni_{11}Al_{7,5}$. The developing of hydrogen induced damping spectra, for H concentrations in the range from 0,001 to 0,5 H/M, was studied in structurally relaxed amorphous as well as in quasicrystalline and crystalline specimens. The theory for the calculation of the activation energy E_a for classical hydrogen hopping in a model amorphous structure [1] has been applied to our glasses: both the ongoing of $\langle E_a \rangle$ with the hydrogen concentration and its theoretical distribution $P_{th}(E_a)$ agree well with the respective experimentally determined quantities, especially at low H concentrations. No significative difference could be found in the shape of the internal friction peaks for the amorphous and icosahedral states, meaning that a similar short range order dominates in both phases. Due to such similarity, the nucleation of quasicrystals from the glassy state is energetically favorable and plays an important role in the destabilisation of the undercooled melts.

Contents

Chapter 1

Introduction

1.1 General problem

The new type of Zr-based metallic glasses first discovered by the groups of Inoue [2] and Johnson [3], are characterized by a large difference between the glass (T_g) and the crystallization (T_x) transition temperatures; this feature allows the production of such glasses with cooling rates ranging from 10^3 to 1 $\mathrm{K\,s^{-1}}$ [4] in the form of bulk samples. Before the introduction of this new type of alloys, much faster cooling rates, of the order of 10^6 $\mathrm{K\,s^{-1}}$, were necessary for getting a solid amorphous metallic glass. The drawback of such technique was, that only specimens with reduced linear dimensions could be fabricated, typically in the form of splats or ribbons with a thickness in the range of some tens of microns.

The main difference existing between *conventional* and *bulk* metallic glasses, is the ease with which their melt destabilizes through the nucleation and growth of energetically more favorable crystalline phases. One central question concerning the stability of the melts is then under which conditions the formation of such phases can be suppressed. In particular we can ask if there exists a specific combination of local chemical and geometrical atomic order for which the rearrangement of the atomic species from the disordered to an ordered state, e.g. an intermetallic phase, is considerably hindered.

In the frame of the research program *Undercooled melts: phase selection and glass formation*, funded by the Deutsche Forschungsgemeinschaft, the knowledge of the short range order (SRO) and its role in the destabilization of the melts was a central topic. In particular, as far as the new Zr-based bulk glasses are concerned, two kinds of problems were of particular interest:

1. Structural reasons for the unusual thermal stability of these new materials as, for example, peculiarities of the SRO in comparison to the normal metallic glasses.

2. The occurring or missing of structural similarities between the amorphous and the respective metastable phases which are built during the devitrification process.

While on one side there is a great need for information concerning the local atomic structure of these disordered states, on the other side there is a lack of methods which allow a quantitative study of such problem. In fact, most of the known techniques like, for example, X-ray diffraction, neutron scattering or positron annihilation, only give a limited set of information on amorphous structures.

In Zr-Ti-Cu-Ni-Be and Zr-Cu(-Ni)-Al bulk glasses, there is the additional possibility of using *hydrogen as a probe* for getting information on their SRO. Hydrogen is highly soluble in these alloys and is accommodated in definite interstitial sites, like tetrahedra formed by four Zr atoms. There exist several examples of measurements (based in particular on electromotive force techniques) which used hydrogen for gaining detailed information on the microscopic structure of a material as, for example, the SRO of glasses based on transition metals [5], the thickness of the grain boundaries in nanocrystalline Pd [6], the number and strain fields of dislocations [7] and other kinds of defects [8].

Beside the techniques based on electromotive force, the reorientation relaxation of hydrogen is also a promising method for studies of the local atomic structure in disordered systems. Under the influence of an external stress, the hopping and the consequent reorientation of the elastic dipoles formed by hydrogen as an interstitial impurity in a given material induce a dissipation of mechanical energy into heat and an anelastic behavior which can be observed e.g. in the form of characteristic damping spectra as a function of temperature. The parameters related to these spectra are closely connected to the local surroundings of the dissolved hydrogen atoms [1] and, in this sense, we can speak of hydrogen as a probe of the SRO of the host material.

1.2 State of the art

We must distinguish between two different aspects: on one side we have the new type of Zr-bases bulk metallic glasses with the questions concerning their atomic structure and, on the other side, we have a relatively new methodology for the investigation of the SRO in materials capable of accommodating hydrogen. As regards the first point we can summarize as follows:

1. One of the decisive factors influencing the good stability of an undercooled melt is the suppression of the nucleation and growth of crystalline

phases: the presence of several atomic species (at least three) with different dimensions (a ratio of approximately 12% between the diameter of the bigger and the smaller atom type), promotes a close packing of the components and reduces, in turn, the diffusional mobility which is necessary for the rearrangement of the alloy into different phases [9, 10].

2. There are indications that the SRO of the new metallic glasses (e.g. La-Al-Ni, Zr-Ni-Al, Zr-Y-Ni-Al) is quite different from the one of the respective crystalline phases [11]; this is an interesting topic which needs further investigation, possibly with new and independent methodologies.

3. Several alloys belonging to the Zr-Cu-Ni-Al and Zr-Ti-Cu-Ni-Be type have been proven to favor the formation of a metastable icosahedral quasicrystalline phase prior to crystallization [12, 13, 14]; this observation poses the question of the role assumed by icosahedral SRO in metallic glasses and how this can influence the destabilization of the melts.

Concerning the methodological aspect, we already mentioned that information on the SRO of a material can be gathered through the analysis of the hydrogen-induced damping spectra. Such spectra can be measured by using the "vibrating-reed" technique, through which the internal friction properties of a thin slab of material, previously excited to its resonance frequency of vibration, can be analyzed, for example as a function of temperature.

In a metallic glass, hydrogen acts in a similar way as C in $\alpha-$Fe, giving rise to a Snoek-type relaxation mechanism. If we assume that the reorientation jump of H depends on its interactions with the metal atoms in its immediate surroundings, then the parameters of the relaxation are related to the local geometry and chemistry of the interstitial site itself. In this case, the theoretical model introduced by Richards [1] can be used for the relationship between the parameters of the relaxation kinetic (activation energy, damping peak temperature) and the local atomic distances. This use of H-induced damping spectra for getting knowledge on the SRO of a system has been named *Mechanical Hydrogen Spectroscopy* (MHS) [15, 16].

This method is rather new, but it has already been used with success in the Co-Zr system, where some structural statements could be made. In particular: a wider distribution of Zr-Zr distances, in comparison to the one characteristic of the amorphous state, was found in the grain boundaries of a nanocrystalline phase of $CoZr_2$ [15, 17]; from the comparison of the damping spectra between the amorphous and crystalline phases, it was concluded that the amorphous $CoZr_2$ alloy contains elements of SRO deriving from the equilibrium C16 crystalline state as well as from the $E9_3$ metastable state [15]; the variation of the average activation energy for the H relaxation with the chemical composition

of different Co-Zr alloys, was understood in terms of an increase of the average Zr-Zr nearest neighbor distances for alloys with lower and lower Zr content [18].

1.3 Scope of the work

In the general frame of the problematic concerning the structural reasons for the stability of the undercooled melts and, in particular, of the Zr-Ti-Cu-Ni-Be and Zr-Cu-Al(-Ni) systems, our aims can be summarized as follows:

1. From the methodological point of view, MHS seems a very promising technique which should be capable of extracting information on the SRO of different amorphous or (quasi)crystalline phases, provided that the materials to be investigated are capable of storing hydrogen. Even though this method has already given significative results, as was clear in the preceding discussions, the connection between the experimentally accessible quantities, on one side, and the microscopic structure of the host material, on the other side, which is contained in the model of Richards [1], has only been used until now on a semi-quantitative base. For example, as regards the calculation, from first principles, of the average activation energy for H-reorientation, a simplified use of the model has been made in order to show the quantities relative to *single* interstitial sites. While this is very sensible when speaking of regular crystalline structures [19], in the case of disordered glassy phases it is better to speak of average values over a *range* of interstitial sites. Therefore, we wish to apply the *complete* theoretical analysis of Richards to our Zr-based bulk glasses, in order to get information on their SRO and, at the same time, to establish on a more quantitative base the applicability of MHS.

2. The recent discovery of a metastable quasicrystalline state in $Zr_{69,5}Cu_{12}Ni_{11}Al_{7,5}$ [12] has opened the opportunity of investigating this fascinating state of the matter through MHS. In fact, this material can be prepared in a relatively easy way in its icosahedral phase by annealing from the precursor amorphous state. Moreover, the system can absorb a big amount of hydrogen without changing its structure considerably. Such characteristics are ideal for an MHS investigation. We want to see firstly if a H-reorientation relaxation is possible at all in a quasicrystalline phase and, secondly, we want to compare the damping behavior of amorphous and icosahedral states. This should bring additional elucidations on the role of icosahedral SRO in the glassy phase.

3. The crystalline states formed during the devitrification of our Zr-based glasses are also interesting from the MHS point of view. A comparison of the damping spectra between these phases is in fact necessary for establishing whether or not some similarities of SRO exist in comparison to the precursor disordered systems.

In Chapter 2 we are going to discuss the basic theory of anelastic relaxation in solids, with particular attention to those parts concerning the relaxation due to point defects. Emphasis will also been given to the calculation of a distribution of activation energies for thermally activated processes by starting from the knowledge of a damping spectrum. Chapter 3 is dedicated to the description of our experimental setup and to the characterization of the materials. In Chapter 4 we will show our experimental results and the annexed discussions. Finally, Chapter 5 contains the summary and conclusions of this work.

Chapter 2

Theory of anelastic relaxation

This chapter illustrates some basic principles of anelastic relaxation which are a necessary introduction for the proceeding of this work; the treatment has not the aim of being complete, but only to give an overview on anelasticity and on the reasons for its occurrence in crystalline as well as in non-crystalline solids. The interested reader can find more detailed information in the well known book of Nowick and Berry [20], which has been the basis for most of the following treatment, or, alternatively, in the text written by de Batist [21].

2.1 Elasticity and anelasticity

An *elastic* solid is characterized by a series of properties that are a direct consequence of Hooke's law, which states that the stress σ and the strain ε acting on a system are proportional to each other at every instant of time according to the equations

$$\sigma = M\varepsilon \qquad \text{or} \qquad \varepsilon = J\sigma, \tag{2.1}$$

where the proportionality factors M and J are called modulus (of elasticity) and compliance, respectively, and are the inverse of each other. In reality σ and ε should be written as second order tensors but, for our purposes, this would add unnecessary complications since we will consider only simple deformations like pure shear or uniaxial stress (strain).

For a system obeying Eqs. (2.1) the following rules hold: 1) the strain response to every level of applied stress has a unique equilibrium value; 2) the equilibrium is achieved *instantaneously*; 3) the response is linear. On the other side for an *anelastic* solid the second of these conditions does not apply anymore and the response of the system to an applied stress becomes time dependent. The situation is shown in Fig. (2.1), where the difference between the elastic ($\varepsilon_{\mathsf{el}}$) and anelastic ($\varepsilon_{\mathsf{an}}$) behavior upon sudden loading and unloading

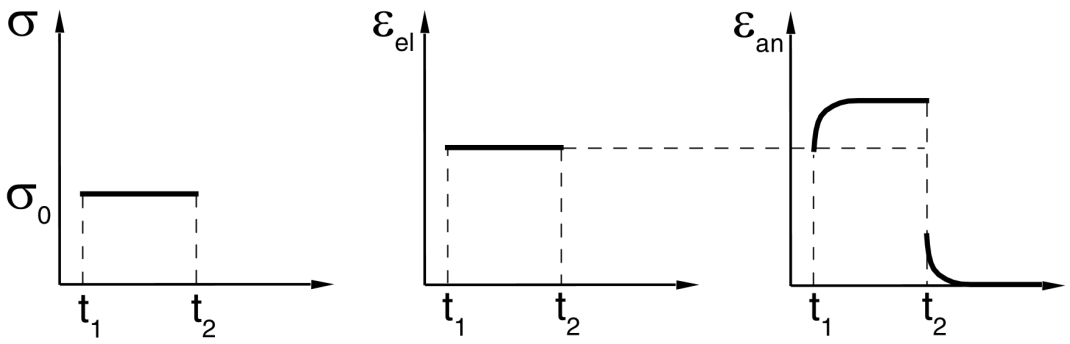

Figure 2.1: *Response of an elastic ($\varepsilon_{\mathsf{el}}$) or anelastic ($\varepsilon_{\mathsf{an}}$) solid subject to a stress σ_0 between t_1 and t_2.*

is apparent; it can be seen moreover that the recovery of the system in both cases is complete. Anelasticity is mainly a phenomenon of thermodynamical nature, in the sense that the response of the system to an external stress is the effect of a time dependent rearrangement towards equilibrium, through kinetic processes like diffusion, of some internal variables (point defect relaxations, dislocation movements etc.).

If we further reduce the conditions imposed by Hooke's law and, in particular, we don't require the uniqueness of the equilibrium value for the strain to an applied stress, then we obtain a *viscoelastic* response. In such a system the strain will change continuously, instead of reaching a steady value, as long as the stress is active. Upon unloading, it will not totally recover to its original state, in contrast to the case of (an)elasticity, due to the occurrence of some processes of irreversible type.

2.2 Response functions

After having given a general idea of the concept of anelasticity, we will now deal in more detail with the response of a system reacting to an external mechanical stress. For a quantitative description of a material's elastic properties - where elastic must be taken in a general sense and includes also non conservative phenomena like viscoelasticity - it is useful to introduce the *quasi-static* and *dynamic* response functions. We will consider hereafter the results derived starting from the second of Eqs. (2.1), even though the theory can be equally well developed for the first one.

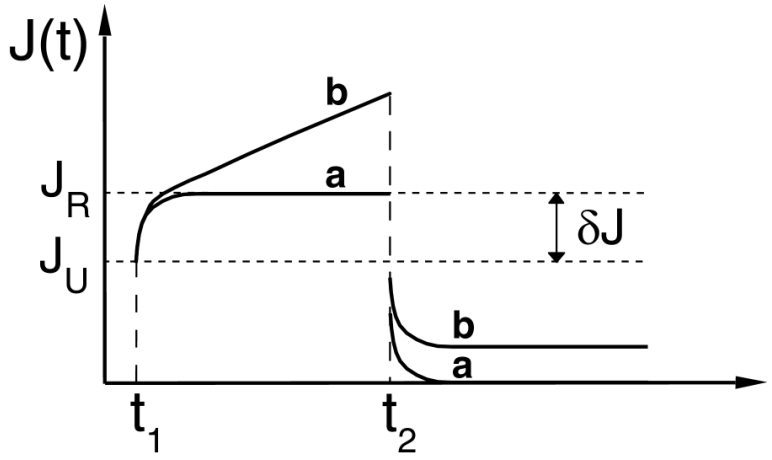

Figure 2.2: *Creep and elastic aftereffect behavior for anelastic* (a) *and viscoelastic* (b) *materials.*

2.2.1 Creep and elastic aftereffect

Speaking of quasi-static type relations, we distinguish between *creep*, which is the appropriate response function when an applied stress is active, and *elastic aftereffect*, which describes the behavior of the system once the stress has been removed. Starting from Hooke's law, we define

$$J(t) \equiv \varepsilon(t)/\sigma_0 \tag{2.2}$$

when the stress applied to the system is

$$\sigma = \begin{cases} 0 & ; \quad t < t_1 \\ \sigma_0 & ; \quad t_1 \leq t \leq t_2 \\ 0 & ; \quad t > t_2 \end{cases} . \tag{2.3}$$

Referring to Fig. (2.2), for $t_1 \leq t \leq t_2$ $J(t)$ defines the creep function whereas for $t > t_2$ it defines the elastic aftereffect. The difference between anelastic (a) and viscoelastic (b) behavior is here evident: in the first case the recovery is complete but in the second case the material undergoes some irreversible deformation and does not return to its original state after unloading. The quantities J_U and J_R are called the unrelaxed and relaxed compliance, respectively, and their difference is δJ. The ratio

$$\Delta \equiv \frac{\delta J}{J_U} \tag{2.4}$$

defines the *relaxation strength* and represents a measure of how important is the anelastic response of the system with respect to the elastic one.

2.2.2 Dynamic response functions

The response functions of the preceding paragraph are used when the excitation acting on the sample lasts several seconds or longer, and are therefore called quasi-static. To obtain information on the behavior of a material at much higher frequencies, a dynamic-type experiment is more appropriate. Then if we write the stress as

$$\sigma = \sigma_0 \mathrm{e}^{i\omega t}, \tag{2.5}$$

where ω is the angular frequency of excitation, the associated strain will be

$$\varepsilon = \varepsilon_0 \mathrm{e}^{i(\omega t - \phi)}. \tag{2.6}$$

The phase lag $\phi(\omega)$ which characterizes the strain response is typical of the anelastic behavior of a material and would reduce to zero in an ideally elastic specimen. Noting that Eq. (2.6) can be rewritten as

$$\varepsilon = (\varepsilon_1 - i\varepsilon_2)\mathrm{e}^{i\omega t} \tag{2.7}$$

where $\varepsilon_{1,2}$ are, respectively, the components of the strain in phase and 90° out of phase with the stress, and defining the complex compliance $J^*(\omega) \equiv \varepsilon/\sigma$, in analogy with Eq. (2.2), we end up with

$$J^*(\omega) = J_1(\omega) - iJ_2(\omega). \tag{2.8}$$

If we draw on the complex plane the vector J^* and its components $J_{1,2}$, and we observe that ϕ is the angle between J^* and J_1, it becomes clear that $\tan\phi = J_2/J_1$.

J_1 is also called *storage* compliance, because it is proportional to the maximum energy W stored in the system according to

$$J_1 \propto W = \int_0^{\frac{\pi}{2}} \sigma \, d\varepsilon; \tag{2.9}$$

on the other side J_2 is known as *loss* compliance, because it is related to the energy ΔW dissipated over an entire cycle, that is

$$J_2 \propto \Delta W = \oint \sigma \, d\varepsilon. \tag{2.10}$$

The ratio $\Delta W/W$ represents the *specific damping capacity* of a material and is linked to $J_{1,2}$ and ϕ through the following identity:

$$\Delta W/W = 2\pi(J_1/J_2) = 2\pi \tan\phi. \tag{2.11}$$

Since ϕ is directly connected to the fractional energy loss of the system due to anelastic behavior, it is also called *internal friction* of the sample.

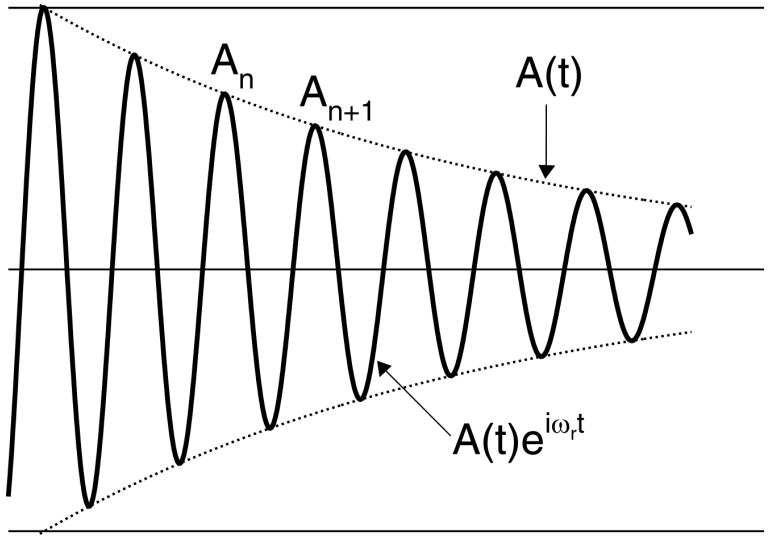

Figure 2.3: *Decay of the free vibrations of an anelastic solid.*

2.2.3 Measurement of the internal friction

The problem of measuring the internal friction (damping) of a material can be solved experimentally with several techniques which are in principle divided in three categories, depending on the relation between the frequency ω of the probing field and the natural eigenfrequency ω_r of the material to be analyzed. In particular we can speak of *sub-resonance* methods if $\omega \ll \omega_r$, of *resonance* methods if $\omega \simeq \omega_r$ and finally of *wave propagation* methods if $\omega \gg \omega_r$. Among the most used procedures, we mention the measurement of the decay of the free oscillations of a system which has been previously excited to its resonance frequency. Since we adopted this technique for our investigations, we will analyze it in some more detail: the equation which describes the free vibrations of a sample in the presence of damping is

$$x = x_0 \exp(-\delta f_r t)\, \exp(i\omega_r t) = A(t)\, \mathrm{e}^{i\omega_r t}, \tag{2.12}$$

where $f_r = \omega_r/2\pi$ is the frequency, $A(t)$ the amplitude of the vibrations and δ is the *logarithmic decrement* defined as

$$\delta = \ln\left(\frac{A_n}{A_{n+1}}\right). \tag{2.13}$$

In Fig. (2.3) we can see a schematic plot of Eq. (2.12) where the envelope of the free decay as well as two successive vibrations A_n and A_{n+1} are emphasized. If a solid is characterized by a low damping, that is $\phi \ll 1$, then as a first approximation we can write

$$\delta = \pi\phi\,; \tag{2.14}$$

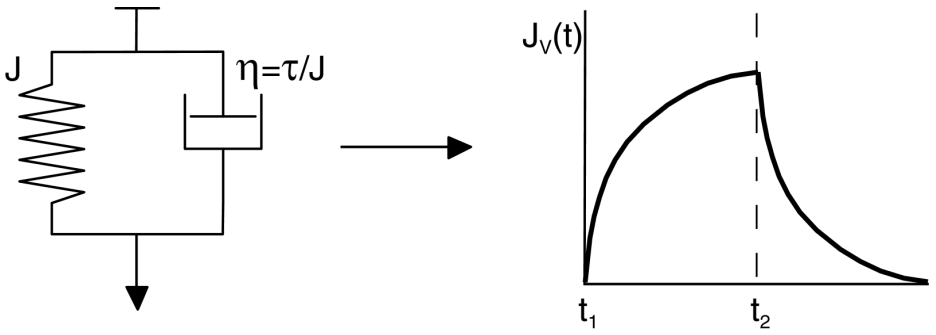

Figure 2.4: *Voigt model and its behavior upon loading and unloading.*

computing the internal friction of the sample reduces therefore to the measurement of the logarithmic decrement of the free vibrations.

2.3 The standard anelastic solid

The response functions represent one way of describing an anelastic solid. Another approach consists in the use of a generalized differential stress-strain equation of the form

$$a_0\sigma + a_1\dot{\sigma} + a_2\ddot{\sigma} + ... = b_0\varepsilon + b_1\dot{\varepsilon} + b_2\ddot{\varepsilon} + ... \tag{2.15}$$

in combination with elementary mechanical models whose basic constituents are ideal springs and newtonian dashpots (a piston moving in an ideally viscous fluid). The simplest combinations of such elements are represented by the so called Voigt and Maxwell models, respectively the parallel and the series of a spring and a dashpot. As we will see, these are not enough to describe the behavior of an anelastic material, for which at least an additional element is required (*three-parameter model*).

2.3.1 The Voigt and Maxwell models

For the characterization of the Voigt model, it is convenient to describe the spring with its compliance J and the dashpot viscosity with the quantity $\eta = \tau/J$ (τ has the dimension of time). In Fig. (2.4) we can see the behavior of this model when a stress σ_0 is applied for $t_1 \leq t \leq t_2$: at first the response $J(t)$ increases continuously until when the spring sustains the whole load and, after release of the stress, the force exerted by the spring makes the system go gradually back to its original state. The model is able therefore to describe the complete recovery of an anelastic material, but does not account for the instantaneous elastic response at the moments of loading and unloading. For

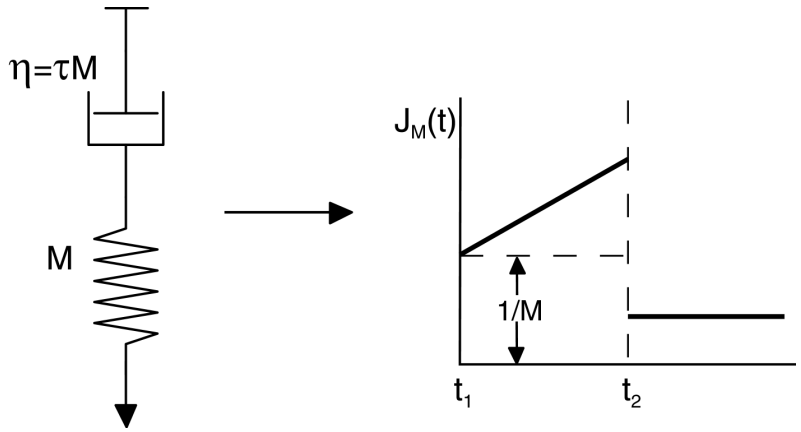

Figure 2.5: *Maxwell model and its behavior upon loading and unloading.*

a quantitative analysis we consider that the spring obeys the relation $\varepsilon_1 = J\sigma_1$ while the dashpot is described by $\dot{\varepsilon}_2 = J\sigma_2/\tau$. Remembering that for a parallel combination of these mechanical elements the strains are equal and the stresses are additive, that is $\varepsilon = \varepsilon_1 = \varepsilon_2$ and $\sigma = \sigma_1 + \sigma_2$ (vice versa for a combination in series), we end up with

$$J\sigma = \varepsilon + \tau\dot{\varepsilon}. \tag{2.16}$$

This represents nothing else than Eq. (2.15) with all the coefficients set equal to zero apart from a_0, b_0 and b_1. From the solutions of Eq. (2.16) it is then possible to derive the quasi-static or the dynamic response functions.

The situation for the Maxwell model is different and is described in Fig. (2.5): if at t_1 a constant stress is applied the spring reacts instantaneously showing a typical elastic response; successively the dashpot creeps until when the external stress is removed; finally for $t > t_2$ the system is permanently set to a new equilibrium level. Apart from the sudden response at t_1, this model clearly cannot describe the typical anelastic behavior and will not be further considered. It is only worth mentioning that also in this case we could derive the differential stress-strain relation starting from Eq. (2.15) and from the conditions $\sigma_1 = M\varepsilon_1$ and $\sigma_2 = M\tau\dot{\varepsilon}_2$; the computation of the response functions would consequently be possible.

2.3.2 The Three-Parameter model

The simplest mechanical model which can describe the behavior of an anelastic material must include at least three different parameters; this kind of description is so important that every material behaving as forecasted by it is called *standard anelastic solid*. There are different ways of combining springs and dashpots, but some of them have no practical meaning (e.g. a Maxwell unit

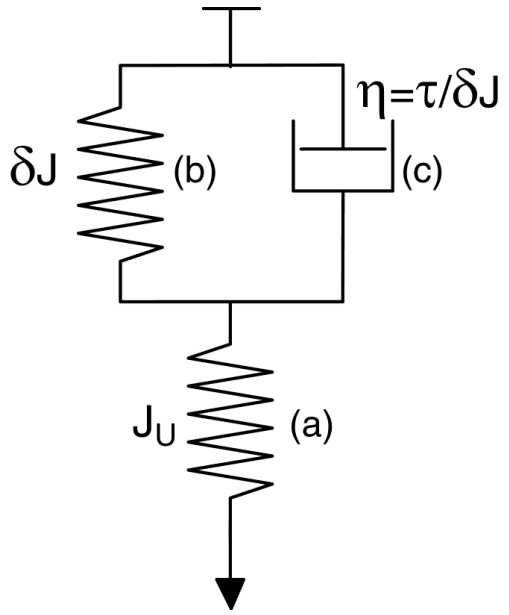

Figure 2.6: *One of the possible Three-Parameter models, made by a Voigt unit combined in series with a spring.*

in series with a spring) and some other give results which are equivalent to each other, like a spring connected in series (parallel) with a Voigt (Maxwell) unit. For brevity we will consider only one of these combinations and derive the respective dynamic response functions. Starting from Fig. (2.6), the temporal development of the strain under a constant load is the following: at the beginning only spring (a) moves leaving the Voigt unit steady (because of the reaction offered by the dashpot) and accounts for the initial elastic response of the whole system; successively the dashpot creeps until when the load is wholly sustained by the combination of (a) and (b). Upon unloading, spring (a) immediately returns to its original state followed then slowly by the Voigt unit. The situation is completely described in Fig. (2.2 a), where the unrelaxed and the relaxed compliances J_U and J_R are represented, respectively, by the element (a) and by the combination of (a) and (b); moreover, since $\delta J = J_R - J_U$, the symbolism adopted in Fig. (2.6) is justified.

If we follow a procedure similar to the one adopted for the Voigt unit, we can derive the differential stress-strain equation governing the behavior of the three-parameter model. The mechanical elements can be described by $\varepsilon_a = J_U\sigma_a$, $\varepsilon_b = \delta J\sigma_b$ and $\dot{\varepsilon}_c = \delta J\sigma_c/\tau$; these relations together with the rules for the combination in series and parallel of springs and dashpots give, after rearrangement,

$$J_R\sigma + \tau J_U\dot{\sigma} = \varepsilon + \tau\dot{\varepsilon}, \tag{2.17}$$

which has once again the form of Eq. (2.15) with an appropriate choice of the coefficients $a_0 \dots a_n, b_0 \dots b_n$. From the solution of Eq. (2.17) we can derive

directly the creep function, that is

$$J(t) = J_U + \delta J[1 - \exp(-t/\tau)]; \tag{2.18}$$

through this relation it is possible to interpret τ as a *relaxation time*, in the sense that at $t = \tau$, $J(t)$ has reached all but $1/e$ of its final value.*

We are now interested in the analytical form of the dynamic response functions, $J_1(\omega)$ and $J_2(\omega)$, that can be derived inserting the expressions $\sigma = \sigma_0 e^{i\omega t}$ and $\varepsilon = (\varepsilon_1 - i\varepsilon_2)e^{i\omega t}$ into Eq. (2.17): the result of such substitution is

$$J_1(\omega) = J_U + \frac{\delta J}{1 + \omega^2\tau^2} \tag{2.19}$$

$$J_2(\omega) = \delta J \frac{\omega\tau}{1 + \omega^2\tau^2}. \tag{2.20}$$

These are called *Debye equations* and are plotted in Fig. (2.7) as function of the product $\omega\tau$ and on a logarithmic scale, in order to emphasize peculiar features of the curves such as the peak shape of J_2 and its symmetry about $\omega\tau = 1$ or the step-like behavior of J_1, which goes from J_U at high frequencies to J_R at low frequencies.

Using the definitions of internal friction ϕ and of relaxation strength contained in Eqs. (2.11) and (2.4), respectively, we can also write $\tan\phi$ in the form of a Debye peak, at least in the approximation of small Δ, that is

$$\tan\phi \equiv Q^{-1}(\omega) \simeq \Delta \frac{\omega\tau}{1 + \omega^2\tau^2} \qquad (\Delta \ll 1). \tag{2.21}$$

We have introduced here the widely used notation of damping as the inverse of a quality factor Q, in analogy to what is commonly done in the description of resonant electrical circuits.

The last expression is very important for our purposes because the experiments made in this work, in which the damping was measured directly according to the method described theoretically in paragraph 2.2.3, were always characterized by small relaxation strengths, typically less than 0.1, giving us the opportunity of starting from Eq. (2.21) for the interpretation of data.

2.3.3 Multiple relaxations spectra

We have seen that the three parameter model is the simplest combination of mechanical elements through which an ideal anelastic solid can be described.

*Correctly speaking, there exist two different relaxation times τ_ε and τ_σ obtained, respectively, when the theory is developed following the first or the second of Eqs. (2.1). Since for small relaxation strengths we have $\lim_{\Delta\to 0}(\tau_\sigma - \tau_\varepsilon) = 0$, it is here tacitly assumed that we deal with processes characterized by very small Δ and consequently $\tau = \tau_\sigma = \tau_\varepsilon$.

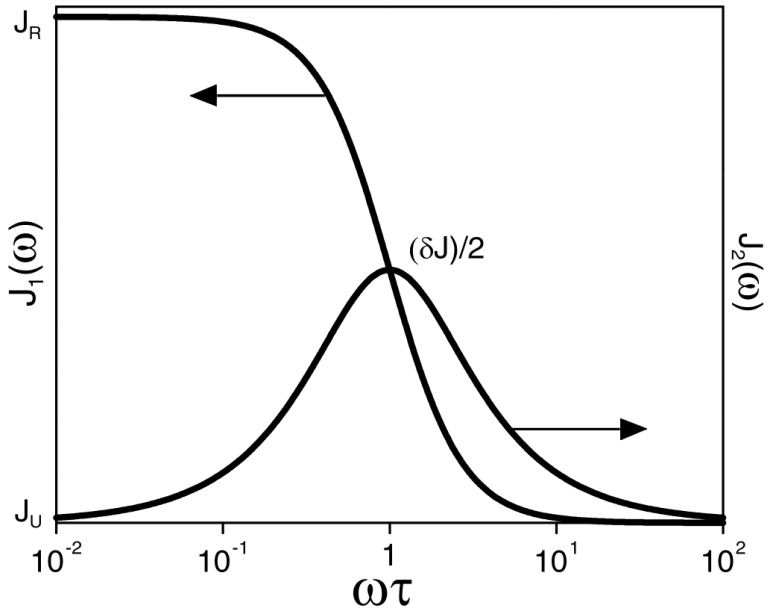

Figure 2.7: *The dynamic response functions for a standard anelastic solid.*

Now we could ask what happens if we add a series of Voigt units characterized by a discrete set of compliances $\delta J_1 \ldots \delta J_n$ and relaxation times $\tau_1 \ldots \tau_n$ to the model of Fig. (2.6). The answer for the dynamic response function J_2 (analogous arguments and formalism apply also to J_1) is contained in the generalization of Eq. (2.20) which becomes

$$J_2(\omega) = \sum_{i=1}^{n} \delta J_i \frac{\omega\tau_i}{1+\omega^2\tau_i^2}. \tag{2.22}$$

The effect on the shape of the Debye function J_2 is a broadening of the full width at half maximum or, if the relaxation times are sufficiently separated and the δJ_i of comparable magnitude, the presence of several maxima located at different frequencies.

The transition from discrete to continuous parameters is accomplished by setting τ as a continuous variable and by the substitution $\delta J_i \to X(\ln\tau)\, d(\ln\tau)$, where the last quantity represents the contribution to the total δJ for values of the relaxation time ranging from $\ln\tau$ to $\ln\tau + d(\ln\tau)$; the choice of a logarithmic scale for the spectrum is only dictated by convenience.[†] In Eq. (2.22) we must then replace the sum with an integral and the final result is

$$J_2(\omega) = \int_{-\infty}^{+\infty} X(\ln\tau) \frac{\omega\tau}{1+\omega^2\tau^2}\, d(\ln\tau). \tag{2.23}$$

[†]A more correct notation would require $\ln(\tau/\tau_1)$ as independent variable, where τ_1 is some appropriate reference relaxation time, but we will neglect this in the following.

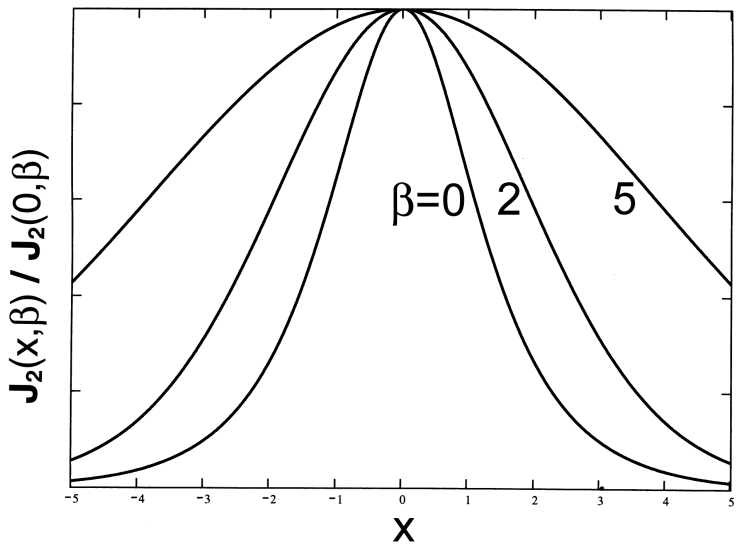

Figure 2.8: *Behavior of the normalized Eq. (2.25) for increasing values of* β.

At this point the problem of describing the behavior of an anelastic solid when its spectrum of relaxation times is known or, on the contrary, of obtaining the spectrum once the dynamic response function has been measured is, at least theoretically, solved. We are now interested in the second of these problems, for the solution of which there exist two different procedures, a direct and an indirect one. In the *direct* approach the knowledge of an analytical expression for the response function is advantageous, so that appropriate mathematical or numerical methods can then be used to invert integrals of the type shown in Eq. (2.23); this can often be a very difficult task and it is out of the scope of this work to investigate it further. In the *indirect* method a reasonable guess must first be made for the shape of the spectrum; successively this distribution must be inserted in Eq. (2.23) and the resulting response function must be calculated. From the comparison with the experimental data it is then possible to judge the quality of the guess. Clearly the shape of the distribution should be as close as possible to the real spectrum of relaxation times and, at the same time, should have an analytical form which minimizes the problem of solving Eq. (2.23). These requirements are often fulfilled by the Gaussian distribution and we will now consider it more in detail. With the substitution $z = \ln(\tau/\tau')$, where τ' is an average relaxation time, we can write

$$\Psi(z) = \frac{1}{\beta\sqrt{\pi}} \exp[-(z/\beta)^2], \tag{2.24}$$

where the adjustable parameter β is the half width at relative height $1/e$. By

defining the variables $w = z/\beta$ and $x = \ln \omega\tau'$ and substituting Eq. (2.24) into (2.23), we reach after rearrangement

$$\frac{J_2(x)}{\delta J} = \frac{1}{2\sqrt{\pi}} \int_{-\infty}^{+\infty} \mathrm{e}^{-w^2} \mathrm{sech}(x + \beta w)\, dw. \tag{2.25}$$

The term δJ appears explicitly on the left side of the equation because we have used a normalized spectrum defined as $\Psi(z) = (\delta J)^{-1} X(z)$. Eq. (2.25) is interesting because it can describe the behavior of an anelastic solid characterized by a continuous spectrum of relaxation times with an appropriate choice of only a single parameter. The effect of a variation of β can be seen in Fig. (2.8): the case of $\beta = 0$ corresponds to the standard anelastic solid and for increasing values of the adjustable parameter the effect is a broadening of the response function associated at the same time to a lowering of the peak height (not visible here because the curves have been normalized).

2.4 Dynamical properties as function of temperature

Until now it has been tacitly assumed that the dynamical response functions were obtained by considering the relaxation time τ as a parameter and the frequency ω as the independent variable. In the practice anyway this is not a very comfortable procedure, especially when a resonance method, like the one described in paragraph 2.2.3, is used; in this case, in order to draw a reasonable Debye peak, the inertia of the specimen must be changed and higher harmonics must be used for covering a frequency range of about two decades.

Luckily a wide range of phenomena causing anelasticity are of thermally activated type and for them the relaxation time can be expressed in the Arrhenius form

$$\tau = \tau_0 \, \mathrm{e}^{E_a/kT}, \tag{2.26}$$

where E_a is the activation energy, k the Boltzmann's constant, τ_0 a reciprocal frequency factor and T the temperature. If we multiply both sides of this equation with ω and take the natural logarithm of it, we obtain the important relationship

$$\ln \omega\tau = \ln \omega\tau_0 + \frac{E_a}{kT}. \tag{2.27}$$

As a consequence, a plot of a response function on a T^{-1} scale will differ only by a constant factor from the one on a $\ln \omega\tau$ scale, giving us the possibility of measuring the anelastic properties of a sample by varying the temperature

and keeping the frequency fixed. For the particular case of a true Debye relaxation, characterized by a single value of τ, we know that the peak maximum is situated at $\omega\tau = 1$ and in this position Eq. (2.27) becomes

$$\ln \omega = \ln \tau_0^{-1} - \frac{E_a}{kT_P}. \tag{2.28}$$

Thanks to this relation, if we measure the positions $T_{P1}^{-1} \dots T_{Pn}^{-1}$ of several peak maxima taken at different frequencies $\omega_1 \dots \omega_n$ and we put the results on a $\mathrm{Log}\,\omega$ vs. T^{-1} plot, the slope of the resulting straight line gives the quantity $E_a/(2.303\,k)$ and its intercept with the y-axis gives τ_0. [‡]

We are ready at this point to write the expression of the internal friction for the standard anelastic solid as a function of temperature: starting from Eq. (2.21), by inserting Eq. (2.27) in combination with Eq. (2.28) we finally obtain after rearrangement

$$Q^{-1}(T) = \frac{\Delta}{2} \,\mathrm{sech}\left[\frac{E_a}{k}\left(\frac{1}{T} - \frac{1}{T_P}\right)\right], \tag{2.29}$$

which is again a Debye peak centered about T_P^{-1} and of height $\Delta/2$.

If the relaxation time of Eq. (2.26) is not single valued but distributed in a continuous way, some caution must be taken when generalizing the expression for the internal friction given by Eq. (2.29). First of all a distribution in τ can arise by a distribution in τ_0, in E_a or in both these quantities. Let's restrict ourselves to the case of a spread in activation energies and let's rewrite Eq. (2.26) in the following way

$$\Psi(\tau) = \tau_0 \,\exp\left[\frac{N(E_a)}{kT}\right]. \tag{2.30}$$

In order for the distribution in relaxation times to be *compatible* with a distribution in activation energies, $\Psi(\tau)$ must have the same functional form at all temperatures; this is indeed a very restrictive requirement which is only met by few types of distributions [22]. It can be shown anyway that a sufficient condition for the compatibility consists in letting the spectrum of relaxation times depend on the composite variable $b^{-1}\ln(\tau/\tau')$, where τ' can be taken as the average value of the distribution and b is a parameter which must depend on the temperature according to $b \propto T^{-1}$. In this case we will have

$$\Psi(\tau) \to \Psi[b^{-1}\ln(\tau/\tau')] = \Psi\left(\frac{E_a - E_a'}{bkT}\right) \tag{2.31}$$

[‡]The factor 2.303 comes from the transformation $\ln x \to \mathrm{Log}\, x$.

where the last equality follows from the Arrhenius form of the relaxation time and $E_a{}'$ is the energy value corresponding to τ'. Thanks to the temperature dependence of the parameter b, the spectrum of Eq. (2.31) satisfies the compatibility criterion.

In the case of the distribution of Eq. (2.24), after the substitution $z \rightarrow \ln(\tau/\tau') = (E_a - E'_a)/kT$ we obtain

$$P(E_a) = \frac{1}{\beta kT\sqrt{\pi}} \exp\left[-\left(\frac{E_a - E'_a}{\beta kT}\right)^2\right], \tag{2.32}$$

which is related to the expression of Eq. (2.24) by $\Psi(z) = kTP(kTz)$. By assuming $b = \beta$, Eq. (2.32) takes the form of Eq. (2.31) meaning that a Gaussian spectrum of relaxation times is compatible with a distribution of activation energies. With this particular form of $P(E_a)$ we can then define $\beta = \beta_E/kT$, where β_E is the half width at $1/e$ of the distribution in E_a.

Finally, if we want to rearrange Eq. (2.25) showing its dependence on T and E_a instead of x and w, by making use of Eq. (2.32) and remembering that for $\Delta \ll 1$ we have $J_2/\delta J = Q^{-1}/\Delta$, we get

$$\frac{Q^{-1}(T)}{\Delta} = \frac{1}{2\,\beta_E kT\,\sqrt{\pi}} \int_0^\infty \mathrm{e}^{-\left(\frac{E_a - E'_a}{\beta_E}\right)^2} \operatorname{sech}\left[\frac{1}{k}\left(\frac{E_a}{T} - \frac{E'_a}{T_P}\right)\right] dE_a\,, \tag{2.33}$$

which is the general expression for the internal friction as function of temperature for an anelastic solid characterized by a Gaussian distribution of activation energies. Here T_P simply represents the peak temperature of the damping spectrum. This equation is not solvable analytically, but it is possible to plot it by using an appropriate commercial software.

2.5 Physical reasons of anelasticity

The reasons for the dissipation of mechanical energy which takes place in a solid subjected to an external field range from the movement of point defects and dislocations, to the diffusion of thermal currents, to phase transformations and grain boundary effects, or again to magnetoelastic phenomena. The occurrence of one or more of these processes depends on several factors, among which are the characteristics of the material and the choice of the probing field; it is the aim of *Mechanical Spectroscopy* (MS) to study and possibly to distinguish all these different physical effects.

We will hereafter concentrate on the thermoelastic damping and on the reorientation relaxation of point defects (especially interstitial hydrogen atoms), which are the main sources of anelasticity in the metallic glasses that we investigated. As we will see, a strong effect due to other movements of the

host matrix atoms in the range between the glass (T_g) and first crystallization (T_x) temperatures is easily distinguishable from the other processes and in particular does not overlap with the hydrogen reorientation relaxation.

2.5.1 Thermoelastic damping

The classical picture of the thermoelastic effect has been given more than fifty years ago by Zener [23]. He understood that a deformation can generate temperature gradients inside a specimen, or between the specimen and its surroundings, giving rise to a heat flow which brings the sample back to thermal equilibrium, but at the same time dissipates energy and causes anelasticity.

It can be shown that the temperature change of an elastic solid due to the presence of an external stress is

$$\Delta T = -(\alpha T/C_\sigma)\,\sigma \tag{2.34}$$

where α is the linear thermal expansion coefficient and C_σ the thermal capacity per unit volume at constant stress. Consequently if we bend a sample and produce an initial strain, which we call ε_U (the subscript means "unrelaxed"), the resulting ΔT will be negative in the zones of tension and positive in the zones of compression. This temperature gradient will be then equilibrated by heat flow and, after this process has taken place, the outcome will be an additional strain due to thermal expansion (contraction); the final value of the strain is then called ε_R or "relaxed". The relaxation strength for such process can be written as

$$\Delta_T = \frac{\varepsilon_R - \varepsilon_U}{\varepsilon_U} = \frac{\alpha^2 E_U T}{C_\sigma} \tag{2.35}$$

where E_U is the unrelaxed elastic modulus. This equation states that in an experiment where the damping is measured as function of temperature, the contribution of the thermoelastic effect is represented by a linear background going through the origin of the axes, at least in the limit of a weak temperature dependence for the parameters α, E_U and C_σ.

If the stress is not static but oscillates with angular frequency $\omega = 2\pi f$, it can be shown that the thermoelastic internal friction is expressed as a Debye peak centered on a frequency f_0 determined by the relaxation time τ for thermal equilibration [24]: in particular

$$Q_T^{-1} = \Delta_T \frac{\omega\tau}{1+\omega^2\tau^2} = \Delta_T \frac{f f_0}{f^2 + f_0^2}\,. \tag{2.36}$$

The most straightforward application of this effect is the computation of the thermal conductivity k_{th} of a specimen of thickness d, which can be done by

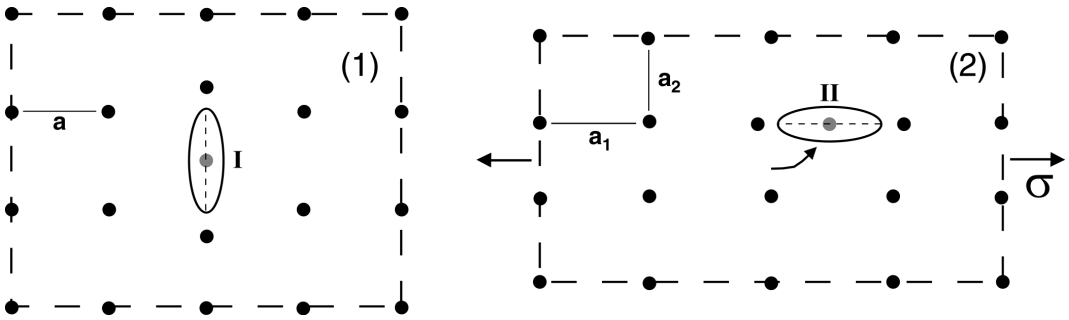

Figure 2.9: *Reorientation of an elastic dipole in two dimensions upon application of an external stress.*

measuring the peak frequency of Q_T^{-1} and using the equation

$$f_0 = \frac{\pi k_{th}}{2d^2 C_\sigma}. \tag{2.37}$$

2.5.2 Point defect reorientation relaxation

Anelasticity can be produced by a stress-induced rearrangement of point defects between their equilibrium positions if the presence of the external perturbation changes the energy levels of these positions relative to each other. A schematic 2-dim representation of this process is given in Fig. (2.9): (1) in the externally unperturbed lattice (black dots) with parameter a, the presence of an interstitial impurity (grey dot) in position I generates locally an elastic distortion field which, if characterized by non-spherical symmetry, is called *elastic dipole*, in analogy with the corresponding electric or magnetic quantities; (2) if we now apply a stress σ, the lattice will be modified and characterized by the new parameters $a_1 > a$ and $a_2 < a$. In such conditions it becomes energetically favorable for the impurity to jump to position II, generating at the same time a change in the orientation of the main distortion axis (reorientation). Let's now imagine a population of such point defects which, in thermal and mechanical equilibrium conditions, are randomly distributed in the host matrix. The application of an external stress will then cause a redistribution of the elastic dipoles along a preferred orientation; since each impurity generates a microscopic elongation, the net effect on the macroscopic sample will be an additional anelastic strain in the direction of the applied stress.

A more complete description of this phenomenon requires the definition of a quantity, the $\boldsymbol{\lambda}$ - tensor, which includes all the information on the elastic distortion field created by a point defect. In the previous example we have seen how an elastic dipole is characterized by an axis along which the distortion is maximum: we call this direction the *orientation* of the dipole. If we introduce

in a solid a mole fraction c_p of defects all oriented along the direction p, then we define

$$\lambda_{ij}^{(p)} \equiv \frac{\partial \varepsilon_{ij}}{\partial c_p}\,, \tag{2.38}$$

which represents the change of the strain component ε_{ij} $(i,j=1,2,3)$ per unit mole fraction of point defects having the same orientation p. This tensor is symmetric and consists in general of six independent components; moreover it can be characterized by a strain ellipsoid with three mutually perpendicular axes, which is nothing else than the 3-dim generalization of the elastic dipole of Fig. (2.9). The number of independent components can then be reduced by making considerations on the symmetry system of the defect[§]: for example a defect of cubic symmetry is characterized by a $\boldsymbol{\lambda}$-tensor whose diagonal values are identical to each other, while a defect of tetragonal symmetry has e.g. $\lambda_{11} \neq \lambda_{22} = \lambda_{33}$ (in both cases the off diagonal components are equal to zero).

In the previous example we have seen how the form of the $\boldsymbol{\lambda}$ -tensor, in the sense of which values are assumed by each λ_{ij}, is only determined by the symmetry system of the defect. As a consequence it is possible that different defect orientations give rise to the same $\boldsymbol{\lambda}$, as it happens for example in the case of an unlike pair which produces the same distortion field either in its original position or after exchanging the places of the atoms (reversed pair). The important point is that defects having the same $\boldsymbol{\lambda}$ are indistinguishable in terms of their behavior under stress: if we denote with n_t the number of independent $\boldsymbol{\lambda}$ -tensors, $n_t = 1$ means that all the defects look alike to an external stress and that no change in the statistical distribution of the elastic dipoles will take place. On the other hand, if $n_t > 1$ a stress field interacts differently with defects having different $\boldsymbol{\lambda}$ so that one of them is energetically favored with respect to the others; this gives rise to a redistribution of defects and to anelasticity.

2.6 Anelastic relaxation of hydrogen

After some general remarks on the theory of the point defect reorientation relaxation we want to give a short overview on similar effects created by the presence of hydrogen as an interstitial impurity in metals and alloys. Generally speaking, in order to observe a particular relaxation as a damping peak, at least two quantities must lay in a suitable range, that is the *strength* Δ and the *rate* τ^{-1} of the relaxation itself. The first one is proportional, according

[§]The defect symmetry is defined as the collection of symmetry elements which are common both to the defect when isolated from the crystal and to the site on the perfect crystal about which the defect is built.

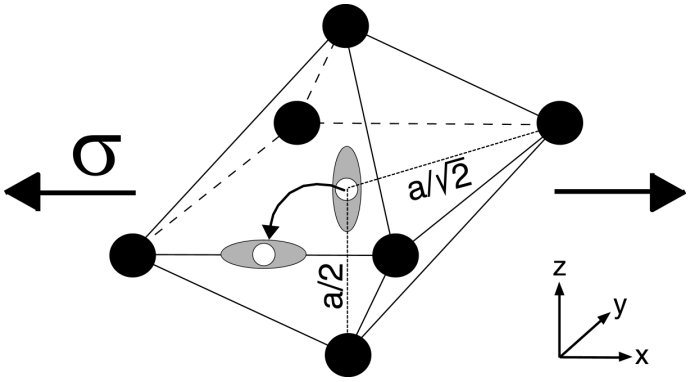

Figure 2.10: *Snoek effect of C (white dots) in bcc Fe (black dots). Emphasized is the reorientation of the elastic dipole (grey oval) upon application of the stress* σ.

to the theory, to the product $c\,(\delta\lambda)^2$, where c is the total concentration of defects and $\delta\lambda$ represents the difference between some appropriate principal values of the $\boldsymbol{\lambda}$-tensor, which is a measure of the anisotropy of the elastic distortion field around the impurity. The relaxation rate on the other side accounts for the diffusional mobility of the point defect: its value should be considerably different from the corresponding quantity related to the atoms of the host matrix, in order to avoid undesirable overlapping effects in the measured damping spectra.

The short range reorientation relaxation of hydrogen can be described following the example of the *Snoek effect* of carbon in *bcc* iron [20, 25] whose principle is shown in Fig. (2.10); in this case the impurities consist of C atoms sitting in the octahedral sites available in the Fe matrix. Since the C-Fe nearest neighbors distances are characterized by two different values ($a/\sqrt{2}$ the longest and $a/2$ the shortest), the elastic distortion field created by the defects is anisotropic and elongated in a particular direction. In equilibrium conditions the elastic dipoles are equally distributed along the x, y, z axis; the application of a stress as in the example of Fig. (2.10), generates a redistribution of the elastic dipoles mainly in one direction, and therefore anelasticity, through a process consisting of thermally activated jumps of the C atoms between adjacent octahedral sites. This example applies also for reorientation processes in other structures, or other type of interstices (e.g. tetrahedral), and with other interstitial impurities like, in particular, hydrogen.

The experimental observation of this type of hydrogen induced anelastic relaxation in form of internal friction spectra depends on several factors that we now summarize: a) the symmetry system of the interstitial H atom must be lower than the one characterizing the host matrix (or, if we think about

the $\boldsymbol{\lambda}$-tensor, $n_t > 1$); b) since the relaxation strength depends on the defects concentration, a good solubility for H in the material of interest is required; c) in order to distinguish the effects due to the interstitials from the ones due to the matrix, the defect mobility must be much higher than the one of the host atoms (which is in many cases true for H). Given these general conditions it is now interesting to see briefly in which kind of structures such a Snoek-type effect of hydrogen has been, or can be, observed (a more complete overview on this topic can be found in the work of Sinning [16] and references within):

- *bcc metals*: no hydrogen induced Snoek effect. In fact the symmetry of the elastic distortion field of a H atom turns out to be cubic, which is identical to the one of the matrix, instead of tetragonal (as it is for heavier interstitials like C, N, O). The reason is probably some delocalisation of H among the tetrahedral sites surrounding an octahedral one. On the other side anelastic relaxation is observed if hydrogen is trapped by some other defects of the host matrix.

- *fcc metals*: the symmetry of the interstices is cubic both for the tetrahedral and the octahedral sites, meaning that a Snoek type relaxation is in principle impossible. The situation is different for *alloys*, because the size difference of the components changes the surroundings of an interstitial H atom and consequently the form of the elastic distortion field. It should be mentioned anyway that another relaxation mechanism prevails in pure fcc metals, that is the Zener reorientation [20, 26] of H-H pairs.

- *hcp metals*: here too the predominant anelastic relaxation mechanism is the Zener effect relative to H-H pairs.

Until now we have spoken about the occurrence of a Snoek type reorientation relaxation in crystalline structures and we have mentioned what are the main conditions for such process. It is interesting for our purposes to extend the analysis to *amorphous* alloys, for which the picture of anelastic relaxation of hydrogen presents peculiar characteristics. In fact it is experimentally well known that, unlike in *bcc* metals, in completely disordered structures the Snoek effect due to hydrogen exists and manifests itself as broad and asymmetric internal friction peaks[¶] as in the example of Fig. (2.11). The increased peak width can be understood by making the following considerations: in crystalline structures made by a single component, the elementary atomic jumps of a particular type of impurity, giving rise to the Snoek effect, are characterized by a *single* value of the relaxation time (and therefore of the activation energy, if we assume thermally activated processes following an Arrhenius behavior and

[¶]In comparison to the Debye peak of Eq. (2.29).

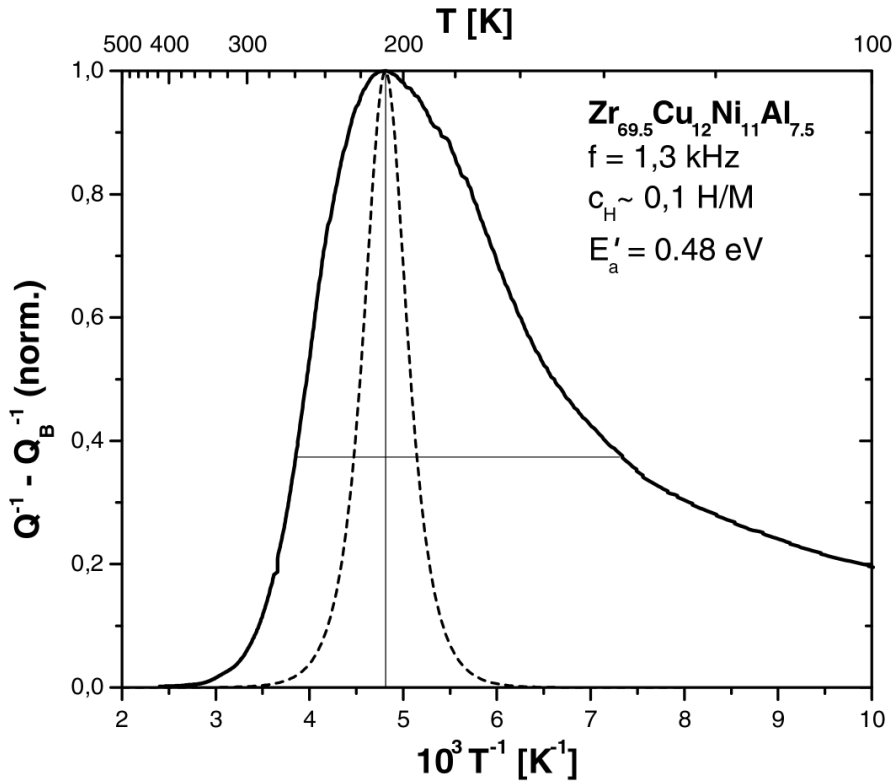

Figure 2.11: *Normalized H-induced damping spectrum after a linear background subtraction for an amorphous alloy. The dotted line is a theoretical Debye peak calculated for the average activation energy* $E_a{}'$.

we take τ_0 as a constant). For such processes the theory predicts a damping spectrum given by Eq. (2.29), which describes a pure Debye relaxation. If we make a step forward and consider a crystalline alloy, we must generally deal with a *discrete set* of values for the activation energy, since the geometry as well as the chemistry of the interstitial sites can assume different configurations; this already turns out in a broader outline of the internal friction spectrum which is now composed by the sum of several Debye peaks. If we want to have a more quantitative, even if somewhat approximative, picture of the problem we can estimate the energy barrier for a jump of a hydrogen atom from its equilibrium site (E) to the saddle point (S) by writing

$$E_a = \sum_{i=1}^{n_S} V_i(r_i^S) - \sum_{i=1}^{n_E} V_i(r_i^E) - \frac{3}{2}\hbar\omega; \tag{2.39}$$

in this equation n_S represents the number of atoms situated at the vertices of the surface through which the H atom jumps to the neighboring interstitial site.

On the other side n_E is the number of atoms constituting the cage where the hydrogen originally sits. V_i is the potential between the ith metal atom and H and r_i the distance between them; the zero point energy of H in its equilibrium site is also taken into account. By looking at Eq. (2.39) it is clear that the influence of chemistry on the activation energy is reflected in the form of the M-H potential (M stands for metal atom), while the geometry of the interstitial site plays a role in the definition of the distances r_i. Considering now an amorphous alloy, it is natural to expect a *continuous* set of activation energies since the distribution of pair distances, which has generally a Gaussian shape, reflects itself in a distribution in r_i and therefore in E_a. For the description of the H-induced internal friction in amorphous structures it is then necessary to use a convolution of a Debye peak with some continuous spectrum of activation energies, as in the example of Eq. (2.33), resulting therefore in a broad outline of the damping curve.

The second important feature of Fig. (2.11), namely the low-temperature tail causing the asymmetry of the damping peak, originates from a contribution to the overall process coming from hydrogen atoms jumping through surfaces offering particularly low values of the saddle point energies (this includes also tunnelling effects); in particular it has been postulated that such process is correlated with the existence of non triangular side faces of the polyhedron enclosing the H atom [27].

Other noteworthy characteristics of the hydrogen Snoek effect in amorphous metals are the shift of the damping peaks to lower temperatures with increasing c_H and the dependence of the peak height on the amount of dissolved H. The first effect is a consequence of the site occupation of hydrogen, which obeys a Fermi-Dirac statistics [28]: while at low c_H the impurities prefer to sit in the energetically more favorable places, at higher concentrations the H atoms must look for other sites. Assuming that the activation energy for the reorientation jumps becomes lower for those impurities sitting in the energetically unfavorable interstitial places and keeping in mind that for thermally activated process there is a proportionality between the internal friction peak temperature T_p and the average E_a as stated by Eq. (2.28), it follows that the increase in c_H involves a decrease of the average E_a and, consequently, of T_p. As regards the second effect, if we only consider the changes of the peak of the damping spectrum, we observe firstly an increase of the peak height with successive hydrogen uptake, at least up to a certain limit, which reflects the dependence of the relaxation strength on c_H as previously discussed. Successively, by inserting more hydrogen, the damping maximum decreases giving an indication that some suppression of relaxation centers takes place, for example because of nearest neighbor (NN) blocking effects. This happens because two H atoms in a metallic matrix cannot be closer than 2,1 Å (Switendick crite-

rion [29]) and this in turn restricts the number of interstitial sites which are available for the reorientation process. In $CoZr_2$ metallic glasses for example it was found that this H concentration limit lay at about $c_H = 0,6\,H/M$ [30].

As yet there are very few theoretical models describing the relationship between the relaxation parameters of the hydrogen Snoek effect and the microstructure of the glassy host system. That some link between quantities like the activation energy for the H reorientation process and the short range order (SRO) of the atoms enclosing the H defect must exist is clear, as can be seen for example in Eq. (2.39). The problem consists in finding some experimentally accessible structural parameters that can be correlated to the internal friction data, without considering in detail the form of the potential M-H, which is generally not known. Richards [1] has done this for a model glass consisting of a dense random packing (DRP) of soft spheres and has successfully applied his theoretical results to the H anelastic relaxation data on $Pd_{80}Si_{20}$. Without going into the details, the author has shown that with the knowledge of the bulk modulus K, of the volume change ΔV per H atom and of the pair radial distribution function (RDF), it is possible to calculate the statistical variation of the H *equilibrium site* energies correlating it to the distribution of the total edge lengths of the polyhedra enclosing the H atoms. For the *saddle point* energies a knowledge of the potential was necessary, but it could be estimated by using simple analytical expressions which fit the observed lattice expansion ΔV and the zero point vibrational frequency of hydrogen in the respective crystalline metal hydride system. One of the main results of this model is the possibility of correlating the measured activation energies of the H reorientation jumps to the shape of the main structural units (tetrahedra or octahedra for example) containing the impurity. This use of the H-induced internal friction spectra as a probe of the SRO of the host matrix has been further developed and represents the basic concept of *Mechanical Hydrogen Spectroscopy* (MHS) [16, 15, 17], which will be more extensively described in section 3.4.

Other theoretical models of the H-induced internal friction in amorphous alloys deal mainly with the calculation of the relaxation strength by following a statistical approach. In particular Stolz [31] applied the Fermi-Dirac occupation statistics to the relaxation process, concluding that only the H atoms in the proximity of the Fermi level contribute to the overall anelastic relaxation. This model, which cannot describe for example the effects deriving from NN blocking, was criticized by Berry and Pritchet first [32], who introduced the concept of H-H repulsion and pointed out the microscopic nature of the reorientation jumps between adjacent sites, and by Sinning afterwards [30], who considered for the calculation of the relaxation strength also a next nearest neighbors occupation probability.

The manifestation of the hydrogen Snoek effect in amorphous alloys has been up to now very well established from the experimental point of view, but a completely satisfactory theory which can describe the behavior of the damping spectra still lacks. The situation is different in crystalline intermetallic compounds because, due to the severe embrittlement caused by hydrogen loading in such structures, it is complicated to perform anelastic relaxation measurements and a systematic collection of data is therefore missing. A satisfactory treatment was performed anyway in the case of $CoZr_2$ and $NiZr_2$ glasses which were firstly crystallized in a vibrating reed chamber and successively loaded in situ with hydrogen. A theory based on Richards' model explaining the relaxation parameters was also successfully attempted [33, 19, 34].

Very interesting for the purposes of this work is the recent discovery of a H-induced anelastic relaxation peak also in Zr- [35] or Ti-based *quasicrystals* [36]. The analogous explanation of this peak also in terms of a Snoek-type mechanism, to be discussed further below in chapter 4, is in some contrast to the interpretation of the relaxation peak observed in (non-H-absorbing) Al-based single icosahedral quasicrystals, where such mechanism (due to C, N and O) was rejected in favor of an explanation involving phason type or other intrinsic defects [37, 38]. Moreover the authors pointed out that almost all the physical parameters necessary for the description of the Snoek effect are unknown for quasicrystals. This opens therefore a new field where a lot has to be done both on the experimental side and on the developing of an anelastic relaxation theory in icosahedral structures.

Chapter 3

Materials and methods

In this chapter we are going to discuss in some detail the experimental technique we used for the anelastic relaxation measurements as well as the characteristics of the materials which we investigated. The first section is dedicated to the description of the vibrating reed device, while the second contains the details on the Zr-based bulk metallic glasses and on the various phases which are successively formed upon annealing from the amorphous state. Another section is dedicated to the description of the hydrogen charging of the samples from the gas phase. The final part of the chapter describes briefly the method of Mechanical Hydrogen Spectroscopy.

3.1 The vibrating reed technique

In the former chapter it has been mentioned that the experimental techniques which are used for anelastic relaxation measurements can be divided in subresonant, resonant and wave propagation methods. The vibrating reed technique belongs to the second of these categories and its main operating principle can be described following the scheme of Fig. (3.1): a thin slab of material, which in our case comes from "splats" or melt spun ribbons of rapidly quenched melts, is securely clamped between a steel and a copper plate. An electrode is placed in close proximity to the sample, in order to form with this one a capacitor. The application of an oscillating voltage with a frequency close to the natural eigenfrequency f_r of the reed promotes the vibration of the sample thanks to the force due to the electrostatic induction between the plates of the capacitor. At regular intervals the excitation is switched off and the signal coming from the oscillating reed is collected from the electrode and elaborated in the measuring unit of the electronics, with the purpose of calculating the damping of the free vibrations of the specimen.

In order to describe how a voltage V applied to the system electrode-sample

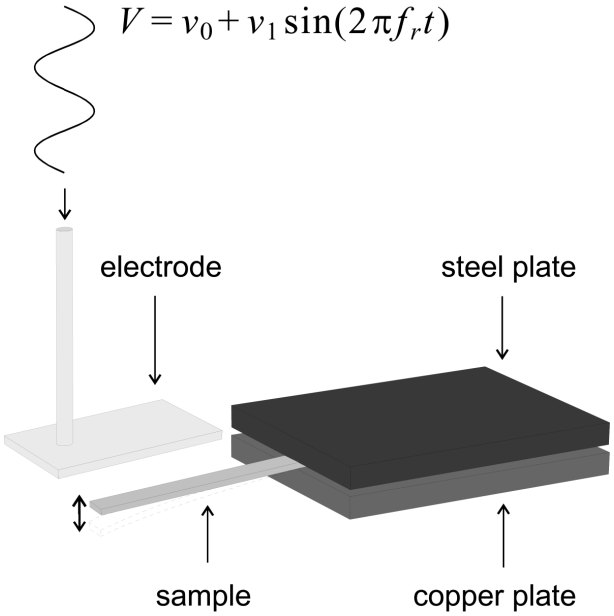

Figure 3.1: *Operating principle of the vibrating reed technique in the "clamped-free" configuration.*

generates an oscillating force on the reed, we can start by writing

$$V = v_0 + v_1 \sin(2\pi f_r t)\,, \tag{3.1}$$

where v_0 (v_1) is the static (dynamic) polarization. The general expression for the force acting between the plates of a capacitor is

$$F = \frac{qV}{d}, \tag{3.2}$$

where q is the electric charge and d the distance between the plates. In our specific case, considering that $q = CV$ and $C = \frac{\varepsilon_0 A}{d}$ for a planar condensator (C is the capacity, A the surface of the condensator's planes and ε_0 the dielectric constant of vacuum), Eq. (3.2) becomes

$$F = \frac{\varepsilon_0 A}{d^2}[v_0 + v_1 \sin(2\pi f_r t)]^2 \tag{3.3}$$

or, after rearrangement,

$$F = \frac{\varepsilon_0 A}{d^2}\left[v_0 v_1 \sin(2\pi f_r t) - \frac{1}{4}v_1^2 \cos(4\pi f_r t) + \frac{1}{2}\left(v_0^2 + \frac{1}{2}v_1^2\right)\right], \tag{3.4}$$

which represents the electrostatic force acting on the sample when a periodic voltage is applied. Eq. (3.4) provides two terms that can be used for the

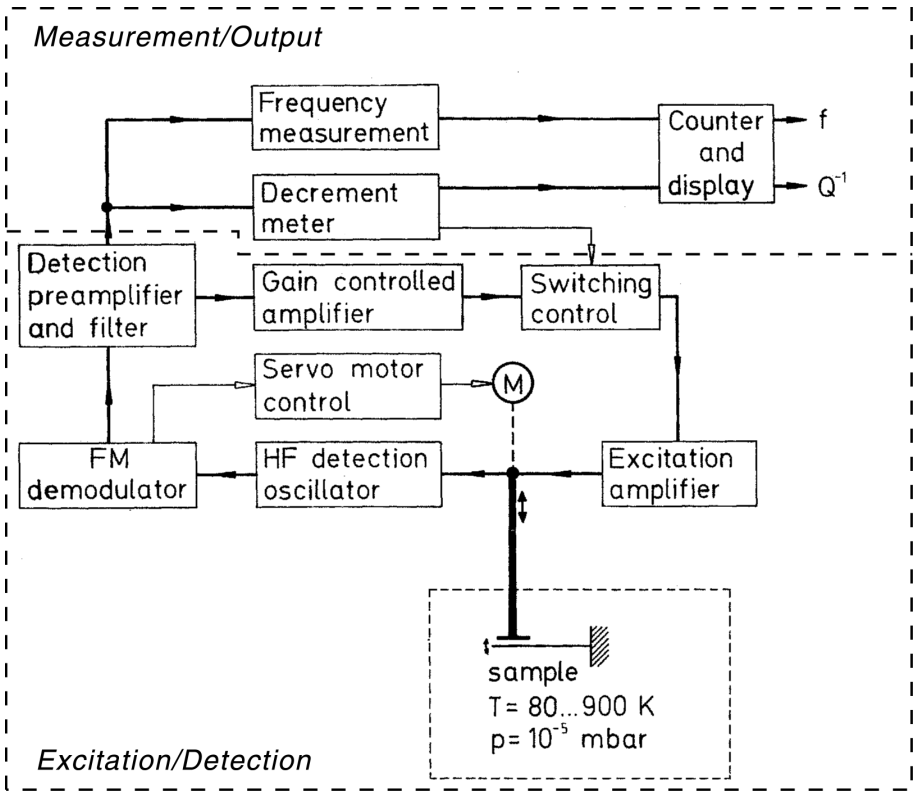

Figure 3.2: *Scheme of the vibrating reed electronics.*

excitation: the first with frequency f_r and the second with frequency $2f_r$. In our case, by adjusting the oscillating excitation electronically to coincide with the resonance frequency f_r of the sample, only the first term is used.

The core of this experimental technique is the electronics [39]; on one side it takes care of the excitation of the sample and of the detection of the signal, while on the other side it gives at its output the resonance frequency and the damping of the material, as is schematically described in Fig. (3.2). One of the most interesting part of the circuitry is the one dedicated to the detection of the signal: an external oscillator works at a ground frequency of approximately 40 MHz (HF oscillator). The determination of this operating frequency depends on the electrode-sample capacity and in particular on the distance $d = d_0 + \Delta d$ between electrode and specimen. The base distance d_0 is chosen by the initial placing of the sample holder and by the regulation through an electric motor of the electrode's position, while Δd is the variation caused by the vibration of the sample. This one in turn changes the value of the capacity, causing a modulation Δf in the base frequency of the HF oscillator. This modulated high frequency is then sent to a demodulator, which gives at its output a signal proportional to Δf, and successively amplified and directed to a phase

locked loop system, which serves to maintain the stable vibration of the sample between successive measurements.

Since most experiments are performed as function of temperature, there is a natural tendency of the mechanical parts, including the specimen itself, to move with respect to each other; in particular d_0 does not remain constant and it is necessary to add a compensation which contrasts this tendency. This is done by the servo motor control, which acts on a micrometer screw directly connected to the electrode and changes the distance electrode-sample according to the specific needs.

The measurement/output part of the electronics gives the values of the resonance frequency of the reed and a quality factor Q, whose reciprocal represents the damping of the material. In particular, for the computation of Q, the decrement meter counts the periods n of the free oscillations of the sample whose amplitudes satisfy the condition $A_L < A < A_H$, where A_L (A_H) is a low (high) amplitude reference value. With the knowledge of this number and remembering Eq. (2.13), it is straightforward to write

$$\delta = \frac{1}{n} \ln \left(\frac{A_H}{A_L} \right). \tag{3.5}$$

From the proportionality between the logarithmic decrement δ and the damping $\phi \simeq Q^{-1}$ which is stated in Eq. (2.14) and considering that the ratio A_H/A_L in this electronics is fixed to the value 1,481 we obtain for the quality factor the expression $Q = 8\,n$.

Speaking about the mechanical part of our experimental setup, the most important thing is the sample holder which can be seen in Fig. (3.3). The position of a reed of material, approximately 40 μm thick, as well as the metal plates used for the clamping are emphasized; moreover the hole which serves for the positioning of a NiCr-Ni thermocouple, used for the monitoring of the temperature, is indicated. All the measurements have been performed in a range between 90 and 900 K with a heating rate of 1-2 K/min and at a pressure of about 10^{-5} mbar. In particular the vacuum was necessary on one side to avoid those damping effect caused by the presence of air and on the other side to hinder an excessive heating of the whole system, as well as to prevent the oxidation of the samples.

At this point it is useful to consider the result of a typical measurement, where the resonance frequency as well as the internal friction of the material are plotted at the same time as function of temperature. This is shown in Fig. (3.4) where we notice the following features: as far as the frequency is concerned, the complex ongoing of the curve with increasing temperature reflects, as we will see in more detail afterwards, the devitrification sequence of the material. On the other side the damping curve is characterized by the peaks indicated

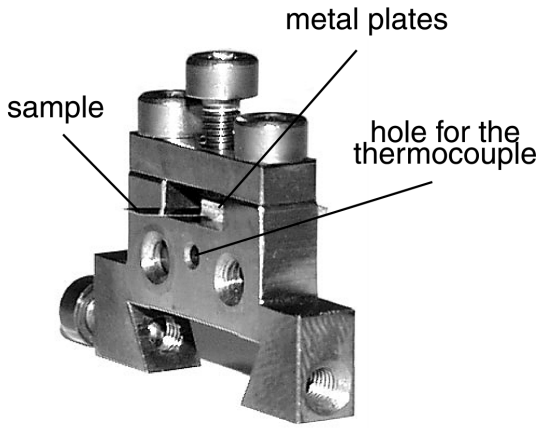

Figure 3.3: *Sample holder used for our vibrating reed measurements.*

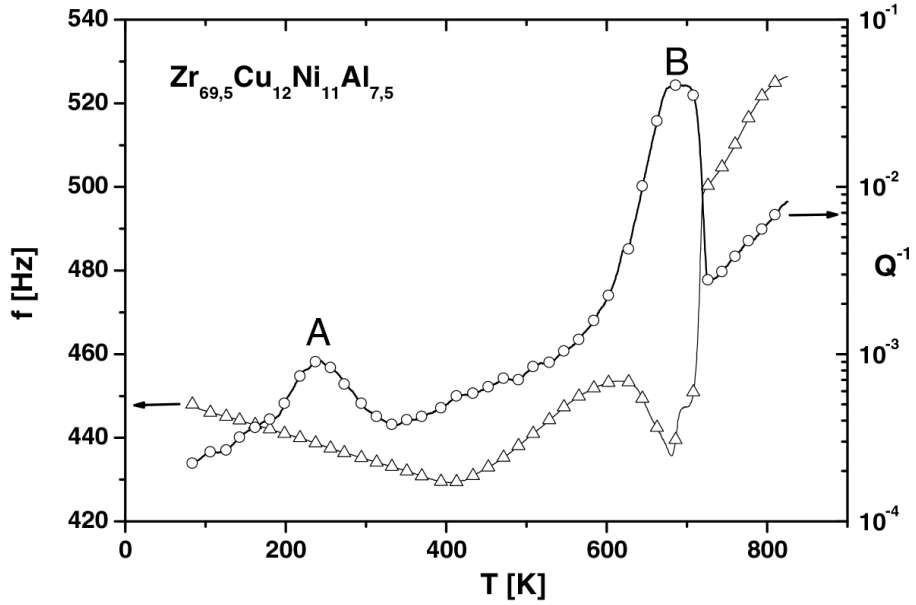

Figure 3.4: *Typical vibrating reed measurement for a bulk metallic glass across the whole temperature range; only few data points are shown and the line is a guide to the eye.*

with A and B which represent, respectively, a true relaxation effect caused by the hydrogen reorientation mechanism and a phase transition effect, reflecting the movements of the atoms composing the host matrix when going from the amorphous to the metastable intermediate states and then to a final crystalline structure.

3.2 Materials selection and characterization

In this section we are going to specify which kind of materials we have used for our investigations and what are their characteristics. In particular we will concentrate on the phase transformations of the samples upon annealing and on the correspondence between the change of resonance frequency and the devitrification of the glasses. This has been done by comparing literature data and self made differential scanning calorimetry (DSC) and transmission electron microscopy (TEM) measurements with the results obtained by using the vibrating reed technique.

3.2.1 Choice of the materials

Generally speaking the materials with which we are concerned belong to the family of the metallic glasses. Until the beginning of the 90's it was customary to produce these alloys from their melts using techniques capable of a very rapid cooling rate, typically of the order of 10^5-10^8 $\mathrm{K\,s^{-1}}$, which implied that the sample thickness was limited to about 50 μm. Successively a range of multicomponent alloys was discovered which showed a very good stability against crystallization upon cooling from the liquid state; as a consequence it was possible to cast specimen with much slower cooling rates and linear dimensions of the order of centimeters, from which the definition of *bulk* metallic glasses arises.

In this work we have studied those bulk glass forming alloys belonging either to the Zr-Cu-Al(-Ni) (which, for brevity, will be referred to as "Inoue" type, even though the alloy containing the highest amount of Zr has been actually introduced by the group of Köster [12]) [2] or to the Zr-Ti-Cu-Ni-Be ("Johnson" type) [3] families. The materials were produced by splat quenching at the university of Augsburg and at Caltech, Pasadena, or by melt spinning at the university of Dortmund, and the different compositions that we analyzed are listed below:

1. $Zr_{41}Ti_{14}Cu_{12,5}Ni_{10}Be_{22,5}$ (V1)
2. $Zr_{46,8}Ti_{8,2}Cu_{7,5}Ni_{10}Be_{27,5}$ (V4)

3. $Zr_{69,5}Cu_{12}Ni_{11}Al_{7,5}$

4. $Zr_{65}Cu_{17,5}Ni_{10}Al_{7,5}$

5. $Zr_{65}Cu_{27,5}Al_{7,5}$.

Although all of these alloys have been studied, some more attention has been given to the first and the third one, because of the interesting intermediate phases which are build upon annealing before the final crystallization. In particular the $Zr_{69,5}Cu_{12}Ni_{11}Al_{7,5}$ glass forms a metastable quasicrystalline state [13], while the $Zr_{41}Ti_{14}Cu_{12,5}Ni_{10}Be_{22,5}$ is characterized by a decomposition stage with related formation of nanocrystals [40].

3.2.2 Phase transformations

The operation of clamping a thin reed of material in our sample holder was quite delicate, especially when handling brittle samples originating from the devitrification of our Zr-based alloys. This is one of the reasons why the materials were placed in the holder *before* the annealing treatment, when the reeds were in the amorphous state and rather ductile. Since one of our main goals was to study the hydrogen induced damping in the different phases originating from the glasses, we needed a method with which it was possible to monitor the phase transformations of the materials upon annealing *without* being compelled to remove the specimen from its holder. The change of resonance frequency of the reeds with a heating rate of 1-2 K/min has proven to give a rather precise picture of the complex sequence which brings our metallic glasses from the initial amorphous to the final crystalline state. Of course, a sort of calibration was necessary before a good interpretation of the data could be done. This is the reason why we compared DSC and TEM measurements (self made and/or taken from literature) with the results obtained with the vibrating reed technique on the same materials. In Fig. (3.5) are shown the measurements made with a Perkin-Elmer DSC 7 calorimeter for two Zr-Cu-Al-Ni alloys with a heating rate of 20 K/min; the most important features of such thermograms are the large exothermic peaks which appear between 700 and 760 K and which reflect, respectively, the formation of quasicrystals and the transformation of the icosahedral phase into a more stable crystalline structure. This interpretation is supported by the results obtained, especially for the Zr-richer material, by the group of U. Köster [13]. In this reference the DSC measurements for the $Zr_{65}Cu_{17,5}Ni_{10}Al_{7,5}$ are anyway quite different from ours; in particular a single large exothermic peak appears, instead of two as in the case of Fig: (3.5). This effect is a consequence of the different impurity content, in particular oxygen, between our samples and the one of reference

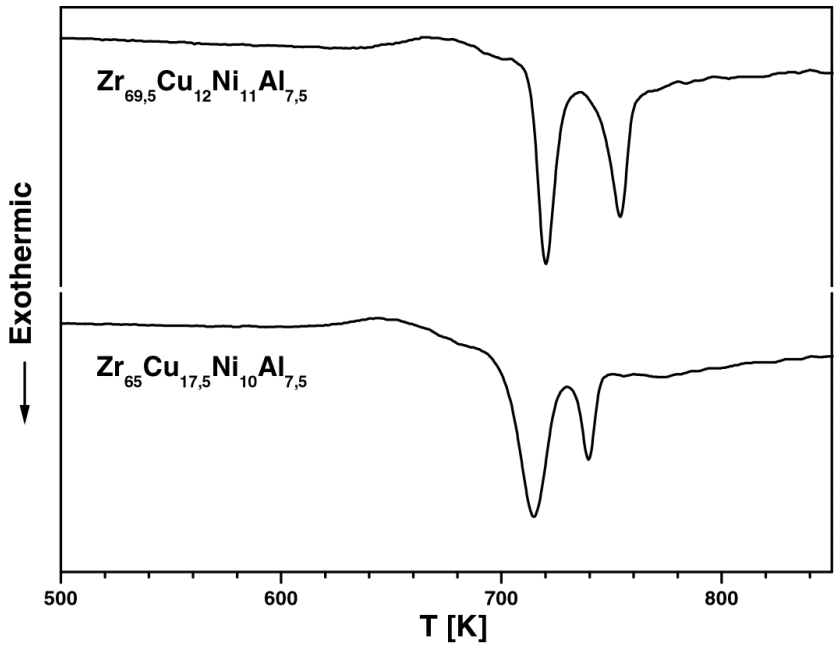

Figure 3.5: *DSC thermograms for two different Zr-Cu-Ni-Al alloys; heating rate 20 K/min.*

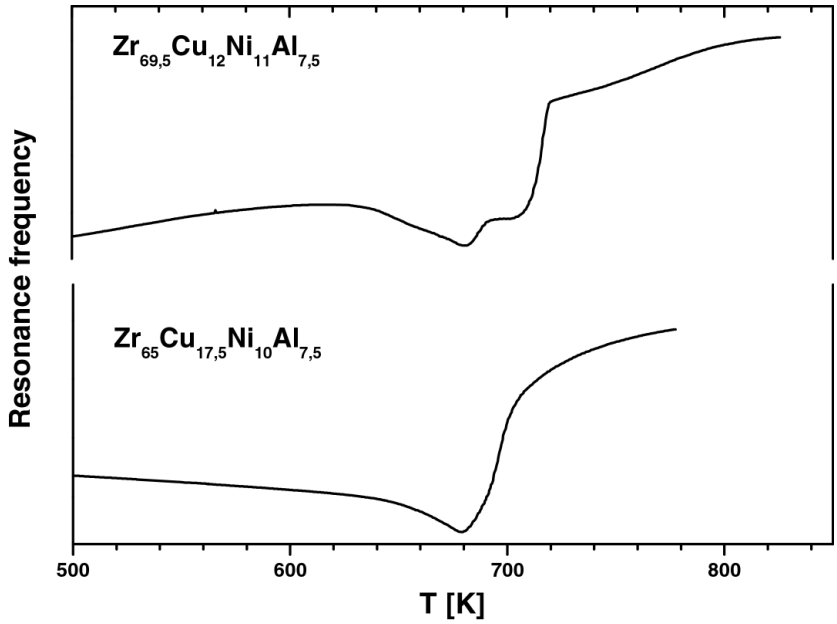

Figure 3.6: *Resonance frequency changes upon annealing for vibrating reeds of two different Zr-Cu-Ni-Al alloys; heating rate 2 K/min.*

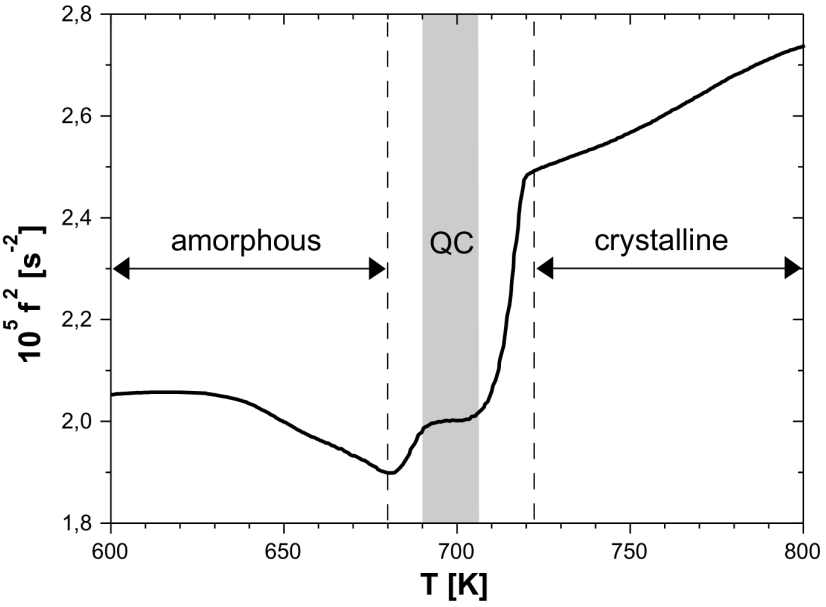

Figure 3.7: *Relation between resonance frequency and phases for the* $Zr_{69,5}Cu_{12}Ni_{11}Al_{7,5}$ *alloy; heating rate 2 K/min.*

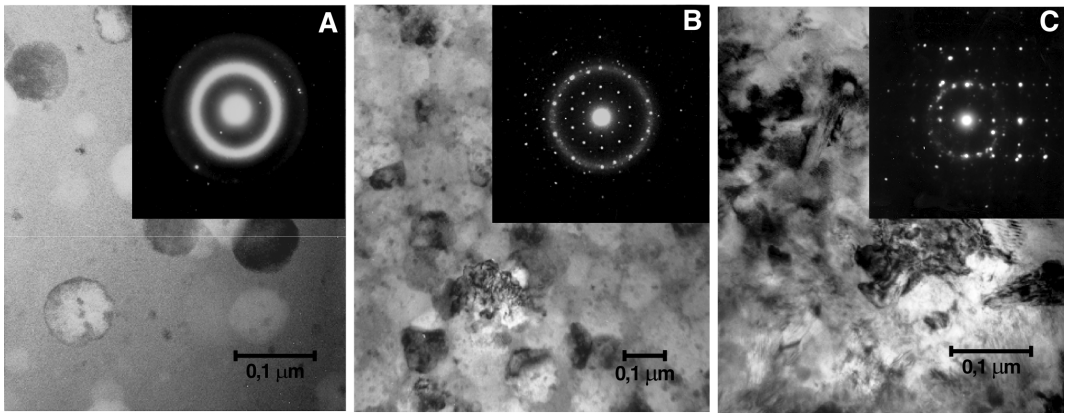

Figure 3.8: *Bright field TEM images and respective diffraction patterns for three* $Zr_{69,5}Cu_{12}Ni_{11}Al_{7,5}$ *samples annealed with 2 K/min up to 673 K (A), 700 K (B) and 720 K (C).*

[13]. In fact it has been demonstrated that even a low oxygen amount of 0,8 at.% promotes the nucleation of an icosahedral phase before other crystalline structures become energetically favored [41]. This in turn changes the behavior of the material so that in the DSC curves two exothermic reactions appear instead of only one. A comparison with the curves of Fig. (3.6) reveals that, at least qualitatively, a correspondence can be made between the increase of resonance frequency in the temperature range 680-720 K and the exothermic peaks of the DSC measurements. Since the separation of the DSC peaks for the Zr-richer alloy is bigger than the same quantity for the Zr-poorer material, the devitrification sequence manifests itself as well definite step-like increase of frequency in the first case and in a smoother variation in the second case. The temperature shift of the main transformation events is due to the heating rate of 2 K/min, which is much lower than the one used in the calorimetry experiments.

Considering now in some more detail the $Zr_{69,5}Cu_{12}Ni_{11}Al_{7,5}$ alloy, we have taken several samples and annealed them to different final temperatures in the vibrating reed device; successively a qualitative analysis in a Philips CM12 transmission electron microscope operating at 120 kV was made. The conclusions we reached are summarized in Figs. (3.7) and (3.8), where a clear picture of the relationship between resonance frequency changes and phase transformations of the material appears. A heat treatment until about 640 K does not change the structure of the glassy matrix, whereas a further annealing promotes the nucleation and growth of the quasicrystals as is shown in Fig. (3.8 A). Going on until approximately 700 K, the specimen becomes mainly quasicrystalline, as is proven for example by the characteristic diffraction pattern of a 5-fold symmetry axis in Fig. (3.8 B). Further annealing transforms finally the alloy into its crystalline state (Fig. (3.8 C)).

As far as the Zr-Ti-Cu-Ni-Be glasses are concerned, the comparison between DSC and vibrating reed measurements is shown in Figs. (3.9) and (3.10): the V1 alloy is characterized by a complex devitrification sequence, involving an intermediate decomposition stage which is reflected in the first exothermic peak of the thermogram or in the first rapid frequency increase at about 670 K. The main peak of the DSC plot for the V1 represents the primary crystallization which corresponds to the second frequency step at 700 K of Fig. (3.10). The further ongoing of the frequency curve reflects the following transformations of the alloy upon annealing. Quite different is the behavior of the V4 glass, for which a single crystallization peak, as well as a single frequency step, appears.

Having established the relationship between the resonance frequency and the phase transformations of our Zr-based alloys, it was comparatively easy to prepare the specimen in the phase of interest by monitoring the behavior of the frequency curve upon annealing and by letting the material rapidly cool

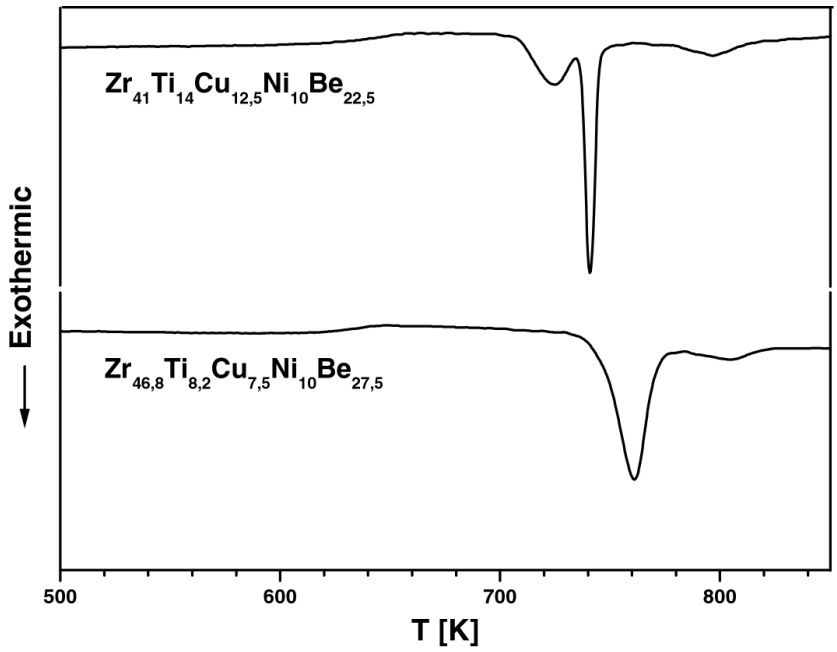

Figure 3.9: *DSC thermograms for the V1 and V4 alloys; heating rate 20 K/min.*

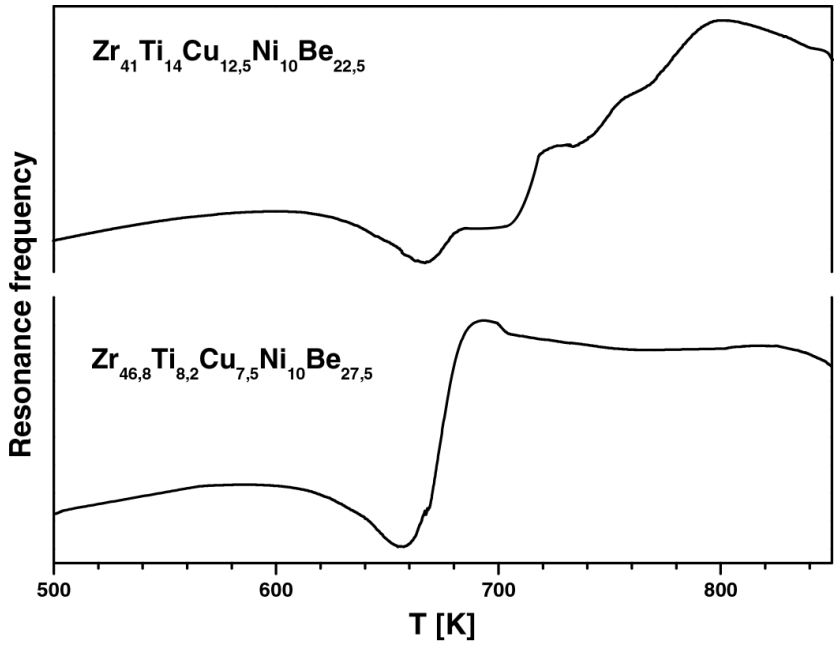

Figure 3.10: *Resonance frequency changes upon annealing for vibrating reeds of the V1 and V4 alloys; heating rate 2 K/min.*

down once the wanted state was reached. The second part of our experiment consisted then in the hydrogen charging of the samples from the gas phase, which we are going to describe in the next section.

3.3 Hydrogenation of the samples

The hydrogenation of a material depends on several factors among which are the modality of the charging (electrochemical or from the gas phase), the affinity of the metal or alloy to hydrogen and the conditions of the sample surface, only to cite a few. In our case hydrogen was introduced into the specimens from the gas phase with different temperatures and pressures. A good balance of such parameters was necessary in order to guarantee an acceptable absorption rate while leaving the structure of the material unaltered. This last aspect was particularly important when the H charging involved metastable states originating from our Zr-based glasses, like the icosahedral $Zr_{69,5}Cu_{12}Ni_{11}Al_{7,5}$ or the decomposed $Zr_{41}Ti_{14}Cu_{12,5}Ni_{10}Be_{22,5}$, for which an excessive temperature or charging time could modify the state of the system. At the end we chose either a temperature of 180 °C at 1 bar pressure, which was ideal for the hydrogenation process taking place in situ in the vibrating reed device, or a temperature of 100 °C at about 350 bar for which a special high pressure vessel was used.

The measurement of the hydrogen concentration could be done only in a destructive manner with a heat extraction method. This technique is characterized by a high sensitivity to the presence of hydrogen, but on the other side it requires specimens with a certain weight, in order to minimize the effects of impurities at the surface of the material. For us this was a problem, since our samples only weighed few milligrams and a careful cleaning of the surface was necessary. In particular, before every concentration measurement, the materials were rinsed in an ultrasonic bath with trichloroethylene and with CCl_4, and successively stored in previously carefully cleaned glass containers.

The second problem was that for several different reasons (like shortage of material, limited availability of operating time of the heat extraction apparatus), such H concentration measurements were only possible on a small number of samples. Our aim was therefore to establish a correlation between the height Q_P^{-1} of the H-induced damping peaks and the concentration c_H of hydrogen; in this way it was possible at least to make a reasonable guess on the order of magnitude of c_H only by the observation of the damping spectra. The conclusions we reached are contained in Fig. (3.11) where the experimental points represent self made measurements on two different Zr-based bulk glasses and the dashed line is a fit of the data. Such a fit of course makes sense only in the range of a monotonic increase of Q_P^{-1} with c_H, i.e. below the concentration

limit $c_H \leq 0{,}6$ H/M mentioned above in section 2.6.

Some comments are at this point necessary: first of all we have noticed that the correlation between charging time and c_H was not as reliable as the one shown in Fig. (3.11). In fact sometimes even if the hydrogenation conditions (temperature, pressure, time) were identical, very different values for the hydrogen concentration were found for different specimens. As already pointed out before, one of the reasons could be the presence of impurities at the sample surface which give a measurable contribution to the overall c_H. Another problem consists in the presence of a thin oxide layer on every reed of material, which significantly hinders the absorption of hydrogen. Since the alloys were not stored in the same conditions and came from different production sets, it cannot be said how thick this oxide layer is and how it influenced the penetration of H inside the specimens. The presence of such barrier is probably the reason why we could not reach the high c_H values of about 1,9 H/M reported in the literature for some Zr-based alloys [42], even extending the H charging to several days and in the high pressure vessel. In order to facilitate the absorption of hydrogen we tried to "activate" the materials surface in several ways. In particular we used thin emery paper for the Zr-Cu-Al(-Ni) alloys, but we could not do the same with the V1 and V4 materials due to the presence of Be, which is toxic. The results of this kind of surface treatment has given anyway only marginal improvements. Much more effective has been the sputtering of a thin layer (approximately 20-30 nm) of Pd; this technique has only been used in the last part of our investigations and on the V1 alloy. The effect on the hydrogen absorption was dramatic, with a reduction of the charging parameters from days to minutes and at room temperature and ambient pressure. Unfortunately a severe hydrogen embrittlement problem appeared, which limited our investigations to the concentration range of Fig. (3.11) and not above.

The problem of embrittlement poses the question of what is the limit above which the presence of hydrogen modifies the initial structure of the host material. Here we want to distinguish between the $Zr_{69,5}Cu_{12}Ni_{11}Al_{7,5}$ alloy, for which information on the effect of H charging can be found in the literature, and the $Zr_{41}Ti_{14}Cu_{12,5}Ni_{10}Be_{22,5}$ system for which, on the other side, interesting data on this problematic are not at hand. We limit our consideration on these two alloys, because they are the ones which were mostly investigated with respect to the H-induced internal friction. For the Zr richer material it is known that an amount of hydrogen of the order of 1,9 H/M has the effect of increasing the quasilattice constant (nearest neighbor distance) of the quasicrystalline (amorphous) phase of approximately 10% (7%) [42]. In the TEM measurements which we made after hydrogenation of the samples in their icosahedral or amorphous states, we could not confirm such observations, which is

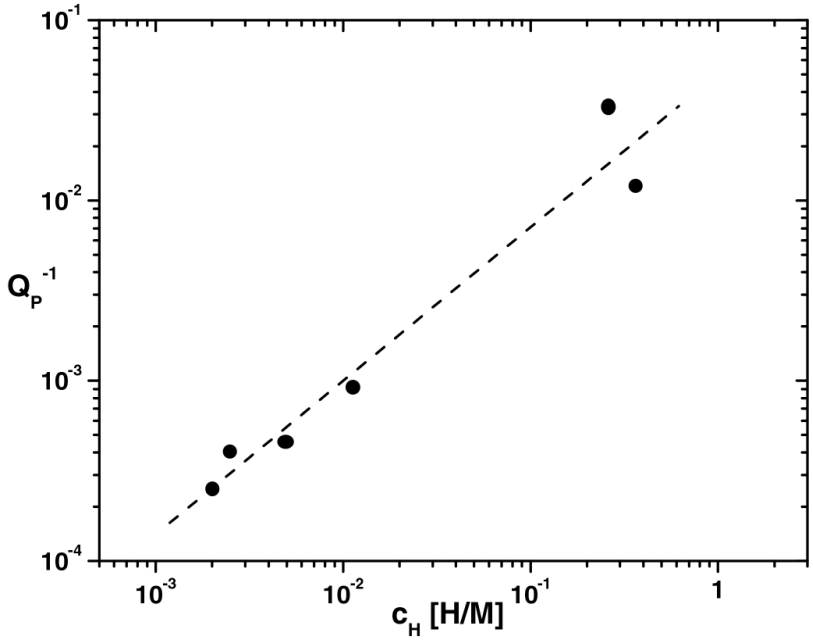

Figure 3.11: *Tentative correlation between the height of the H-induced damping peaks and the concentration of hydrogen in Zr-based bulk metallic glasses.*

an indication of the relatively low c_H reached in our experimental conditions. We think that a similar situation is also true for the V1 alloy; in fact our TEM observation before and after hydrogenation did not show remarkable structural changes. Moreover in this case too the concentration of the dissolved hydrogen remained comparatively low ($\leq$ 0,5 H/M).

3.4 Mechanical Hydrogen Spectroscopy (MHS)

We have seen in section 2.6 how the presence of dissolved hydrogen has an influence, in some cases, on the anelastic relaxation behavior of a material. Generally speaking the way in which the hydrogen atoms influence the internal friction of a system depends on their interaction, at a microscopic level, with the surrounding host matrix. In this sense hydrogen *probes* the local structure of a material in a similar way as other atomic or nuclear probes (NMR, positrons, muons etc.) do. As a consequence materials with different microscopic structures can be characterized by different shapes of the H-induced damping spectra, making therefore possible to define the analysis of such curves as "Mechanical Hydrogen Spectroscopy". This methodology can be used on a purely phenomenological or on a specifically microscopic level: in the first case information can be gathered for example on complex phase

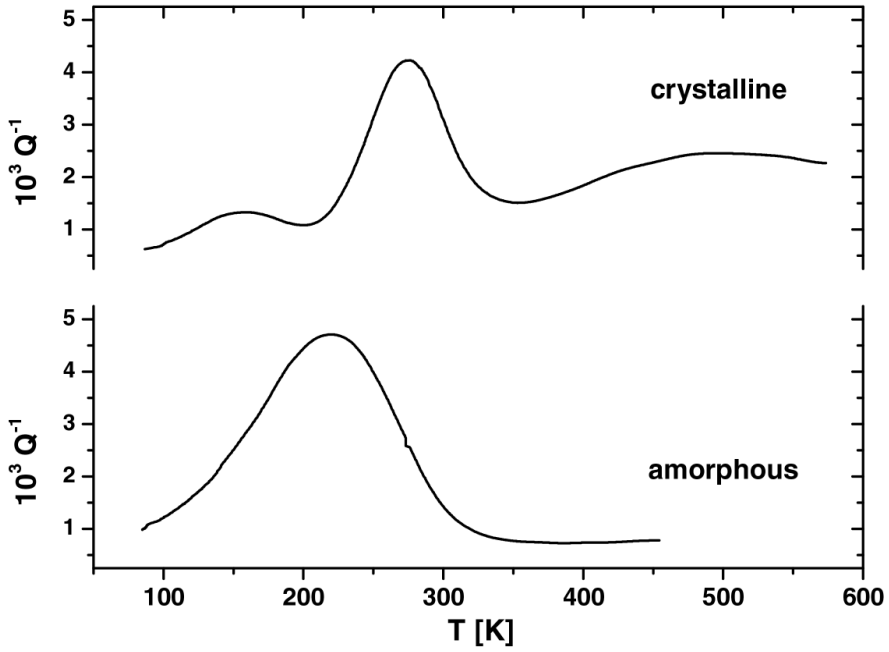

Figure 3.12: *H-induced damping spectra for two different phases of the* $Zr_{69,5}Cu_{12}Ni_{11}Al_{7,5}$ *alloy; heating rate 2 K/min;* $c_H \simeq 0{,}05$ *H/M;* $f_r \simeq 1$ *kHz.*

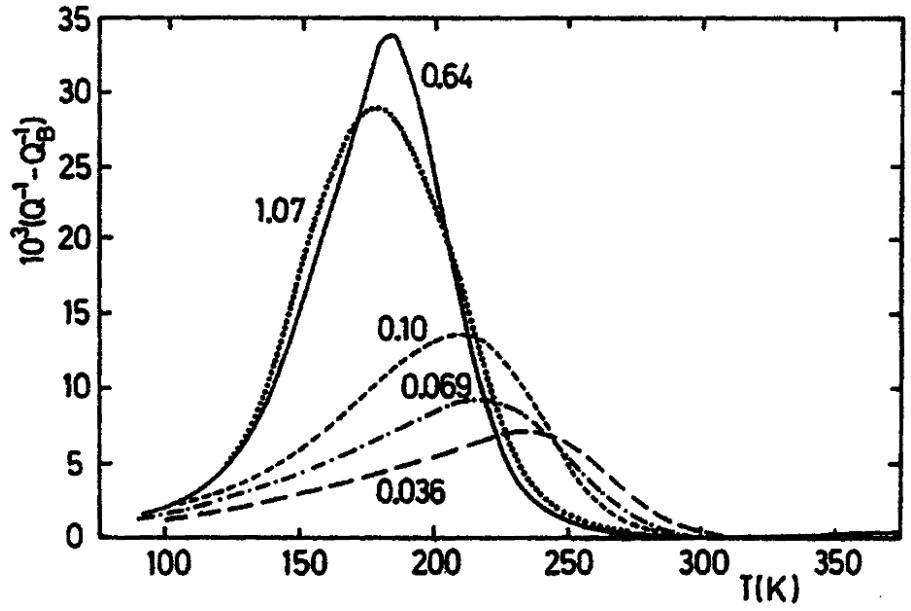

Figure 3.13: *Internal friction spectra, after subtraction of a linear background* Q_B^{-1}*, for glassy* $CoZr_2$ *in a frequency range around 300 Hz; the hydrogen concentration is indicated in H/M* [30].

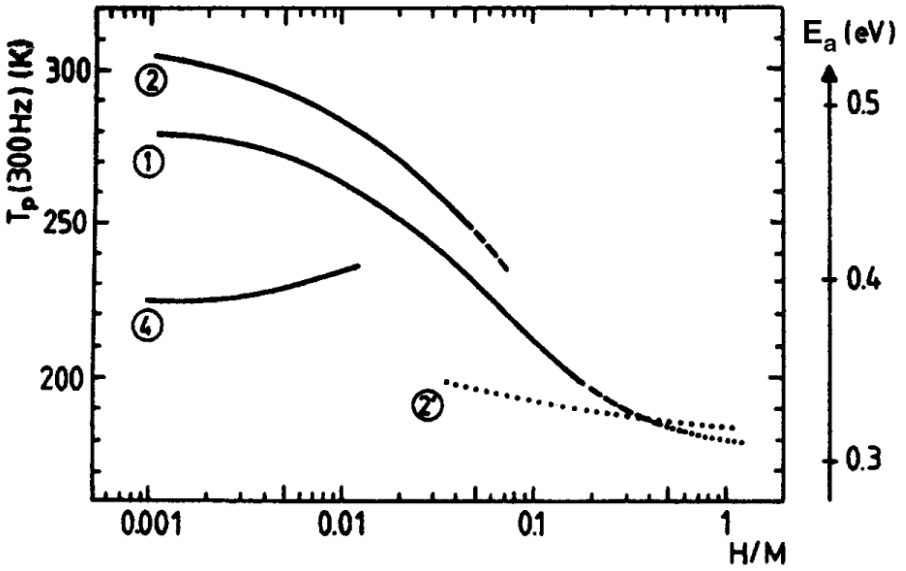

Figure 3.14: *Peak temperatures against H concentration for the internal friction spectra of* $CoZr_2$*: (1), amorphous state; (2-2'), nanocrystalline state; (4), C16 equilibrium phase; energy scale calculated for* $\tau_0 = 10^{-12}s$ [30].

transformation sequences like the ones taking place in metallic glasses. An illustration of this kind of analysis can be seen in Fig. (3.12) where the distinct shape of the spectra is to ascribe to the different anelastic relaxation behavior of hydrogen in going from the amorphous to the crystalline phase of the selected alloy.

Extending the damping measurements to a wide range of hydrogen concentrations, it is possible to draw a series of spectra which are characteristic of the material. An example of such kind of investigations is given in Fig. (3.13) for a set of amorphous $CoZr_2$ samples containing different amounts of hydrogen [30]. The shift to lower temperatures as well as the dependence on c_H of the peak maxima reflects the typical H-induced anelastic relaxation behavior of metallic glasses, as already explained in section 2.6.

When examining alloys characterized by different compositions and/or different (meta)stable phases, it is often desirable to have in a single diagram an overview on the internal friction behavior of several samples. This can be achieved by plotting the peak temperatures T_P of a series of spectra taken at different c_H against the hydrogen concentration itself.* A typical example is shown in Fig. (3.14), once again for the $CoZr_2$ alloy which has proven to

*A common practice is to plot T_P against the height Q_P^{-1} of the peaks, which is more readily at hand; this quantity can successively be correlated to c_H as in the example of Fig. (3.11).

be an excellent case study for MHS investigations [16]. The curves represent measurement made in different states of the material, which means that the method is sensitive to the structural changes of the host matrix. The temperature of the peaks has been "normalized" for a frequency of 300 Hz; this is necessary because for thermally activated processes, like the stress induced jumps of hydrogen between neighboring sites, the relation between frequency and T_P is contained in Eq. (2.28), from which it appears that the position of T_P depends on the eigenfrequency of the sample. By writing Eq. (2.28) for two different frequencies $\omega_{1,2}$ and peak temperatures $T_{P1,P2}$ and by subtracting the two expressions, after rearrangement we obtain

$$T_{P2}^{-1} = T_{P1}^{-1} + \frac{k}{E_a} \ln\left(\frac{\omega_1}{\omega_2}\right); \tag{3.6}$$

using Eq. (3.6) the shift of T_P due to the change of resonance frequency among different samples can be corrected. Always referring to Fig. (3.14), the average activation energy scale has been calculated following an Arrhenius relation for the hydrogen reorientation jumps: according to this scheme, the peak temperatures of the damping spectra and the average activation energy are linearly correlated through the equation

$$E_a = -kT_P \ln \omega\tau_0. \tag{3.7}$$

If an estimate of τ_0 is possible, then an appropriate energy scale can be constructed.

The other interesting and more challenging application of MHS involves the microscopic domain: the aim in this case is to extract some information concerning the local atomic structure of the host material from the H-induced anelastic relaxation parameters. This process requires a detailed knowledge of the relaxation mechanism from which a correlation between experimentally accessible quantities, like the activation energy for the hydrogen jumps between interstitial sites, and some function of the nearest neighbor atomic distances can be made. Moreover an hypothesis is necessary on what kind of sites are probed by the hydrogen atoms at all concentrations. For example in binary amorphous alloys of the type A_xB_{1-x} made by an early (A) and a late (B) transition metal, it has been demonstrated with the aid of electrochemical measurements that H is stored sequentially, with increasing c_H, in $A_4, A_3B_1, A_2B_2, ...$ tetrahedral sites [5]. In multicomponent glasses a similar argument can be used, provided that at least one element of the alloy has a much higher affinity for hydrogen than the others. On the other side, for crystalline structures, where the unit cell is known, it is somewhat easier to formulate hypothesis on the location of H by keeping into account both the

chemical affinity as well as the volume of the interstitial sites, which must be sufficiently large in order to accommodate a H atom.

As yet one of the best examples concerning the application of MHS in the microscopic domain can be found for the $CoZr_2$ alloy, which has been investigated in its several (meta)stable phases (a more extensive overview is contained in [16]). The main results involve firstly the discovery of a structural difference between the glassy state and the grain boundaries of nanocrystalline $CoZr_2$: the main experimental evidence for such conclusions comes from a plot of T_P against a volume related peak height Q_P^{-1}/α (α = volume fraction of grain boundaries [43]), which qualitatively reflects the average activation energy for the H reorientation relaxation as a function of the local hydrogen concentration. Here the nanocrystalline state showed a stronger T_P shift for increasing c_H, indicating a broader distribution of Zr-Zr distances in the grain boundaries than in the precursor glassy phase [15, 17].

A second remarkable result concerns the short range order of amorphous $CoZr_2$: one question was to what extent some elements of local order of the different metastable or stable crystalline phases were already present also in its precursor glassy state. In the C16 phase a hydrogen reorientation relaxation model was proposed and one of its conclusions, valid for dilute H concentrations, was the correlation of the activation energy of the internal friction spectra with a Zr-Zr distance of 3,27 Å [15, 19], which is a characteristic length from a combination of nearest-neighbor distances within a specific relaxation model for this structure. For the amorphous phase it was then possible to conclude that there must be some intermediate H concentration value for which such characteristic Zr-Zr distance related to the average activation energy for H reorientation just coincides with the average Zr-Zr distance in the glassy state.

This use of the MHS method will be the basis for our investigations on the Zr bulk glasses and their derived metastable states. From the phenomenological point of view, an analysis will be made on the similarities or differences which appear among different states of the material under investigation (or among different alloys in the same state), like for example between amorphous and quasicrystalline $Zr_{69,5}Cu_{12}Ni_{11}Al_{7,5}$. In particular we will compare the shape of the damping spectra, similarly to what shown in Fig. (3.12), or of the distribution of activation energies calculated through Eq. (2.33). The evaluation of the relaxation parameters like T_P and Q_P^{-1} will also be used, similarly to what has been done in the example of Fig. (3.14). On the other side the application of MHS on a microscopic level will involve a generalization of the results on $CoZr_2$ previously mentioned, where the microscopic model considered only a single interstitial site (tetrahedron), to the overall amorphous structure of the Zr-based bulk glasses, by comparing the ongoing of the activation energies as

function of the hydrogen concentration (derived from T_P and Q_P^{-1}) with the theoretical model of Richards [1].

Chapter 4

Results and discussion

This chapter is devoted to the description of the experimental results and their interpretation. From the previous discussion it is clear that the vibrating reed technique gives at the same time the resonance frequency f_r of a specimen and the damping Q^{-1} of its free oscillations as a function of temperature; it has already been mentioned how the changes of f_r can be used to monitor the phase transformations of a material upon annealing and the first part of this chapter will be used to give a deeper insight on this subject. In the second part we will concentrate on the hydrogen induced internal friction making a distinction between results concerning different Zr-based bulk glasses in the same state (amorphous or crystalline) and results on the same material prepared in its different (meta)stable phases.

4.1 Young's modulus changes upon heating

In section 3.2.2 it has already been shown how the behavior of $f_r(T)$ can be associated with the devitrification sequence of our Zr-based bulk glasses. This is a direct consequence of the dependence of the elastic properties of a material on its atomic structure: when the latter is modified through appropriate treatments, quantities like the Young's modulus of the specimen can be affected. The connection between resonance frequency f_r and Young's modulus E for a bar of rectangular cross section is contained in the following equation

$$f_r = \frac{\alpha^2 d}{\sqrt{3}\pi l^2}\sqrt{\frac{E}{\rho}}\,, \tag{4.1}$$

where l and d are, respectively, the length and the thickness of the bar, ρ is its density and α is a numerical factor whose value depends on the vibration mode of the sample. If the geometry of the specimen is known with accuracy, then the vibrating reed technique allows a quantitative measurement of the

Young's modulus by making use of Eq. (4.1). In our specific case (clamped bars) it was impossible to perform a precise computation of E because of the uncertainty in the linear dimensions, as well as the density, of our ribbons. Since in particular l and d appear to the 4th and the 2nd power, respectively, when computing the value of E, it is clear how a small error on the values of the length and thickness is reflected in a larger uncertainty in the Young's modulus (approximately $\pm 25\%$ of the average value in our case). Anyway this was not a limitation for the kind of analysis we wanted to perform for which a *relative* change of properties between different states of the material is involved. Additionally we assumed that the geometry of the specimens did not change significantly in the course of our experiments, meaning that relative changes of $f_r^2(T)$ could be taken directly as the modifications of $E(T)$.

The transformation kinetic of our Zr-based bulk glasses could be monitored following a "step by step" anisothermal procedure: the samples were firstly annealed to a temperature T_1 with a heating rate of 2 K/min and let rapidly cool down. Successively a second run was performed to $T_2 > T_1$ again followed by fast cooling. The procedure was repeated several times for increasing final temperatures so the irreversible and reversible part of the transformations could be distinguished. Some examples of such measurements are shown in Fig. (4.1) for two Zr-Ti-Cu-Ni-Be alloys and in Fig. (4.2) for two Zr-Cu-Al(-Ni) glasses. In each plot the roman numbers shown for $T \geq 400$ K denote the ranges where the main transformations of the material occur. These numbers are repeated in proximity of the arrows at $T = 300$ K, which indicate the relative changes of Young's modulus, measured at room temperature, following the respective structural modifications of the alloy upon annealing. The ranges denoted with I, which span approximately from 400 to 620 K, refer to the structural relaxation of the amorphous alloys; from 620 to about 700 K we find the undercooled melt stage (marked with II), from which some materials undergo irreversible structural modifications before crystallization, like the formation of quasicrystals in $Zr_{69,5}Cu_{12}Ni_{11}Al_{7,5}$ [12] or the decomposition into two amorphous phases followed by the formation of nanocrystals in $Zr_{41,2}Ti_{13,8}Cu_{12,5}Ni_{10}Be_{22,5}$ [40]; in range III the main crystallization of all materials takes place and range IV is characterized by further transformations in the crystalline state. A common feature of all the plots is the increase of f_r^2 in range I which is a consequence of the irreversible structural relaxation of the glasses. The only variable thing is the magnitude of the effect among different samples which can be explained by the following considerations: firstly, the irreversible structural relaxation is directly connected with the change of available free volume which is quenched in the glasses during their production. Such observation has been demonstrated for example by positron annihilation studies on $Zr_{65}Cu_{17,5}Ni_{10}Al_{7,5}$ [44] and $Zr_{46,7}Ti_{8,3}Cu_{7,5}Ni_{10}Be_{27,5}$ [45] bulk

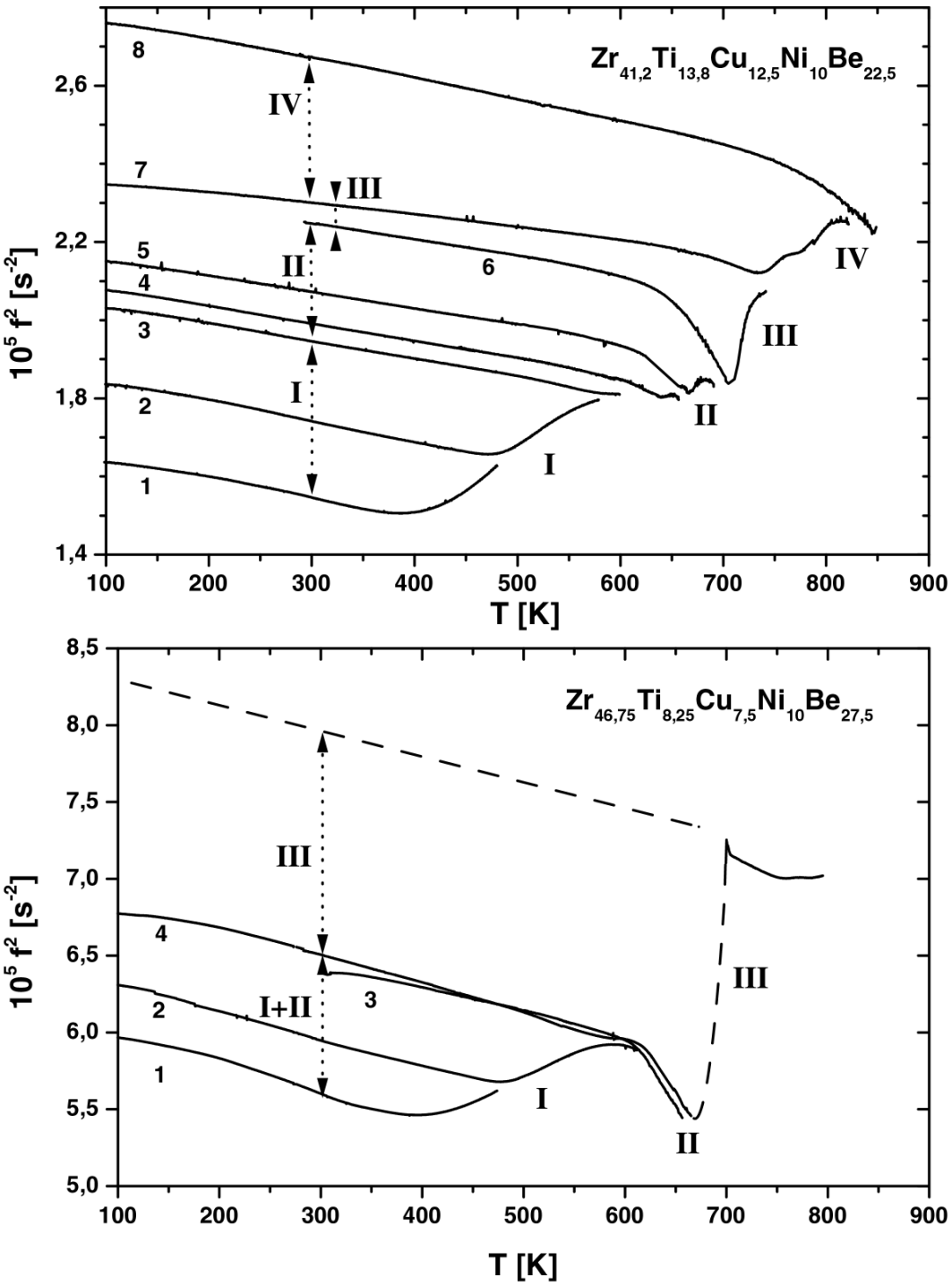

Figure 4.1: $f_r^2(T)$ *plot for two "Johnson" type glasses. Heating rate 2 K/min; integer numbers denote different measurements while roman numbers refer to the phase transformations upon annealing and their relation with the changes of Young's modulus measured at 300 K.*

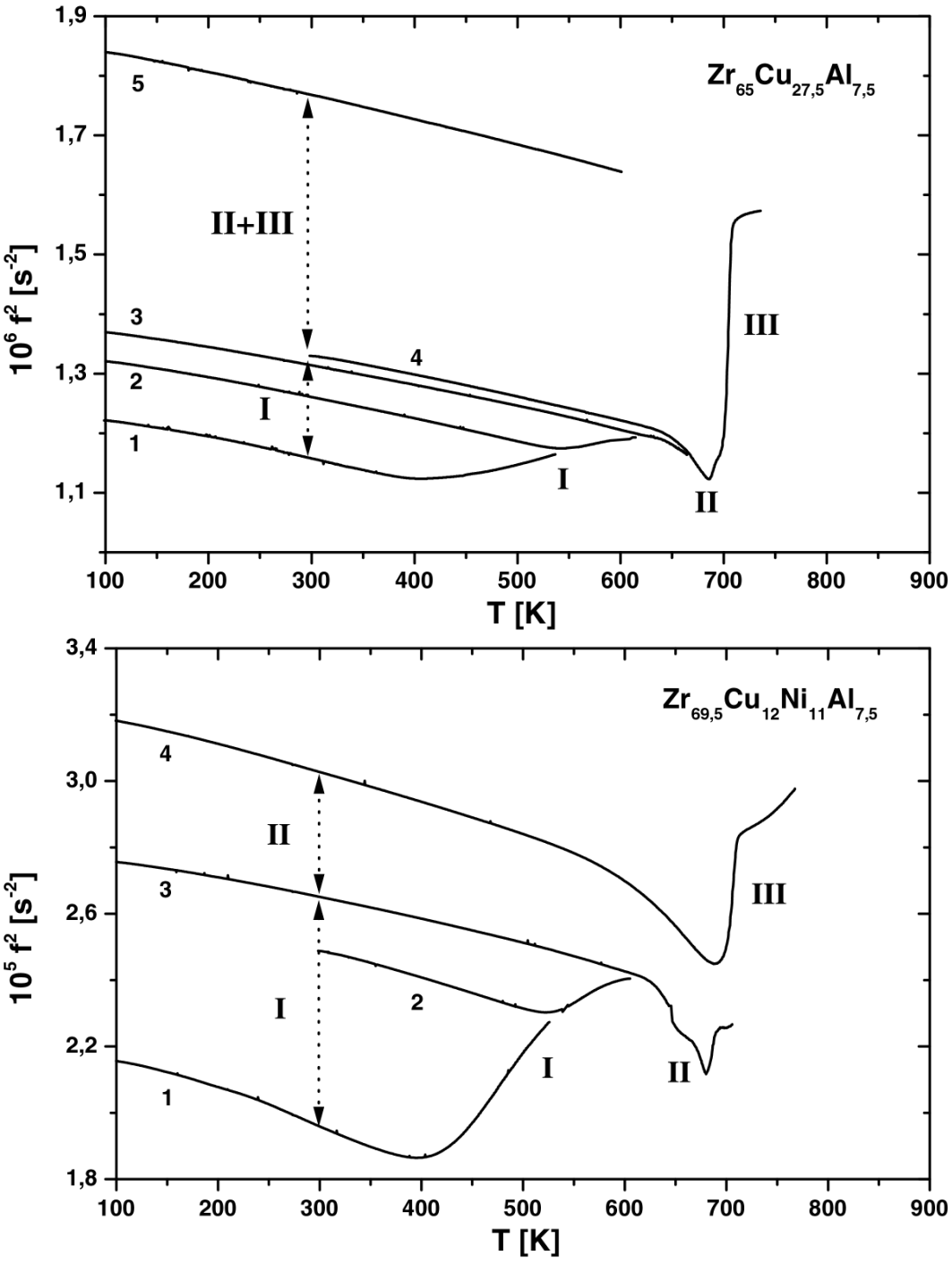

Figure 4.2: $f_r^2(T)$ *plot for two "Inoue" type glasses. Heating rate 2 K/min; integer numbers denote different measurements while roman numbers refer to the phase transformations upon annealing and their relation with the changes of Young's modulus measured at 300 K.*

glasses, in which the authors related the lowering of the average positron lifetime in the materials, after heat treatment, to the annealing of free volume. This result was corroborated by measurements of the density change of the alloys, which showed an increase of 0,1% after structural relaxation. Secondly, considering that our samples have been produced with different techniques (splat quenching or melt spinning) and in different places, it would not be surprising if the amount of quenched in free volume would show remarkable deviations among several specimens, influencing in turn the magnitude of the effects due to structural relaxation. A change of Young's modulus in going from the "as prepared" state to the structural relaxed one has already been observed in a bulk glass with composition $Zr_{57}Cu_{20}Al_{10}Ni_8Ti_5$ [46], which was also interpreted as an effect due to the change of density following the lowering of available free volume after structural relaxation.

In the temperature range denoted with II, which refers to the undercooled melt of our Zr-based bulk glass forming alloys, some materials undergo further irreversible modifications before they crystallize, while others don't. As regards the "Johnson" glasses of Fig. (4.1), the behavior of E for $Zr_{46,7}Ti_{8,3}Cu_{7,5}Ni_{10}Be_{27,5}$ is nearly completely reversible between the end of the irreversible structural relaxation and the beginning of crystallization, so that the glass transition effect as well as the strong temperature dependence of the Young's modulus in the undercooled melt state can clearly be noticed. The situation is different for $Zr_{41,2}Ti_{12,8}Cu_{12,5}Ni_{10}Be_{22,5}$: as already mentioned, in range II such alloy undergoes a decomposition into two amorphous phases immediately followed by the formation of nanocrystals. Here we want to emphasize the effect that this transformation has on the Young's modulus. In particular, we observe a pronounced increase of E at 300 K (arrow between curves 3 and 6) due to the decomposition; the following crystallization step marked with number III at about 720 K, does not produce a similar increase in Young's modulus if measured at room temperature (arrow between curves 6 and 7). A clear interpretation of these measurements is not yet at hand and such effect has not been reported in the literature so far. Experimental evidence nevertheless exists as regards the behavior of the viscosity before and after decomposition of the $Zr_{41,2}Ti_{12,8}Cu_{12,5}Ni_{10}Be_{22,5}$ alloy [47]: here the authors measured an increase of the viscosity of about three orders of magnitude after the phase separation of the alloy and explained the effect by postulating that the amorphous matrix which remains after the formation of nanocrystals has a slightly different chemical composition from the nominal one; the new matrix is a glass which is kinetically "stronger" than the starting alloy. Even though such results cannot directly be applied to our findings, it is tempting to assume that some chemical short range order (CSRO) is formed in the decomposed amorphous matrix and that this influences the elastic properties of the

$\Delta E/E$ *vs. devitrification stages*				
	I	II	III	IV
$Zr_{41,2}Ti_{13,8}Cu_{12,5}Ni_{10}Be_{22,5}$	26	15	3	16
$Zr_{46,75}Ti_{8,25}Cu_{7,5}Ni_{10}Be_{27,5}$	16		22	
$Zr_{69,5}Cu_{12}Ni_{11}Al_{7,5}$	35	14		
$Zr_{65}Cu_{27,5}Al_{7,5}$	15	33		

Table 4.1: *Relative Young's modulus changes (expressed in %) measured at room temperature after successive annealing treatments (heating rate 2 K/min). The values are referred to Figs. (4.1) and (4.2).*

sample. If such CSRO would resemble the structure of the crystallized specimen, then the small difference of Young's modulus between the decomposed amorphous material and its crystallized phase should not be surprising.

Referring now to Fig. (4.2), the ternary "Inoue" alloy shows a behavior similar to the Zr richer "Johnson" glass and, therefore, will not be discussed further. On the other side in the $Zr_{69,5}Cu_{12}Ni_{11}Al_{7,5}$ glass we observed a reversible behavior of E in range II until the onset of the quasicrystals formation at about 690 K. After such phase transformation the material becomes very brittle and its Young's modulus increases (difference between curves 3 and 4 in the respective plot).

The results concerning the change of E due to the devitrification of our Zr-based bulk glasses are summarized in Table (4.1): the values referring to range I (or to range I + II if the material shows a reversible behavior in the undercooled melt stage) have to be taken with caution, because of the remarkable deviations observed among different samples of the same material, which is probably due to inhomogeneities of the "as received" splats and ribbons. On the other side the E variations deriving from the transformations happening in the other ranges are less sensitive to such inhomogeneities, which seem therefore easily removable by an annealing treatment which brings the glasses to the end of the irreversible structural relaxation.

4.2 Damping in Zr-based bulk glass forming alloys: general remarks

As already mentioned in section 2.5, one of the problems which arise when studying the anelastic relaxation behavior of a material is to distinguish among the different physical mechanisms at the origin of a particular damping spec-

trum. In the following we will make some considerations firstly on the influence of the atomic rearrangements due to annealing of an as quenched sample and of the phase transitions of our alloys on the internal friction behavior of the specimens, secondly on the systematic presence of a linear damping background whose origin is to be found in the thermoelastic effect.

4.2.1 Non hydrogen induced damping effects

For the investigation of the hydrogen induced anelastic relaxation it is favorable to assume that the H reorientation jumps take place in an immobile host matrix, meaning that in the respective ranges the damping effects due to movements of the atomic constituents of the host material don't overlap with the ones deriving from the presence of hydrogen. In a metallic glass this is generally not true for an "as quenched" sample: the presence of excess free volume as well as inhomogeneities or plastic deformation [18] have an influence on the damping in the same temperature range where the hydrogen effects are normally visible. Such observation is confirmed for example in the plot of Fig. (4.3), where the resonance frequency and the damping of a $Zr_{69,5}Cu_{12}Ni_{11}Al_{7,5}$ bulk glass specimen are shown for two successive measurements: in the first run we notice a peak just below room temperature whose magnitude is considerably reduced after the annealing treatment (2nd run). This indicates a superposition of the hydrogen internal friction with some other effects due to movements of the atoms composing the host matrix. This is the reason why all our measurements on amorphous samples have been performed after a previous annealing treatment which let the material reach the end of the irreversible structural relaxation. After such procedure we experienced no further anomalous damping effect in the successive measurements.

In conclusion we can say that care must be taken when analyzing the hydrogen induced internal friction spectra in metallic glasses, because of the possible overlapping of effects due to the presence of plastic deformation, inhomogeneities or excess free volume. Only after a proper annealing treatment such side effects can be eliminated.

4.2.2 The linear background

The internal friction of our bulk metallic glasses consists of thermally activated as well as thermoelastic contributions, which reflect atomic and thermal transport processes respectively. The thermoelastic effect has been already described theoretically in section 2.5 and for convenience we write again the equation relating the damping component due to transverse thermal currents

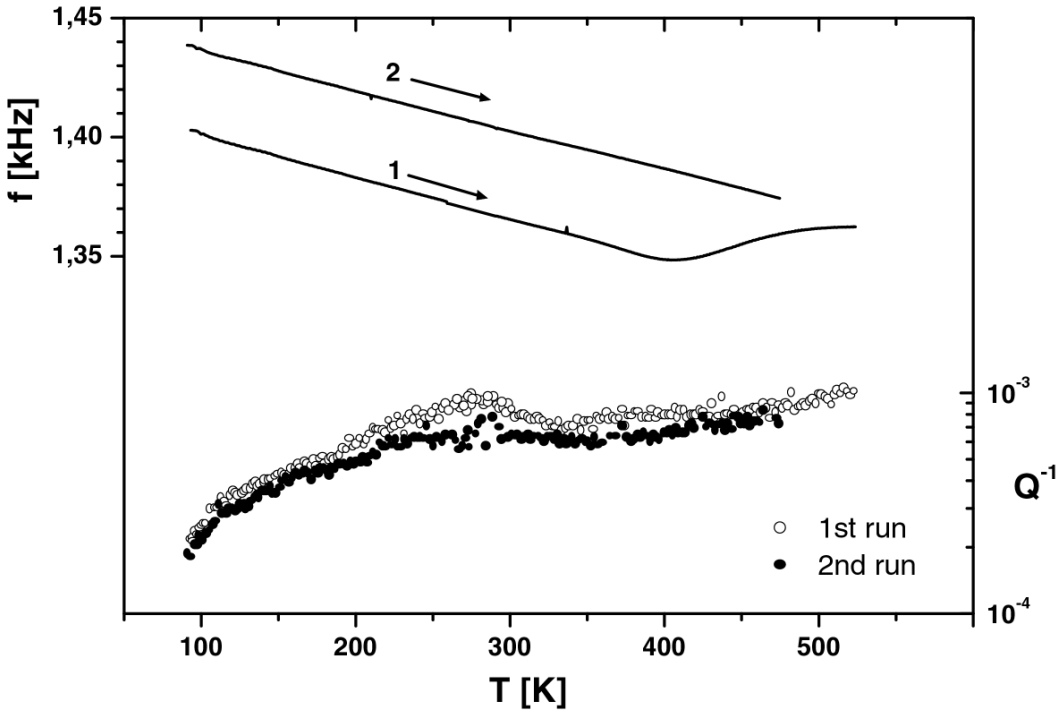

Figure 4.3: *Resonance frequency and damping for a* $Zr_{69,5}Cu_{12}Ni_{11}Al_{7,5}$ *specimen in the "as received" state (1st run) and after structural relaxation (2nd run); heating rate 2 K/min.*

to the frequency and temperature:

$$Q_T^{-1}(T,f) = \frac{\alpha^2 E_U T}{C_\sigma} \cdot \frac{f\, f_0}{f^2 + f_0^2}\,; \tag{4.2}$$

this is nothing else than the combination of Eqs. (2.35) and (2.36) where the first term on the right hand side of the equation represents the relaxation strength Δ_T. In the following we want to justify, through some experimental observations, the assumption that in the damping measurements of Zr-based bulk glass forming alloys there exists a component due to the thermoelastic effect, which manifests itself as a linear background going through the origin of the $Q^{-1}(T)$ plot.

We have measured the internal friction as function of temperature of a $Zr_{41,2}Ti_{13,8}Cu_{12,5}Ni_{10}Be_{22,5}$ specimen; in order to scan a frequency range as large as possible, we have carefully cut, after each measurement, the clamped ribbon, which resulted in a gradual increase of its ground frequency. Moreover we used in some cases the first overtone. Fig. (4.4) represents a series of such internal friction measurements, performed at different frequencies; the straight lines are our estimate of the linear background, from which the thermoelastic

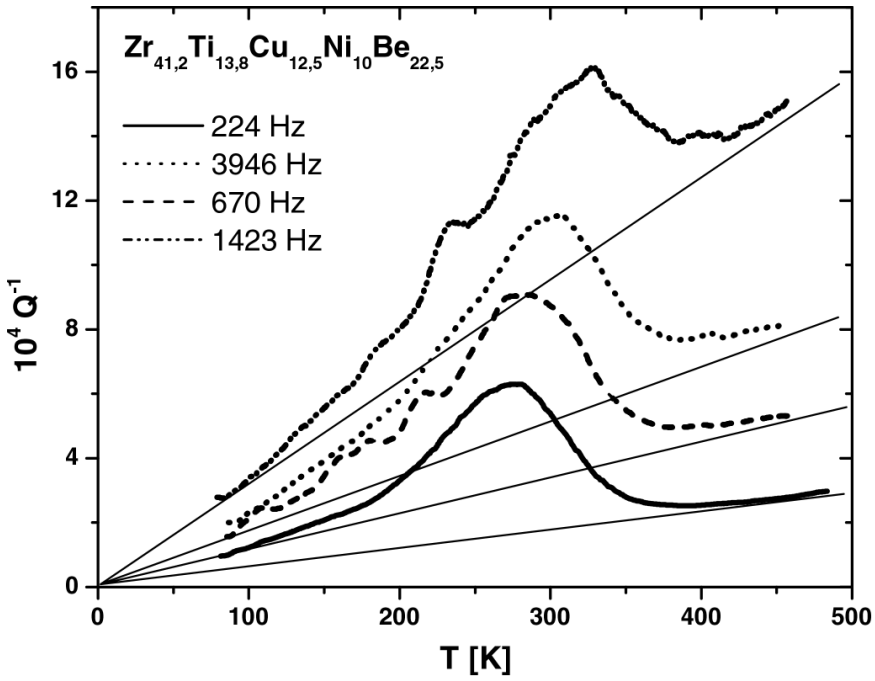

Figure 4.4: *Damping spectra for a Zr-based bulk glass at different frequencies; the straight lines are used to estimate the thermoelastic component of* Q^{-1}.

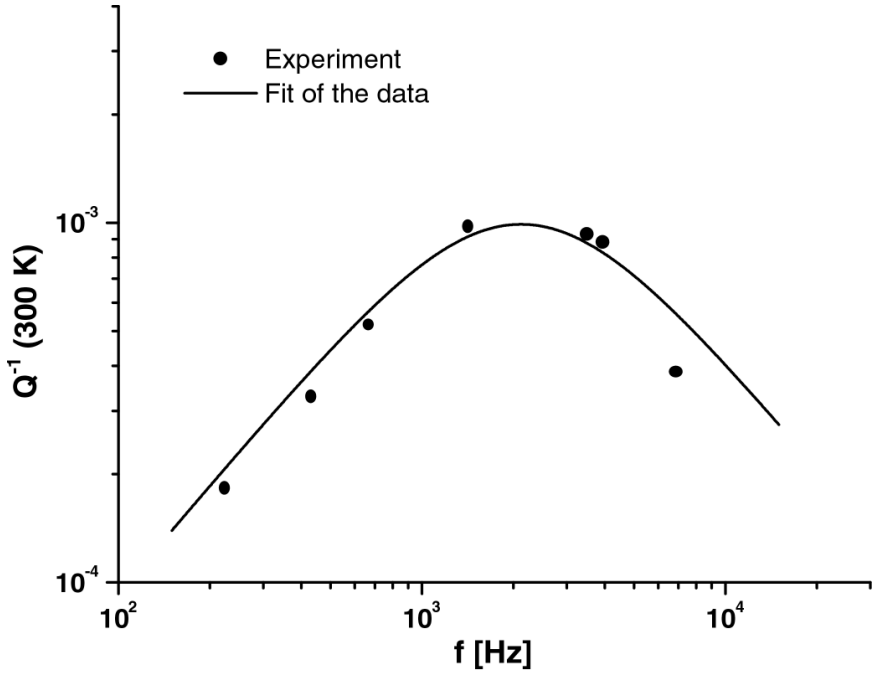

Figure 4.5: *Frequency dependence of the damping measured at 300 K and fit of the experimental data through Eq. (4.2).*

damping has been computed. Successively a $Q_T^{-1}(f)$ plot has been made which could be fitted using Eq. (4.2) with Δ_T and f_0 as free parameters. The results are presented in Fig. (4.5) from which a reasonable agreement between theory and observations emerges. The values of the free parameters obtained from the fit are $\Delta_T = (19,8 \pm 1,1) \cdot 10^{-4}$ and $f_0 = 2120 \pm 195$ Hz.

As a check for our interpretation of the linear background as thermoelastic effect, we have calculated the linear thermal expansion coefficient α by making use of Eq. (2.35): by taking E_U and ρ equal to 90 GPa and 5,9 $\mathrm{g\,cm^{-3}}$ respectively [48], $C_p = 0{,}45\ \mathrm{J\,g^{-1}\,K^{-1}}$ [49] and considering that $C_\sigma = \rho\, C_p$, we obtain $\alpha = 1,39 \cdot 10^{-5}\,\mathrm{K^{-1}}$. The agreement of this result with the value of $1,13 \cdot 10^{-5}\,\mathrm{K^{-1}}$ found in the literature [50] is reasonable, if we consider the experimental uncertainties involved in the estimate of the linear background as well as the pronounced scattering in the internal friction data taken at the highest frequency (not shown in Fig. (4.4)).

Finally, from the value of f_0 we can estimate the thermal conductivity k_{th} of the material by making use of Eq. (2.37): for a typical sample thickness d of 40 μm we get $k_{th} = 5{,}7\ \mathrm{Wm^{-1}K^{-1}}$.

4.3 MHS of amorphous samples

4.3.1 H-induced damping spectra

In this paragraph we want to show firstly the general ongoing of the internal friction caused by the short range reorientation relaxation of hydrogen in our Zr-based glasses; successively we will present our results concerning the evaluation of the average activation energy E_a' and of the pre-exponential factor τ_0 using the frequency shift method based on Eq. (2.28).

The spectra obtained for various alloys present remarkable similarities, like the broad outline deriving from the existence of a distribution of activation energies, the asymmetrical shape with long tails on the low temperature side and the characteristic shift of the peak temperatures with increasing hydrogen concentration. Most of these features can be recognized in Fig. (4.6) where a selection of our experimental results is presented. The shape of the spectra was already argument of discussion in paragraph 2.6 in connection to Fig. (2.11), which refers to the data obtained at the highest c_H for $Zr_{69,5}Cu_{12}Ni_{11}Al_{7,5}$. In that case an inverse temperature scale was chosen because in this way the asymmetry of the curve and its difference from the ideal Debye relaxation could be more clearly seen. The implications of this asymmetry, especially as regards the form of the related activation energy distributions, will be discussed further on in paragraph 4.3.4. For now it suffices to observe that the width at $1/e$ height of a typical internal friction curve is approximately 3-4 times larger than

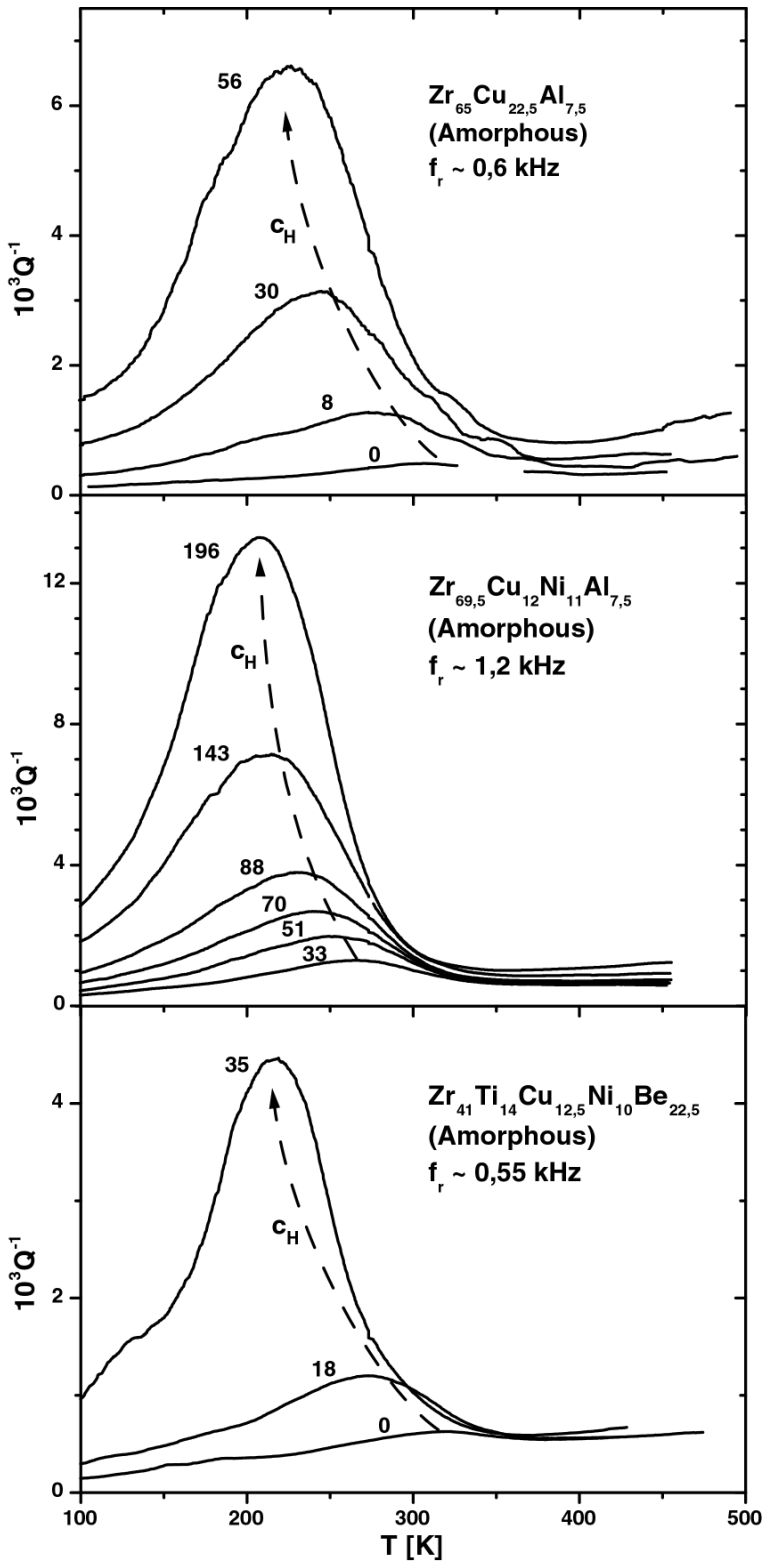

Figure 4.6: *Damping spectra as function of H content; the shift of the peaks to lower temperatures is emphasized by the dashed lines; the H-charging times in hours are also indicated.*

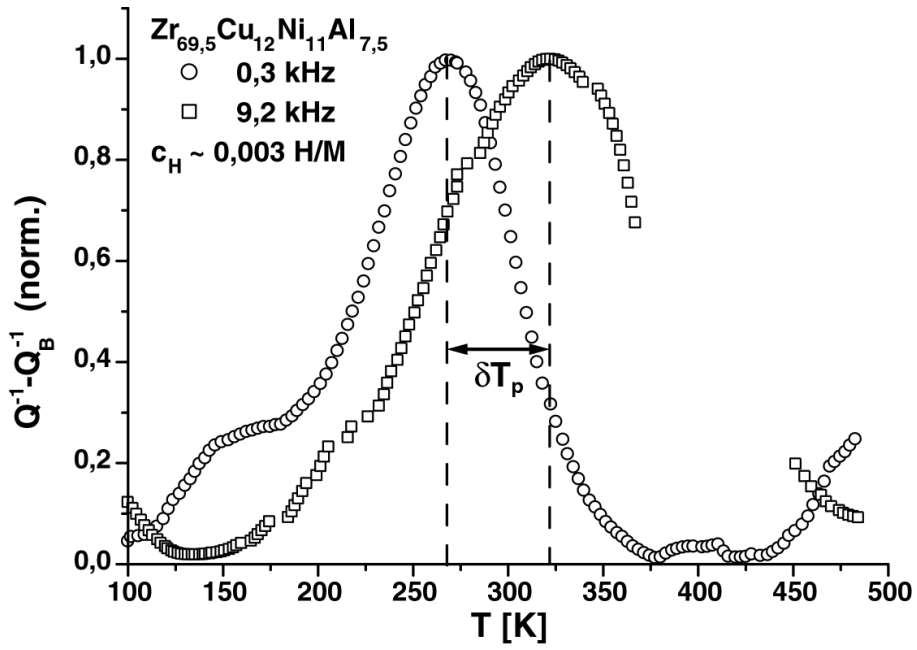

Figure 4.7: *Plot of two normalized damping spectra taken at different frequencies; a linear background Q_B^{-1} has been subtracted prior to normalization.*

the respective quantity of the ideal Debye peak.

After having confirmed that also in the Zr-based bulk glasses the hydrogen reorientation relaxation manifests itself in a similar way as in other known metallic glasses, we were interested in the evaluation of the average activation energy for the stress induced hydrogen hopping in the two classes of Zr-based alloys which we investigated, namely the "Inoue" and the "Johnson" ones. For such purpose we used the characteristic shift of the peak temperature of a damping spectrum linked to the change of the frequency at which the experiment is carried out. An example of this effect is shown in Fig. (4.7) where the temperature shift δT due to the change of frequency from 0,3 to 9,2 kHz is emphasized. The results obtained by applying this "frequency shift" method are summarized in Fig. (4.8) for two different materials: precisely we got $E'_a = 0,48 \pm 0,05$ eV and $\tau_0 = 5 \cdot 10^{-(13\pm1)}$ s for $Zr_{69,5}Cu_{12}Ni_{11}Al_{7,5}$ and $E'_a = 0,58 \pm 0,06$ eV and $\tau_0 = 2 \cdot 10^{-(14\pm1)}$ s for $Zr_{41}Ti_{14}Cu_{12,5}Ni_{10}Be_{22,5}$. It is clear that under the present experimental conditions only an approximate evaluation of the pre-exponential factor τ_0 is possible, also because of the limited frequency range (about two orders of magnitude) which could be investigated with our system. We prefer therefore to focus our attention on the average activation energy which, measured at a hydrogen concentration of about $3 \cdot 10^{-3}$ H/M, has markedly different values for the two classes of amorphous alloys. This

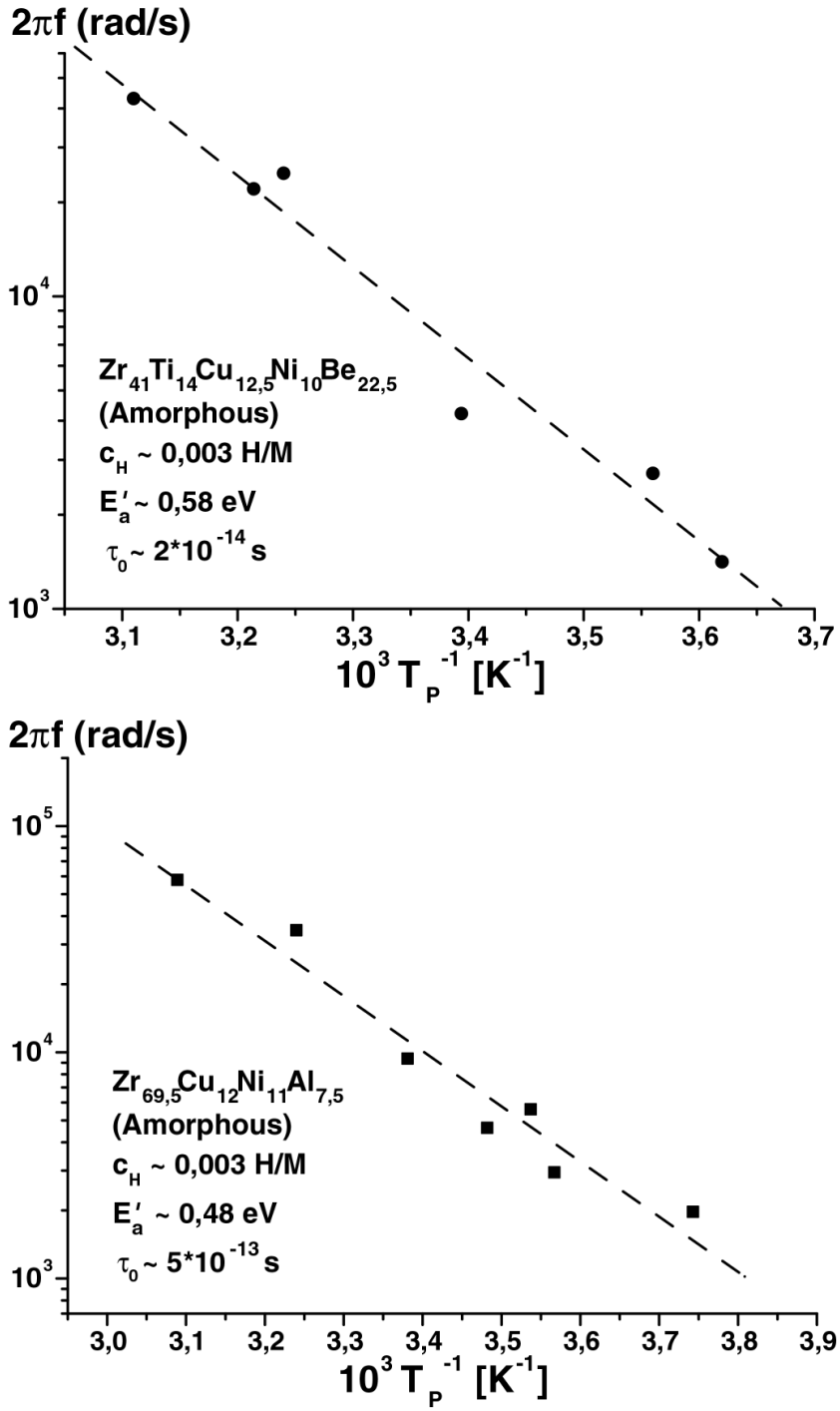

Figure 4.8: *Arrhenius plots of the peak frequencies against the inverse peak temperatures for a Johnson and an Inoue type glass.*

result will be interpreted in the light of the theoretical model from Richards which we will analyze in the paragraphs 4.3.3 and 4.3.4; in particular we will notice how the variation of E'_a at a specific concentration of hydrogen can give information on the influence of chemistry on the short range order of the glasses under investigation.

This kind of result belongs to the microscopic field of application of MHS and requires a detailed description of how the relaxation process takes place at the atomic level. Before dealing in detail with this problem, we want to put our attention to the comparison of MHS data on several metallic glasses, for which a knowledge of the microscopic mechanism at the origin of the internal friction is not necessary. Only the positions of the peak temperatures and their heights, as well as c_H, are useful data for this purpose: in the next paragraph we focus our attention on the comparison of a large data base concerning the H-induced damping results in several classes of metallic amorphous alloys.

4.3.2 Comparative MHS results

One of the questions which arose after the discovery of the bulk glass forming alloys was whether the enhanced stability against crystallization of this new class of materials, in comparison to the conventional metallic glasses, had a structural origin, involving a peculiar chemical and/or geometrical short range order. Direct experimental evidence on the SRO of amorphous structures is as yet very limited, but the well known mechanical loss peak produced by hydrogen in metallic glasses seems to be useful for the characterization of the local order of these materials, as was mentioned in section 3.4. Since, in particular, the hydrogen concentration dependence of the relaxation spectra has proved to give an indication on the different chemical and/or topological SRO according to the specific composition of the amorphous alloy under investigation [30, 18], it is to be expected that similar differences, if existing, should emerge when comparing a larger set of data concerning different metallic glasses. Such comparison has been made using a set of data involving the peak temperatures and the peak heights of the damping curves [51], whose values are easily available in the literature. With the assumption of a constant value for the pre-exponential factor τ_0 in the Arrhenius relation of Eq. (2.26), the peak temperatures are related through Eq. (3.7) to the activation energies of the hydrogen reorientation jumps, while the peak heights reflect roughly the amount of atomic hydrogen dissolved in the material. Therefore a T_P vs. Q_P^{-1} plot reflects as a first approximation the ongoing of E_a vs. c_H, which are the quantities directly connected with the distribution of atomic distances in the host matrix, and in this sense can be considered as characteristic of the structure of the glass under investigation. An important factor to keep in

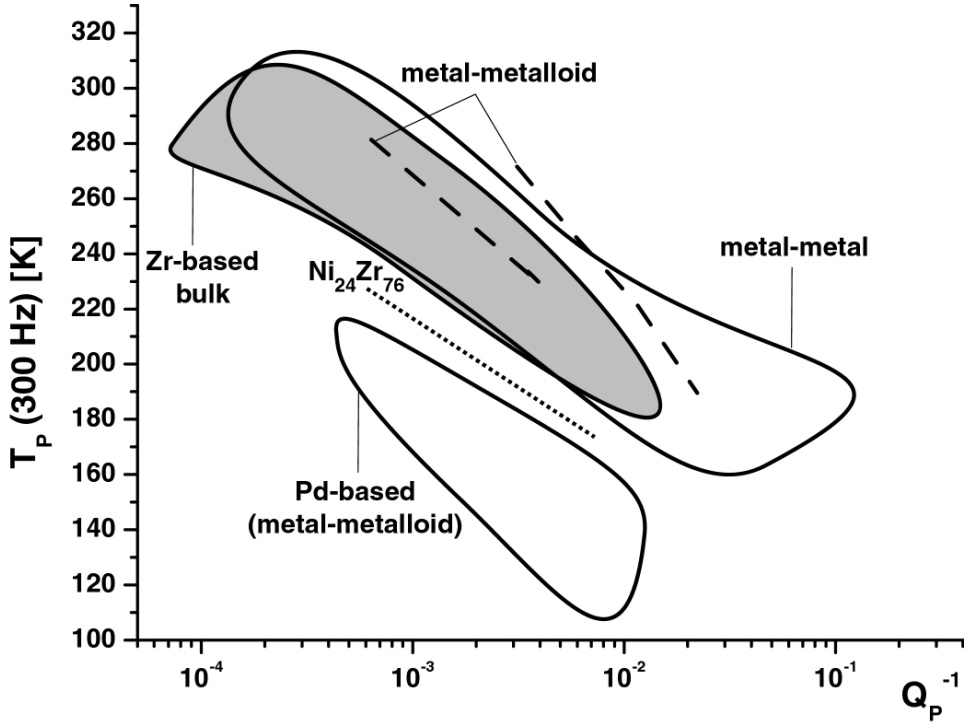

Figure 4.9: *Comparative MHS results on several categories of metallic glasses.*

consideration when taking the T_P values from the literature is the frequency at which the experiment has been performed; as stated in fact by Eq. (3.6), a correction to the peak temperature depending on the measuring frequency is necessary. The problem arises of which frequency must be taken for the comparison of a large data base and, as specified elsewhere [51], a value of 300 Hz has been found suitable for the comparison of most results. Here we want to show the final finding of this literature overview, extending the collection of data already published in the work of Sinning [51] to a broader set of Q_P^{-1} and T_P values for the Zr-based bulk glasses: the summary of such investigation is plotted in Fig. (4.9).

What are the information we can get from the aforementioned plot? First of all we notice that the conventional metal-metal and metal-metalloid glasses behave, with the exception of the Pd-based materials, in a similar way as the Zr-based bulk glasses, at least as appears from our "comparative" MHS measurements. The mechanical relaxation behavior of hydrogenated conventional metallic glasses is supposed to be of the Snoek type [52], with the H atoms sitting in tetrahedral sites and forming strong elastic dipoles. From the similarities among the measurements on different amorphous metallic alloys, it seems that the reorientation relaxation mechanism is very similar in most of

the investigated materials, giving further experimental evidence on the polytetrahedral SRO of such disordered structures. The deviation of the Pd-based glasses from the other alloys in the plot of Fig. (4.9) could be interpreted as a different kind of SRO, involving for example non triangular faces of the geometrical figures constituting the main building blocks where the H atoms are stored; this in turn could adjust the overall activation energy on lower values than what observed in other glasses. Such interpretation, however, does not keep in consideration that in the special case of Pd-H the interaction potential may be exceptionally soft, as indicated e.g. by particularly low activation energy values also for long range H diffusion in Pd [53]. In this case one should be careful on the explanation to give on such experimental observation.

If from the general point of view there seems to be no difference in structure between the Zr-based bulk and the other conventional glasses, a closer look at the data on the bulk amorphous alloys shows some characteristics which depend on the chemistry of the material under investigation. In particular in Fig. (4.10) the data have been divided in two categories, belonging to the Zr-poorer "Johnson" type the first and to the Zr-richer "Inoue" type the second. The experimental points with error bars consist of averages on several data, while the others represent single measurements. Clearly at low hydrogen concentrations the peak temperatures of the Inoue alloys are lower than the corresponding quantity in the Johnson glasses. Such effect has already been noticed on MHS studies in Co-Zr systems [18, 54], an example of which is shown in Fig. (4.11). An interpretation of this dependence of the activation energy for short range hydrogen hopping on the chemistry of the alloy was given in terms of a variation in Zr-Zr nearest neighbor distances in the glass [18]: in fact, an increase in E_a with decreasing Zr content could be compared with the increase of Zr-Zr distances linked to the lowering of the amount of Zr in several Co-Zr metallic glasses [55]. The connection between E_a and the average distances of the Zr atoms comes from a model based on the theoretical approach of Richards [1]. While we will soon deal in detail with this theory, it is useful now to introduce the equations which relate E_a to the sum of edge lengths of a distorted tetrahedron, which are at the basis of the interpretations contained in [18]. Considering the ideal geometry of close packed spheres, we define d_0 as the edge of a *regular* tetrahedron which can be found in such structure; furthermore, taking the same figure, this time *distorted* due to the change from "ideal close packed" to "dense random packed" arrangement of spheres, we set d_i $(i = 1, 2, 3)$ as the edges of the triangular face through which the H atom hops and d_i $(i = 4, 5, 6)$ as the other edges (see Fig. (4.12) further on). With these definitions it is possible to write [18]

$$E_a = \Delta_0 + 3(a_S - 2a_E) + (a_E - a_S)\frac{d_1 + d_2 + d_3}{d_0} + a_E\frac{d_4 + d_5 + d_6}{d_0}\,, \quad (4.3)$$

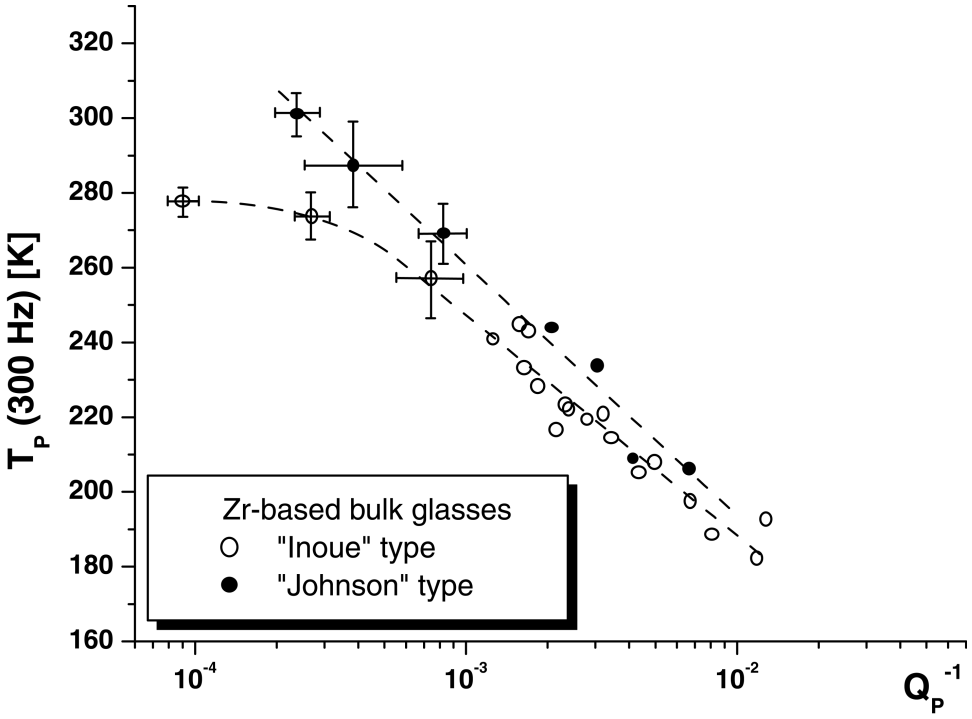

Figure 4.10: *Comparative MHS results on Zr-based bulk glasses.*

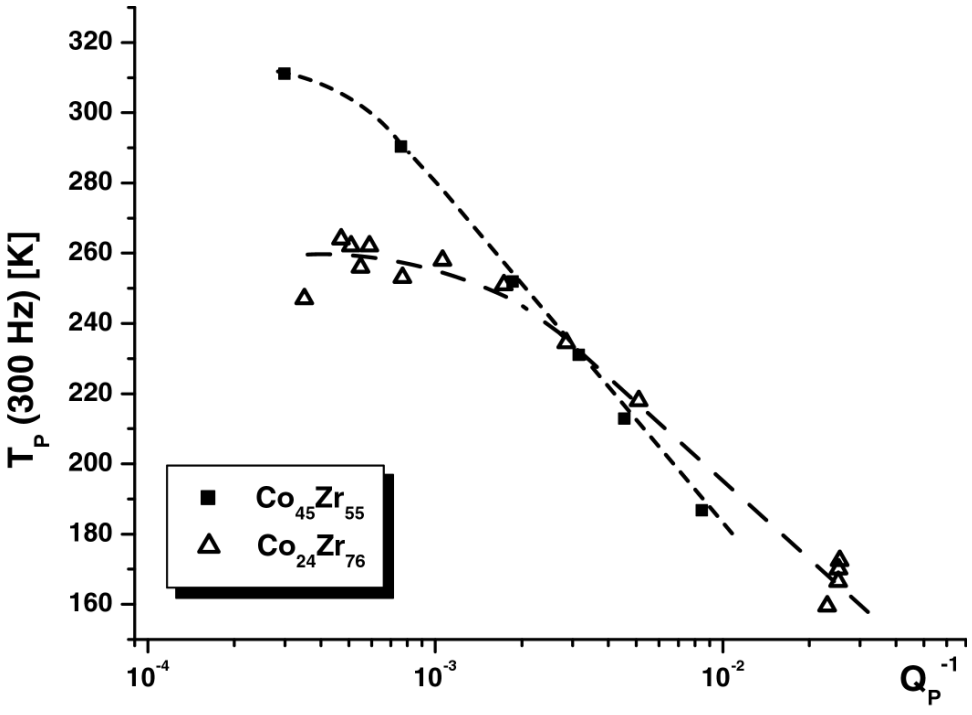

Figure 4.11: *Comparative MHS results on Co-Zr glasses; data from [54].*

where Δ_0 is the activation energy for the hydrogen atom jumping out of the regular tetrahedron and $a_{S,E}$ enclose the metal-hydrogen interactions at the saddle point S (center of the triangular faces of the polyhedron) and equilibrium site E respectively. By assuming a ratio $a_S/a_E = 1,5$ [19], Eq. (4.3) can be rewritten as

$$E_a = \Delta_0 + a_E \left(\frac{D}{d_0} - \frac{3}{2} \right) \tag{4.4}$$

with $D = d_4 + d_5 + d_6 - \frac{1}{2}(d_1 + d_2 + d_3)$. According to this simple model, an overall increase of the atomic distances reflects itself in an increase of D and, consequently, of E_a.

Eq. (4.4) is well worth remembering because its meaning is more general than what seems from the restrictive initial conditions, like the choice of considering only *one* tetrahedron and the relative edge lengths, instead of thinking about the whole structure, and the assumption of the value 1,5 for the ratio a_S/a_E. In the following we will show how such hypothesis finds a confirmation through a comparison of the theoretical model of Richards, where an average activation energy is calculated in dependence on some function of the average edge lengths in the amorphous structure, and our experimental results on the Zr-based bulk glasses.

4.3.3 Theoretical model

The following considerations are, as already mentioned, largely based on the work of Richards [1]. The aim of this model is to find a distribution of activation energies for hydrogen hopping in a model amorphous structure, assuming a classical over-the-barrier jump mechanism governed by the metal-hydrogen distances and potential and neglecting any tunnelling or phonon assisted processes, as in the case of Eq. (2.39). One important result of such work is the possibility of neglecting the detailed form of the metal-hydrogen potential, which is normally not known, for the calculation of the activation energies. Instead, quantities like the bulk modulus and the volume expansion per H atom are used, at least for the computation of the equilibrium site energies; for the saddle point ones the situation is more complex but, assuming that the potential is well behaved and has a simple form, the corresponding energies can be estimated by using the observed lattice expansion and the zero point vibrational frequency of the hydrogen impurity. The salient feature of the model consists of predicting that the activation energy depends on the sum of edge lengths of the distorted polyhedra (tetrahedra or octahedra) enclosing the H impurity and that this quantity has a distribution which is related to the pair radial distribution function (RDF). Since in the Zr-based bulk glasses we suppose that hydrogen sits in tetrahedral sites, we will hereafter consider

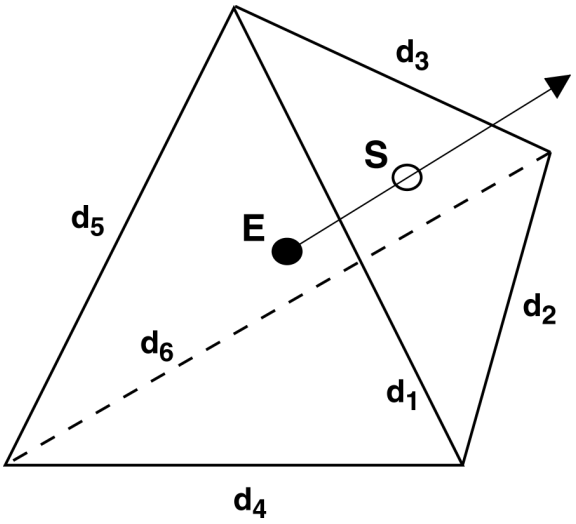

Figure 4.12: *Distorted tetrahedron with indication of its edge lengths; the full and hollow circles denote, respectively, the equilibrium and saddle point positions; the arrow symbolizes the hopping of a H atom out of the interstitial site.*

the expressions of Richards' model only for these kind of interstitial sites.

In general the activation energy E_a for hydrogen hopping out of a distorted tetrahedron turns out to be temperature dependent. Under certain conditions, which will be specified later, such dependence disappears: in particular in the "low temperature" approximation we get

$$E_a = \Delta_0 + a_E Y - a_S Y_{\alpha max} \,. \tag{4.5}$$

Beside Δ_0, which has already been introduced in the preceding paragraph, the other quantities of Eq. (4.5) can be defined as follow: by letting $V(r)$ be the metal-hydrogen potential, r_{0E} (r_{0S}) the distances vertex-equilibrium site (vertex-saddle point) of a regular tetrahedron with edge length d_0, K the bulk modulus of the material under investigation and ΔV_H the volume change per hydrogen atom, we can write

$$a_E = -\frac{2}{3}\, V'(r_{0E}) r_{0E} = \frac{1}{2}\, K \Delta V_H \qquad \text{and} \qquad a_S = -V'(r_{0S})\, r_{0S} \,. \tag{4.6}$$

Moreover, by referring to the distorted tetrahedron of Fig. (4.12), where the equilibrium (E) and saddle point (S) positions are also schematically shown, we have

$$Y = \sum_{k=1}^{6} \left(\frac{d_k}{d_0} - 1 \right) \qquad \text{and} \qquad Y_{\alpha max} = \sum_{k=1}^{3} \left(\frac{d_k}{d_0} - 1 \right) ; \tag{4.7}$$

the suffix αmax indicates that the summation is performed over the *largest* face of the polyhedron. For the particular case in which the ratio a_S/a_E takes the value 3/2 it is easy to convince ourselves that Eq. (4.5) has exactly the same form of Eq. (4.4) with $D/d_0 = Y - \frac{3}{2} Y_{\alpha max} + \frac{3}{2}$.

The considerations made until now regard a single interstitial site. The next step in the model is the generalization of the results to the overall amorphous structure; this requires the passage from the single value of E_a given by Eq. (4.5) to a distribution $P_{th}(E_a)$ which, in the present model, is supposed to be of Gaussian shape. Moreover, also the quantities related to Y will be replaced by the respective average values. In the theory the direct computation of the Gaussian distribution of activation energies is not possible, but its first and second moments, that is the average $\langle E_a \rangle$ and standard deviation δE_a, are given instead:

$$\langle E_a \rangle = \Delta_0 + (a_E - a_S/2)\langle Y \rangle - a_S \langle \delta Y_{\alpha max} \rangle \,; \tag{4.8}$$

$$\langle (E_a - \langle E_a \rangle)^2 \rangle = (a_E - a_S/2)^2 \langle (Y - \langle Y \rangle)^2 \rangle + a_s^2 \langle (\delta Y_{\alpha max} - \langle \delta Y_{\alpha max} \rangle)^2 \rangle \equiv \frac{1}{2}(\delta E_a)^2, \tag{4.9}$$

where $\delta Y_{\alpha max} = Y_{\alpha max} - Y/2$ is the departure of $Y_{\alpha max}$ from the expectation value of any of the Y_α in the conditional distribution $\rho(Y_\alpha|Y)$ and Y_α is the sum of the edge lengths of a generic face α of the tetrahedra.* The average value of $\delta Y_{\alpha max}$, as well as its standard deviation, turns out to be only dependent on the type of interstitial site and not from Y, and it can be calculated with standard software by using an appropriate distribution [1]. On the other side, the quantities related to Y deserve a deeper insight, especially as regards the form of the distribution $\rho(Y)$ to be used for their computation. Since Y is related to a sum of nearest neighbor distances $(d_1, ..., d_6)$ each distributed according to the RDF, considering only the first peak of the RDF and approximating it with a Gaussian, for tetrahedral interstitial sites we get

$$\rho(Y) = \exp(-Y^2 / 6\,\sigma^2), \tag{4.10}$$

where σ is the half width at $1/e$ height of the RDF expressed in units of d_0. Eq. (4.10) is not enough for the computation of $\langle Y \rangle$ because the thermal probability of finding a particle in a specific interstitial site must also be taken into account. In the case of hydrogen this thermal probability is the Fermi-Dirac distribution $F(Y) = \{\exp[-\frac{a_E}{kT}(Y - Y_F)] + 1\}^{-1}$, where Y_F is related to the Fermi energy and depends on the hydrogen concentration according to

$$c_H = \frac{5}{4}\,\mathrm{erfc}(Y_F / \sqrt{6}\,\sigma). \tag{4.11}$$

Consequently, the average and standard deviation of Y can be calculated using the distribution $G(Y) = F(Y)\rho(Y)$. The ingredients for the theoretical computation of the activation energy and its distribution are now at hand and we will now apply such results to our amorphous alloys.

*The conditional distribution $\rho(Y_\alpha|Y)$ is the probability of finding Y_α when Y is given. Its computation is out of the scope of this work, but the interested reader can find the mathematical details in Ref. [1].

4.3.4 Application to Zr-based bulk glasses

One of the basic premises for the application of the theoretical results of the preceding paragraph is that our alloys can be treated as if they were pure amorphous Zr; moreover, it is assumed that the Zr-H potential is the same as in the respective crystalline structure. Such considerations may not be too far away from the reality: in fact for the hydrogen concentration range that we investigated, which has an upper limit of about 0,5 H/M, the relaxation mechanism at the base of the internal friction spectra is supposed to be the hopping of H between adjacent Zr_4 tetrahedral sites. In this sense hydrogen only probes the SRO of the Zr atoms and therefore "sees" a glassy structure made apparently only of this metal. This should be true especially for the Inoue glasses, where the considerable amount of Zr and, at the same time, the high and positive enthalpy for hydride formation of the other elements of the alloys (Cu, Al, Ni), should favor the positioning of H in interstitial sites only surrounded by the early transition metal. Similar considerations should apply also to the Johnson glasses, even though the lower amount of Zr and the presence of Ti could also favor the storage of H in other kind of tetrahedral sites like Zr_3Ti.

In the first part of this paragraph it is our aim to calculate the average activation energy for H hopping according to Eq. (4.8) as a function of the H concentration; the theoretical curve obtained in this way can be then compared with our experimental results. The first quantity needed in the model is the parameter a_E referred to the equilibrium site energy. Following Eq. (4.6), a_E is related to the bulk modulus and the volume expansion per H atom and these values have been taken from the literature, even though it was sometimes very difficult to find the adequate information, especially as regards ΔV_H. Anyway, for the bulk modulus we found $K = 110$ GPa [48], while for the volume change we set $\Delta V_H = 4$ Å^3, which is a compromise between the value observed in the case of crystalline Pd (2,9 Å^3) and the one of 5 Å^3 obtained at the high H concentration of 1,9 H/M in quasicrystalline $Zr_{69,5}Cu_{12}Ni_{11}Al_{7,5}$ [42]. With these choices we get $a_E = 1,37$ eV. The second important parameter is σ, which is the half width at $1/e$ height of the RDF in units of the hard sphere diameter d_0. In particular, we must consider the *partial* RDF referred to the distribution of Zr-Zr nearest neighbor distances and this poses a serious problem due to the lack of experimental evidence on such quantity in the literature. We made therefore a compromise among the data found for other kind of Zr-based bulk glasses and which we report in Table (4.2). According to these information we could make no use of the values referred to the Johnson glass, because they derive from the *total* RDF, which in turn reflects the distribution of Zr-Be distances. In consideration of the other data, more indicative of the Zr-Zr

	$Zr_{41,2}Ti_{13,8}Cu_{12,5}Ni_{10}Be_{22,5}$ (Zr-Be) [56]	$Zr_{60}Ni_{25}Al_{15}$ (Zr-Zr) [4]	$Zr_{33}Y_{27}Ni_{25}Al_{15}$ (Zr-Zr) [4]
d_0 (Å)	2,8	3,17	3,15
w (Å)	1,3	0,87	0,67
σ	0,23	0,14	0,11

Table 4.2: *Summary of the quantities related to the RDF according to a literature survey with indication of the atomic distances to which the RDF is referred; d_0 is the center of the RDF, w the full width at $1/e$ height and $2\sigma = w/d_0$.*

distances distribution, we chose to set $\sigma = 0,13$. A comment is necessary as far as the definition of d_0 is concerned: in the preceding paragraph we stated that this quantity is the edge of a regular tetrahedron in an ideal structure of close packed spheres. It will be from now on assumed that such value corresponds, in the case of our materials, to the center of the Zr-Zr pair RDF and that its value is $d_0 = 3,16$ Å, in excellent agreement with the Goldschmidt radius of Zr.

For the calculation of the activation energy, the knowledge of a_S is also necessary. This can be estimated by using a model potential which reproduces the observed volume expansion and the hydrogen vibrational frequency in a chosen interstitial site. An estimate of the form of the potential is needed because, according to Eq. (4.6), the ratio of the parameters a_E and a_S for a tetrahedron can be written as

$$\frac{a_S}{a_E} = \sqrt{2}\,\frac{V'(r_{0S})}{V'(r_{0E})}. \tag{4.12}$$

Assuming that the potential has a simple form like for example $V(r) = V(r_{0E}) + Ar^{-p}$, with the constants $V(r_{0E})$ and A which do not appear in the computation of a_S/a_E because here only a ratio of derivatives is involved, the problem is to estimate the value of the parameter p.[†] In the model of Richards the zero point vibrational frequency ω_0 of a hydrogen atom of mass m placed at the center of a regular octahedron and the volume expansion per H atom are related to the potential by the equation

$$\frac{r_{0E}\,V''(r_{0E})}{|V'(r_{0E})|} = \frac{m\,\omega_0^2\,r_{0E}^2}{K\Delta V_H} + 2 = 7,63\,; \tag{4.13}$$

[†]It is possible to take for example $e^{-\alpha r}$ or $e^{\gamma/r}$ instead of r^{-p}, but this does not affect the final results in a significant way [1].

the last equality comes by considering the value $\hbar\omega_0 = 80$ meV for H in octahedral sites of Zirconium hydrides [57] and by taking $r_{0E} = d_0/\sqrt{2}$ (vertex-equilibrium site distance in a regular octahedron) with $d_0 = 3,16$ Å. By substituting $V(r)$ in Eq. (4.13) we find $p = 6,63$; with such information we can finally estimate $a_S/a_E = 2,1$ by using Eq. (4.12) and considering the ratio $r_{0S}/r_{0E} = 2\sqrt{2}\,/3$ for a tetrahedron. In evaluating Eq. (4.13) we used the volume expansion ΔV_H for hydrogen stored in tetrahedral sites; this has no significative influence on the calculation because it is possible to show that the ratio $\Delta V_H(T)/\Delta V_H(O)$, for quantities referred to tetrahedral and octahedral sites respectively, is approximately equal to 0,95 [1].

In the considerations made above it was tacitly excluded any effect due to lattice relaxation upon introduction of hydrogen. Such phenomenon should reduce the ratio a_S/a_E, even though the value $\sqrt{2}$ represents a lower limit, since in this case we would assume, by considering Eq. (4.12), that the force exerted on the hydrogen atom at the saddle point is the same as the one at the equilibrium site. For such reason we can at this point only state that $\sqrt{2} \leq a_S/a_E \leq 2,1$; we will calculate the average activation energy for different values of this ratio and, by comparing it with our experimental results, it will be possible to see which is the more reasonable choice.

Before going further, we will briefly go back to consider the validity of the low temperature approximation used in Eq. (4.5); this equation holds if $|a_S Y_\alpha/kT| \gg 1$ and now we can estimate it since we have a value for a_S. At the root-mean-square value $\langle Y_\alpha^2 \rangle^{1/2} = \sqrt{3/2}\,\sigma$ [1] and at $T = 300$ K we get $a_S Y_\alpha/kT \simeq 18$, in reasonable agreement with the chosen approximation, also considering that most of the peak temperatures in our damping spectra lay about and below room temperature.

The theoretical computation of $\langle E_a \rangle$ has been made through Eq. (4.5) as function of the hydrogen content c_H and plotted in Fig. (4.13) for different values of a_S/a_E (continuous lines); at the same time also the experimental data for both our Inoue and Johnson glasses in form of a T_P against Q_P^{-1} diagram are plotted. For the comparison of the theory with the experiment we used the empirical relationship linking the hydrogen concentration with the height of the damping spectra previously shown in Fig. (3.11); moreover we could correlate the peak temperatures to the average activation energy through Eq. (3.7). The parameter Δ_0 has been set equal to 0,5 eV, which agrees very well with the activation energy for hydrogen diffusion in hcp Zr [58, 59], whose structure closely resembles the ideal arrangement of close packed spheres. The energy scale on the right side of the plots has been determined from Eq. (3.7) for the two values $\tau_0 = 10^{-12}$ and $\tau_0 = 10^{-13}$ s. The choice of showing the difference between two energy scales derives from the uncertainty with which the parameter τ_0 can be estimated. In fact under the present experimental conditions the

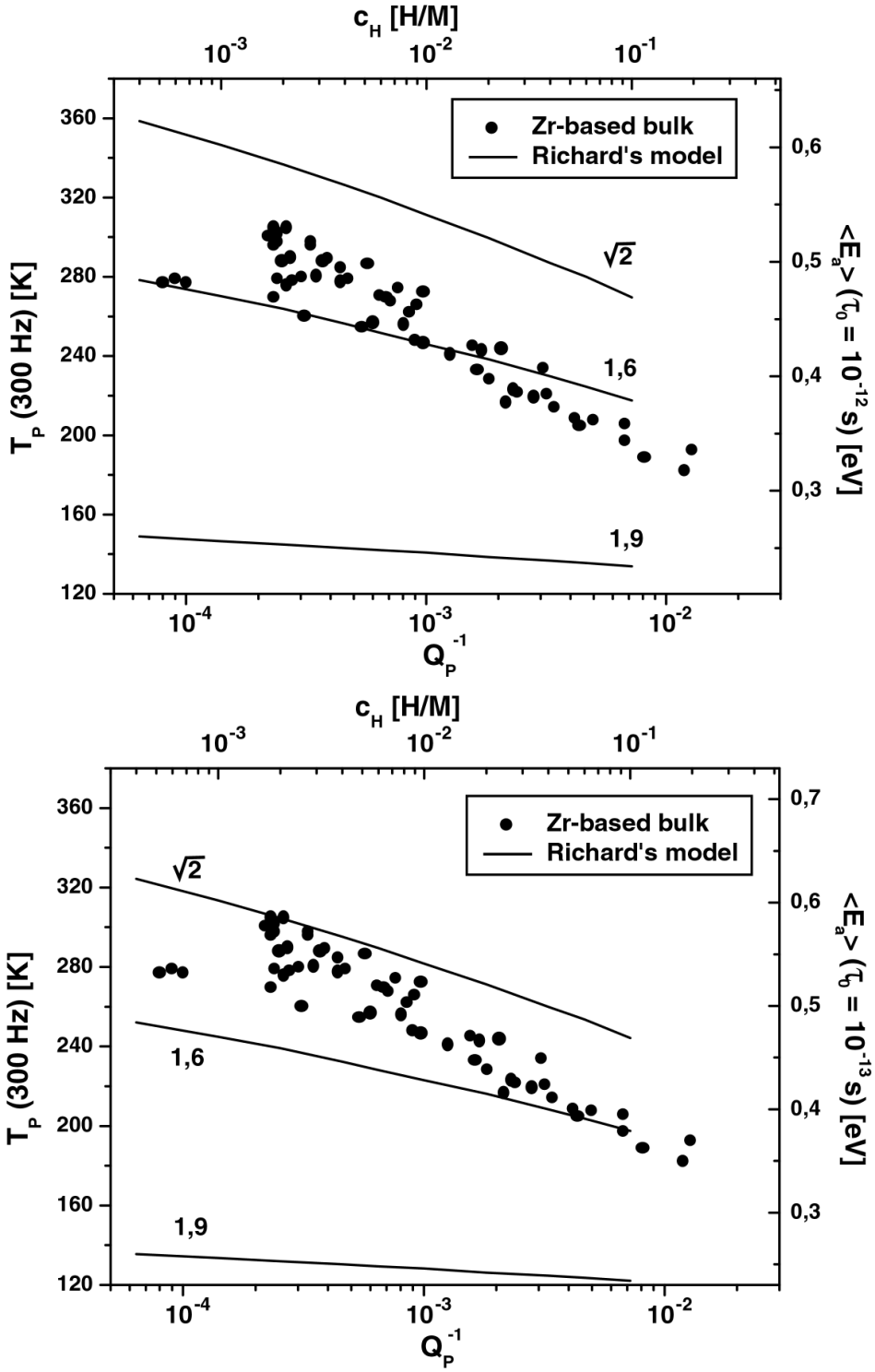

Figure 4.13: *Experimental results on Zr-based bulk glasses and comparison with the theory according to Eq. (4.8). The energy scales are derived from Eq. (3.7) using different values for τ_0. Indicated are also the ratios a_S/a_E.*

frequency shift method, commonly used in mechanical spectroscopy investigations and whose principle is contained in Eq. (2.28), is negatively influenced by several error sources, like temperature gradients inside the experimental setup, limiting therefore the precision in the measurement of τ_0 to an interval of about two orders of magnitude. In consideration of what has been found in the literature as regards the ground frequency of hydrogen placed in tetrahedral sites in Zr hydrides, for which the value $\tau_0 = 3 \cdot 10^{-13}$ s was measured [60] and of our own results as expressed in Fig. (4.8), we will assume in the following that the "true" value of the pre-exponential factor is $\tau_0 = 10^{-13}$ s.

The results concerning the energy parameters a_S and a_E are the argument we are going to analyze next. In particular we can make the following observations: firstly, we see from Fig. (4.13) that the ratio a_S/a_E lies approximately between $\sqrt{2}$ and 1,6. Such a low value means that some lattice relaxation effects do take place upon introduction of hydrogen and influence the overall activation energy for H-hopping in the Zr-based glasses. The value of 2,1 corresponding to a rigid structure is manifestly inappropriate to match the experimental results. Consequently the heuristic choice of $a_S/a_E = 1,5$ made by Sinning [19] and explained in paragraph 4.3.2, appears now justified on the base of a more fundamental model. Secondly, a change of one order of magnitude in τ_0 does not seem to influence in a dramatic way the value of the ratio a_S/a_E: in going from $\tau_0 = 10^{-13}$ to $\tau_0 = 10^{-12}$ s, we can say that a_S/a_E approximately increases from 1,5 to 1,6 but this does not considerably affect the essence of our results.

We can now write the ongoing of the activation energy as a function of quantities related to the Zr-Zr distances by starting from Eq. (4.8) and by taking $a_S/a_E = 3/2$:

$$\langle E_a \rangle = \Delta_0 + a_E \left(\frac{\langle Y \rangle}{4} - \frac{3}{2} \langle \delta Y_{\alpha max} \rangle \right). \tag{4.14}$$

The expression in round brackets represents the generalization to the overall amorphous structure of the corresponding quantity of Eq. (4.4) which, in this sense, has a more general meaning than what appears from the restrictive hypothesis at the base of its derivation.

Now that we have investigated the behavior of the activation energy as a function of the hydrogen content, we want to study the problem from another point of view. Let's fix this time the value of c_H and, from the knowledge of the activation energy for hydrogen hopping in different Zr-based glasses, we will try to make some conclusions on the influence of chemistry on the SRO of such amorphous structures. An interesting value for the hydrogen concentration is $c_H = 10^{-3}$ H/M, which corresponds to a peak height of the damping spectra of about $2 \cdot 10^{-4}$. From the plot shown in Fig. (4.10) we notice that in the

aforementioned range the behavior of the Zr-richer Inoue glasses is different from the one of the Johnson alloys: in particular the average activation energy is lower in the Inoue materials than in the Johnson ones. From the value of $\langle E_a \rangle$ as can be seen from the energy scale relative to $\tau_0 = 10^{-13}$ s in Fig. (4.13) and remembering that $\langle \delta Y_{\alpha max} \rangle$ is a constant, using Eq. (4.14) we estimate $\langle Y \rangle_J = 0,87$ and $\langle Y \rangle_I = 0,7$ for the Johnson and Inoue glasses respectively. From the definition of Y given in Eq. (4.7) we notice that the average value of such quantity can be written as

$$d_0 \langle Y \rangle = \langle \sum_{k=1}^{6} (d_k - d_0) \rangle. \tag{4.15}$$

The right side of this equation represents the average deviation of the perimeter of a distorted tetrahedron from the corresponding value of a regular tetrahedron with edge length d_0. It is possible to consider $\langle Y \rangle$ as the *isotropic* variation of the dimensions of the tetrahedral interstitial site; such variation can be a dilatation, for positive, or a shrinkage for negative values of $\langle Y \rangle$.[‡] By using Eq. (4.15) we can estimate the average deviation of a single edge from d_0 which, for tetrahedral sites, is $\langle d_k - d_0 \rangle = d_0 \langle Y \rangle / 6$. For the Johnson and Inoue glasses we get, respectively, $\langle d_k - d_0 \rangle_J = 0,46$ Å and $\langle d_k - d_0 \rangle_I = 0,37$ Å and this means that the average Zr-Zr distances in these alloys, as seen from the MHS measurements for low hydrogen concentration, are $\langle d_k \rangle_J = 3,62$ Å and $\langle d_k \rangle_I = 3,53$ Å having assumed $d_0 = 3,16$ Å. If we concentrate on the magnitude of such distances, we notice that they are considerably larger than the ideal value of d_0: this is not surprising in consideration of what kind of interstitial sites are probed by hydrogen at such low c_H. In fact, if we look at the distribution $G(Y)$ (as defined in paragraph 4.3.3) used for calculating $\langle Y \rangle$ and plotted in Fig. (4.14), we can see that the sites occupied by hydrogen are limited to the shaded area in the high-end region of the distribution. In such conditions then the H atoms occupy the *largest* tetrahedral sites which are characterized by the highest values of Y. Thinking now about the difference between $\langle d_k \rangle_J$ and $\langle d_k \rangle_I$ and restricting our considerations to that part of the Zr-Zr RDF which is scanned by the H atoms, we can say that the SRO of our materials depends on their chemistry in the sense that with increasing Zr content there is a decrease of the average Zr-Zr distance. Such conclusion is confirmed in the results found in the simpler case of the binary Co-Zr system [55] and, on the other side, strengthens the hypothesis formulated in [18] and discussed in paragraph 4.3.2.

Another interesting question is why at higher hydrogen concentrations the difference in activation energies between Zr-richer and Zr-poorer glasses tends

[‡]The *anisotropic* part is represented by $\langle \delta Y_{\alpha max} \rangle$ which is the deviation of the perimeter of the largest face of the polyhedron from its average value for a generic face.

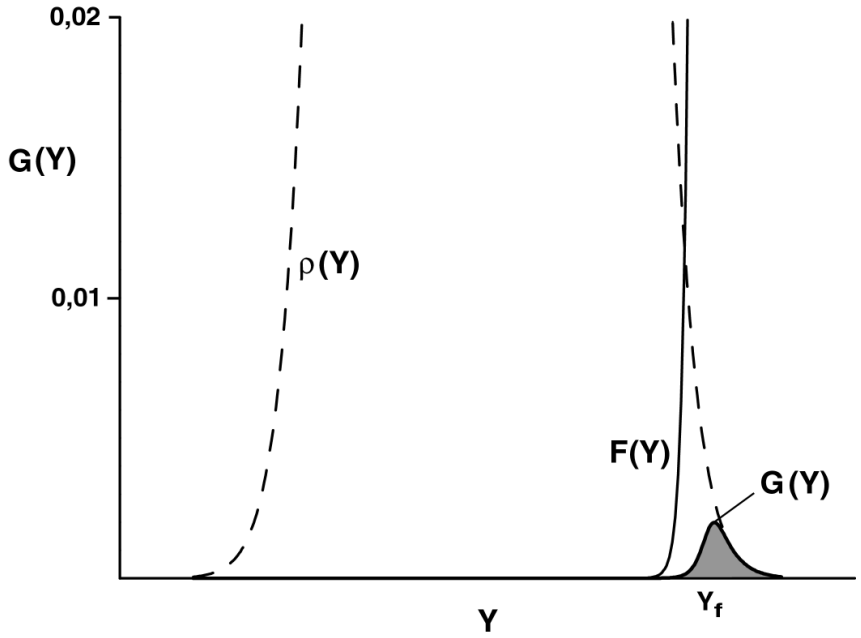

Figure 4.14: *Plot of the distribution G(Y) for* $c_H = 10^{-3}$ *H/M and* $T = 300$ *K together with the Fermi-Dirac distribution F(Y) and the Gaussian* $\rho(Y)$ *of Eq. (4.10); the shaded area symbolizes the sites occupied by hydrogen.*

to level off and eventually to reverse as shown for example in Fig. (4.11). In particular, the tendency of the Zr-poorer alloys to have a steeper E_a vs. c_H curve was clearly measured in the case of Co-Zr, while for our bulk glass forming materials this effect could not be confirmed with certainty because of the relatively low hydrogen content that was reached upon H charging. A tentative interpretation of such effect can be given if we assume that the difference of activation energy for H hopping among the distorted interstitial sites is mainly determined by the variation of *site energies*, rather than by the related saddle point quantities. Moreover, we must consider that a higher amount of Zr means also a greater number of available Zr_4 tetrahedra for H storage in each energy range. With an increase in c_H the H atoms first occupy the sites with lowest energy, which also corresponds to the highest Zr-Zr distances, and then gradually the sites which are energetically less favorable. This observation, together with the assumptions made above, already explains why the average activation energy decreases when c_H grows. Now, in the Zr-poorer glasses there are less "low energy" sites available for hydrogen which, therefore, must occupy more rapidly the unfavorable Zr_4 tetrahedra. Consequently the decrease of $\langle E_a \rangle$ with c_H is faster in these materials than in the Zr-richer ones, explaining therefore the behavior observed in Figs. (4.11) and (4.10).

We have until now analyzed the ongoing of the activation energy for short range hydrogen hopping in dependence of parameters linked to the geometry of the interstitial sites in a random structure. We have not yet used the form of the overall internal friction spectra for such investigation, because only the position of the peak temperatures was necessary. The next step needed for a check of the model is to consider the whole H-induced damping curves and compare the activation energy spectra at the origin of their shape with the Gaussian distribution $P_{th}(E_a)$ obtained from Richards' model and characterized by the quantities defined by Eqs. (4.8) and (4.9).

The starting point consists in using Eq. (2.33) with appropriate values of the parameters β_E and E'_a for the simulation of the internal friction curves.[§] After having noticed that the choice of a simple Gaussian $P(E_a)$ as formulated in Eq. (2.32) was inadequate for the correct fit of the experimental data, we decided to try with asymmetric distributions $P_{12}(E_a)$ consisting of two half Gaussian characterized by different widths β_{E1} and β_{E2}. In this way the fit improved, even though in the temperature range below approximately 180 K the agreement between simulation and experiment remained unsatisfactory. The behavior observed for an Inoue type glass is summarized in Figs. (4.15) and (4.16); for the Johnson alloys we obtained similar results and, therefore, we will generalize the conclusions to be drawn from the aforementioned figures to all the Zr-based glasses considered in this work.

Due to its rather artificial choice, we don't want to give too much importance to the analytical form of $P_{12}(E_a)$ but rather to its broad outline: considering the average of all the experimental half widths at $1/e$ height as seen in Fig. (4.16) we get $\langle \beta_E \rangle = 0,138$ eV, which is a rather large value. The theory predicts on the other side an even wider distribution characterized by $\delta E_a = 0,165$ eV. Such difference should not be very important since the experimental value must be thought of as a lower limit to the width of the distribution. In fact as it appears from the fit of the damping peaks of Fig. (4.15) the low temperature side of the curves remains partly out of the fit, indicating that an even wider (and asymmetric!) distribution of activation energies would be required. The comparison between the theoretical $P_{th}(E_a)$ as calculated from Richards' model and our experimental findings is quite good especially at the lower hydrogen concentrations, where the hypothesis at the base of the theory, referring in particular to the assumption of a pure amorphous Zr host matrix, should be better fulfilled. At the highest c_H the most disturbing fact is the shift of $\langle E_a \rangle$ to lower values which is more pronounced in the reality than

[§]The parameters E'_a and β_E are derived experimentally and represent, respectively, the average value and the half width at $1/e$ height of a Gaussian distribution of activation energies. The corresponding theoretical quantities are given by $\langle E_a \rangle$ and δE_a as defined in Eqs. (4.8) and (4.9).

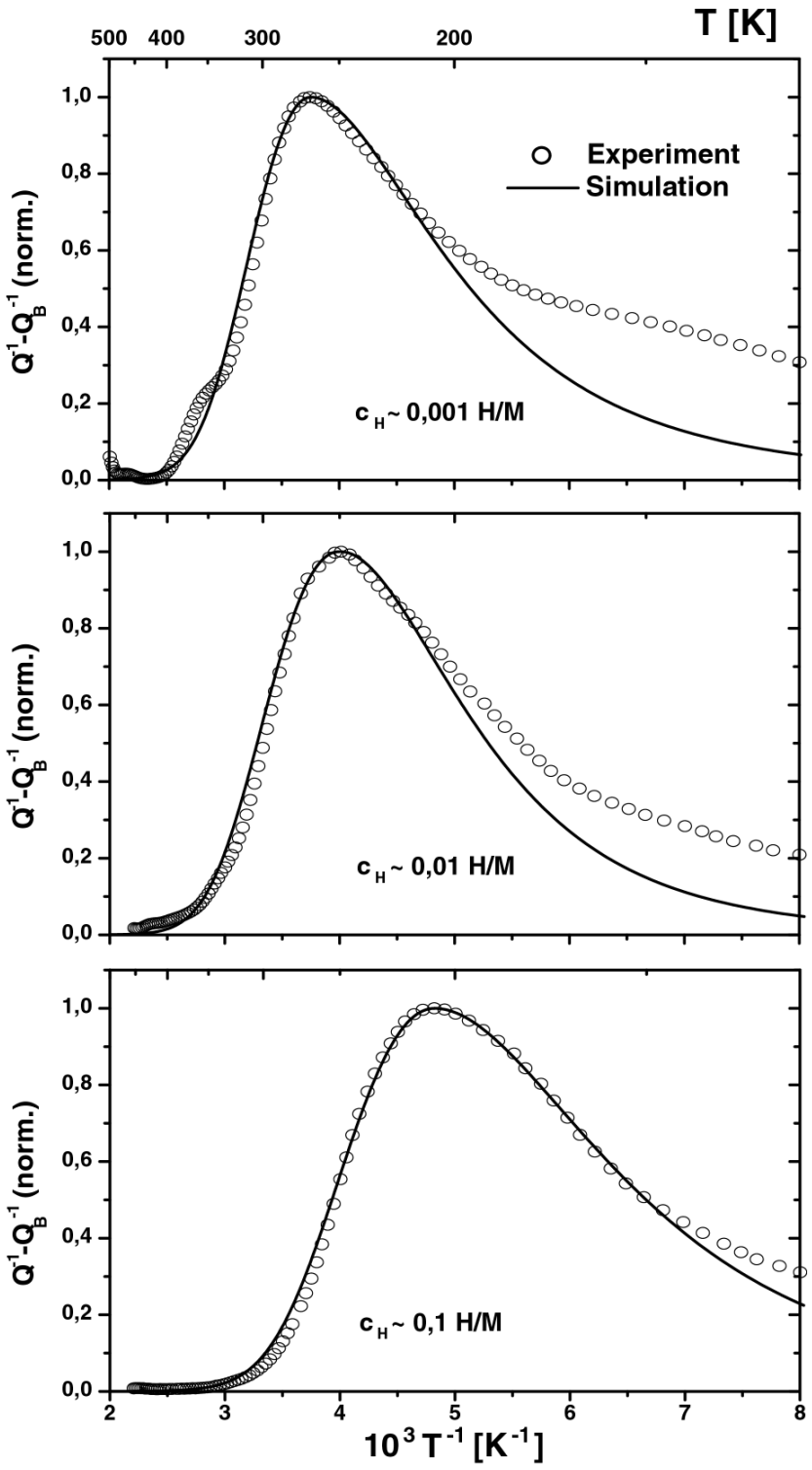

Figure 4.15: *Plots of the H-induced damping spectra for* $Zr_{69,5}Cu_{12}Ni_{11}Al_{7,5}$ *in different H-concentration ranges; the lines are simulations from Eq. (2.33) with activation energy distributions chosen as shown in Fig. (4.16).*

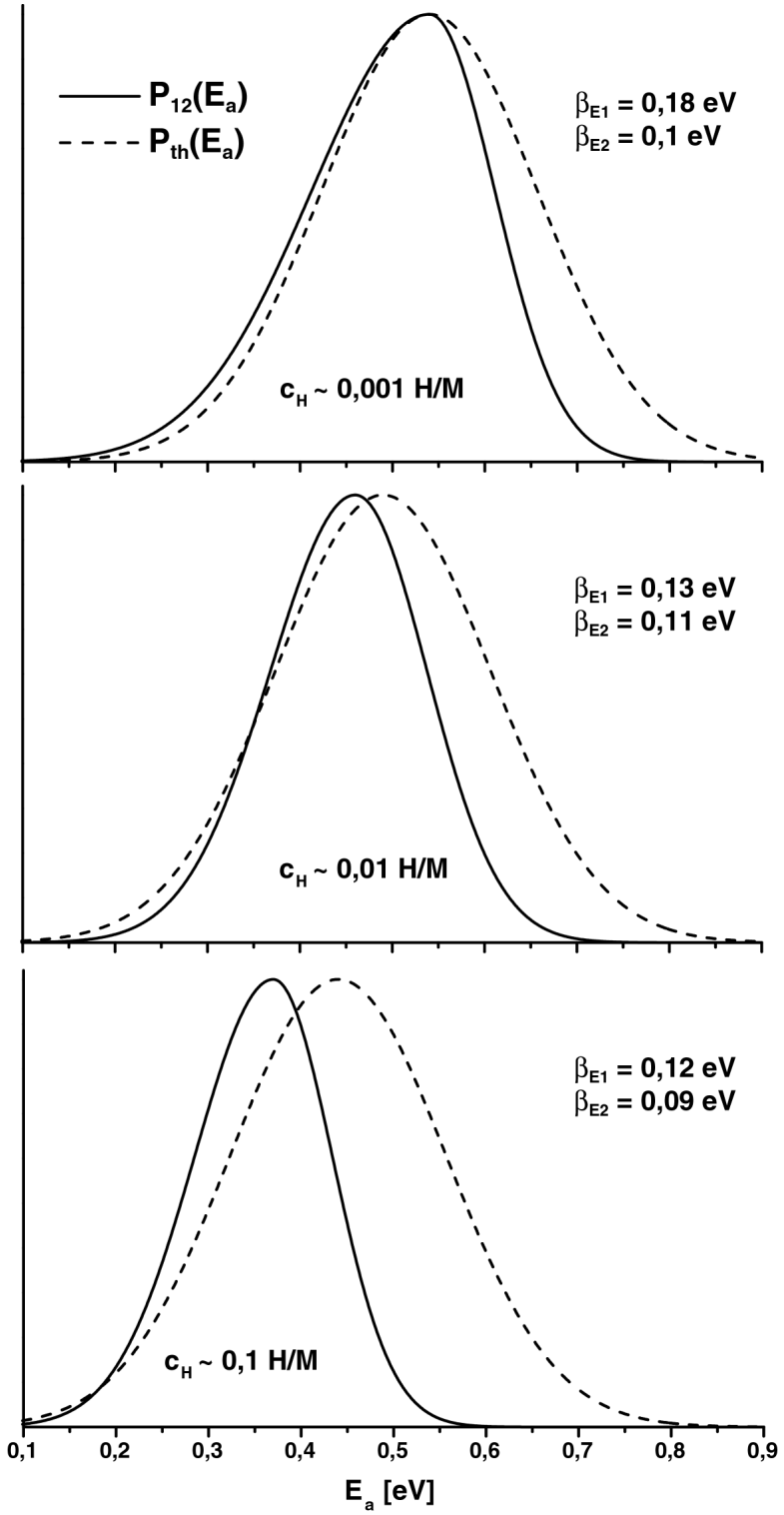

Figure 4.16: *Distribution of activation energies $P_{12}(E_a)$ used for the simulations of Fig. (4.15) and comparison with the theoretical $P_{th}(E_a)$ characterized by the parameters defined in Eqs. (4.8) and (4.9).*

what happens in the model; this effect could already be observed in the plots of Fig. (4.13) where the theoretical curves exhibited a different slope in comparison to the experimental data. Again this could be explained by considering the number of available Zr_4 tetrahedra which, in the ideal case of pure amorphous Zr, is of course greater than in our alloys. The reason for the different slope is then the same as the one we addressed when explaining the similar effect on $CoZr_2$ and in our glasses.

Concluding this paragraph we feel that the model based on Richards' work can explain fairly well several experimental findings concerning the internal friction of hydrogen in metallic glasses. Some aspects which would need further attention regard for example the possibility of choosing an asymmetrical distribution of activation energy which better resembles the reality than a symmetric Gaussian one; this seems anyway a very complicated task which would imply a reconsideration of a significative part of the model. A second point regards the assumption of a pure amorphous Zr matrix for the successful application of the theory. While this constraint seems reasonable for hydrogen concentration up to 10^{-2} H/M, above this value the agreement between experiment and theory became less accurate. In other words, the presence of interstitial sites characterized by a different chemical composition (Zr_3Ti or Zr_3Cu for example) and whose importance became more evident with an increase of c_H cannot be taken into account by the model.

4.4 MHS of quasicrystalline samples

In a previous chapter we pointed out that the observation of a mechanical loss peak depending on short range reorientation of elastic dipoles formed by hydrogen impurities is limited to certain specific crystalline or amorphous structures. When we began our investigations it was not clear if the new class of materials known as quasicrystals possessed the necessary characteristics for the manifestation of the hydrogen induced internal friction. Our measurements pointed out for the first time that such phenomenon exists [35], at least in the metastable quasicrystalline state formed upon annealing of as spun amorphous $Zr_{69,5}Cu_{12}Ni_{11}Al_{7,5}$ ribbons. More work is still in progress for the verification of this experimental evidence on other types of icosahedral quasicrystalline alloys, belonging in particular to the Ti-Zr-Ni family where a related peak of ultrasonic attenuation was discovered independently [36]. In this paragraph we will describe our findings on the H-induced damping in this new and interesting class of materials and we will discuss the implications as far as the existence of an icosahedral short range order in the precursor glassy state of the alloys is concerned.

4.4.1 H-induced damping spectra

The internal friction was measured after the preparation of the samples in their icosahedral quasicrystalline state according to the lines described in chapter 3, and the structure of most samples was examined by transmission electron microscopy after the damping measurements. Several specimens were tested in the temperature range 100-500 K at acoustic frequencies, and some selected results obtained for increasing hydrogen concentration are presented in Figs. (4.17), (4.18) and (4.19). In the captions we refer to different ranges of c_H: in particular we indicate with "low" the range below $5 \cdot 10^{-3}$ H/M, with "intermediate" the range from $5 \cdot 10^{-3}$ to about 0,1 H/M and finally with "high" we mean that the hydrogen concentration should lie above 0,1 H/M. Unfortunately we cannot say with precision what is the upper limit of c_H reached in the case of Fig. (4.19) because of the lack of a specific H concentration measurement for this specimen, which compels us to relay entirely on the approximate $Q_P^{-1}(c_H)$ relationship shown in Fig. (3.11).

A second set of measurements has been devoted to the calculation of the average activation energy for the H hopping by following the same lines as in the case of the amorphous specimens. The results concerning this point are summarized in Figs. (4.20) and (4.21) which represent, respectively, the temperature shift δT_p of the normalized damping spectra taken at different frequencies and the Arrhenius plot of the peak frequencies against peak temperatures. From the slope and intercept of the fit of the experimental points in Fig. (4.21) we get $E'_a = 0,48 \pm 0,03$ eV and $\tau_0 = 2,5 \cdot 10^{-(14\pm1)}$ s, respectively, for a hydrogen concentration of the order of 10^{-2} H/M.

We are going to discuss further on the implications of our experimental results in the light of existing studies concerning the mechanical loss and the hydrogen storage in quasicrystals.

Mechanical relaxation in quasicrystals

As yet a very small amount of research has been devoted to the internal friction behavior of quasicrystals. The pioneering works consisted of mechanical spectroscopy studies on Al-based alloys characterized by a multigrain [61] or by a single grain [62] quasicrystalline structure. In the first case the authors interpreted the intrinsic loss peak observed at 439 K as the result of a phason jump mechanism. In the second case two different peaks were measured: one at about 400 K (peak A), characterized by $E_a = 0,98$ eV and $\tau_0^{-1} = 10^{15}$ Hz, and one at about 900 K (peak B), with relaxation parameters given by $E_a = 4$ eV and $\tau_0^{-1} = 10^{24}$ Hz. The low temperature effect was ascribed to an intrinsic mechanism consisting of local atomic jumps, possibly of phason type, and the high temperature one was interpreted as a consequence of a collective

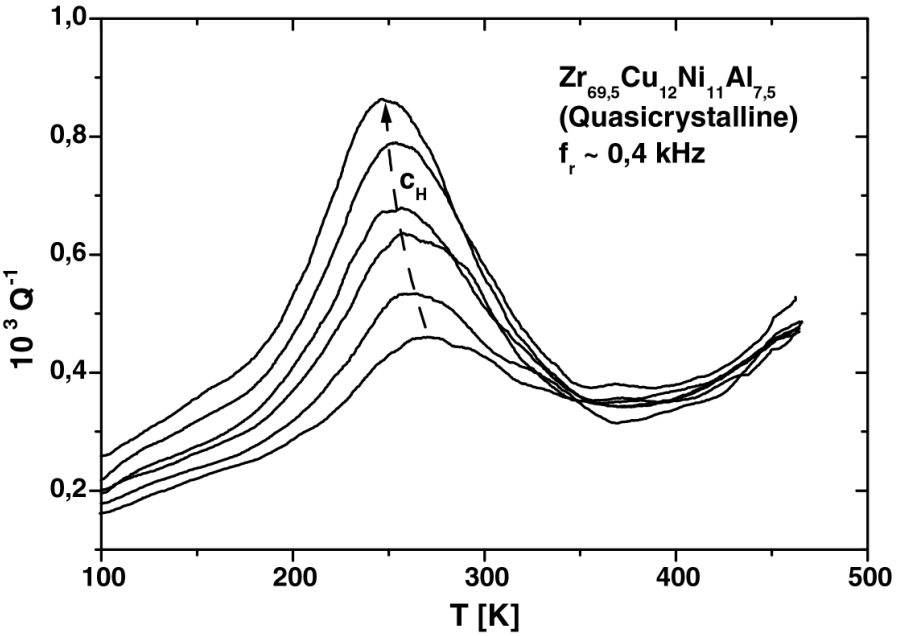

Figure 4.17: *Damping spectra in the "low" c_H range; H-charging time: 4, 9, 14, 19, 24 and 32 hours (1 bar, 457 K); heating rate 2 K/min.*

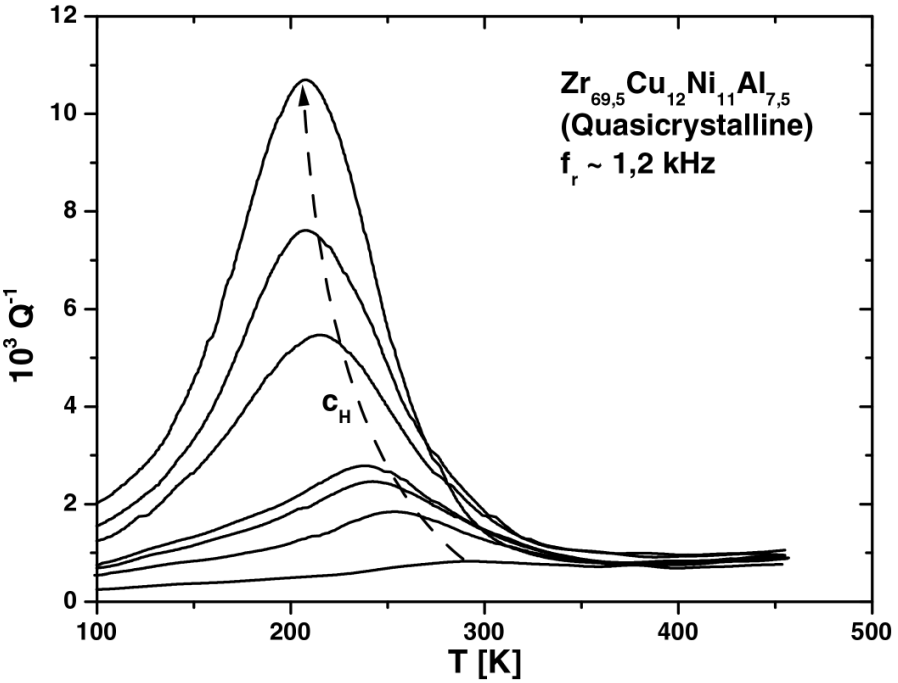

Figure 4.18: *Damping spectra in the "intermediate" c_H range; H-charging time: 17, 83, 101, 143, 228, 245, 280 h (1 bar, 457 K); heating rate 2 K/min.*

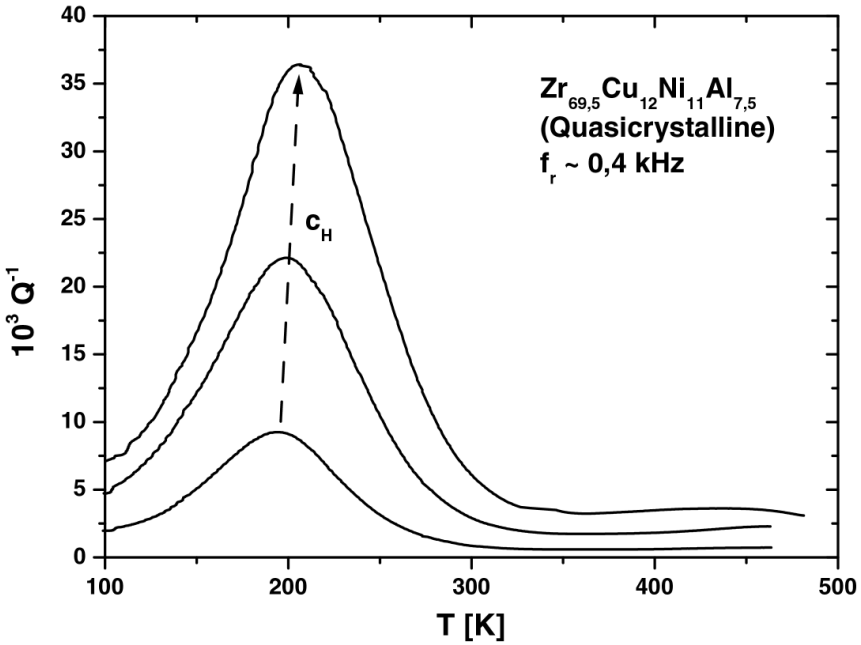

Figure 4.19: *Damping spectra in the "high" c_H range; H-charging time: the top curve was obtained after 80 h (1 bar, 473 K) plus 144 h (300 bar, 373 K). The other curves have been measured after H desorption; heating rate 2 K/min.*

motion of extended defects. Another possible interpretation related to peak A consisted in postulating a reorientation of point defects; this idea was anyway rejected because of the independence of the relaxation strength (peak height) from the concentration of foreign atoms (C, N, O) in the investigated alloy [37].

In the frame of this general picture, in which only mechanical loss effects due to intrinsic properties of the quasicrystals play an important role, it was interesting to discover in our Zr-based icosahedral quasicrystals new damping peaks produced by dissolved hydrogen which, therefore, opened the question whether a Snoek type relaxation is a possible mechanism of internal friction in these materials. The amount of data collected in this work on $Zr_{69,5}Cu_{12}Ni_{11}Al_{7,5}$, the independent results obtained on $Ti_{41,5}Zr_{41,5}Ni_{17}$ in the MHz frequency range with a ultrasonic technique by Foster *et al.* [36] and some recent new investigations carried out on a $Ti_{53}Zr_{27}Ni_{20}$ quasicrystalline alloy [63], strengthen the idea of a H-induced reorientation relaxation in these materials. The problem now is to understand from the structural point of view if a hydrogen atom can create an elastic dipole in the interstitial sites offered by quasicrystals and if such dipoles can re-orientate upon application of an external stress. Since a theory of point defects anelastic relaxation lacks for quasicrystals, we will try

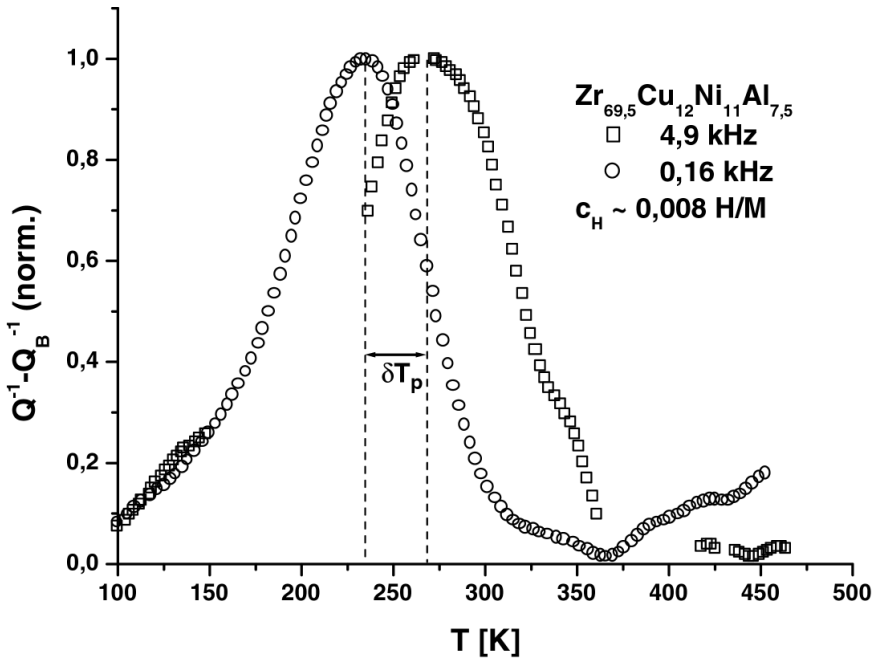

Figure 4.20: *Normalized damping spectra for a quasicrystalline alloy, after a linear background subtraction, for two different measuring frequencies.*

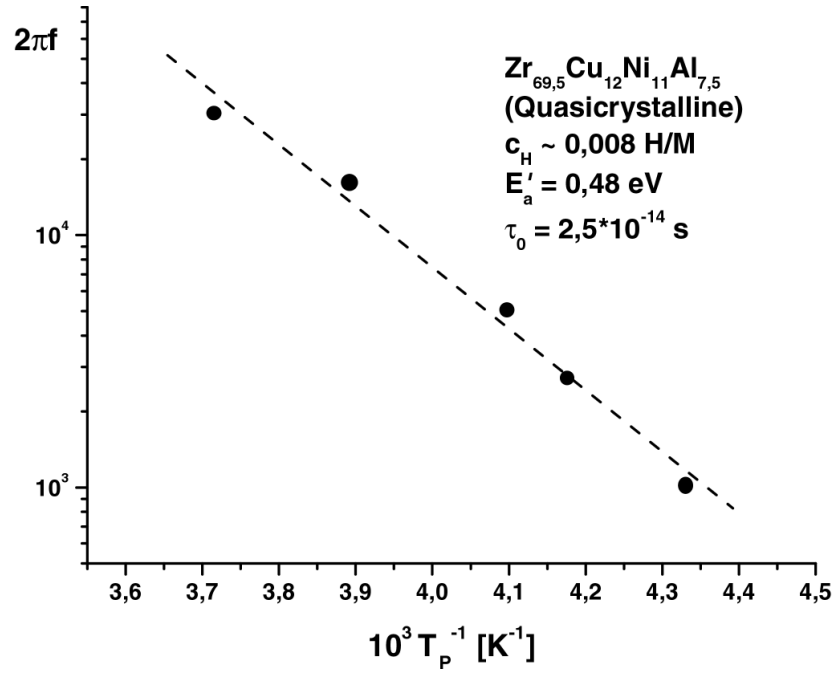

Figure 4.21: *Arrhenius plot of damping peak frequencies against peak temperatures with linear fit of the data.*

to answer to these questions in a qualitative way on the base of the actual knowledge on this topic, starting from the studies on hydrogen storage in the icosahedral phase of the Ti-Zr-Ni system.

Hydrogen in the quasicrystals

Until recently there has been little interest in the hydrogen storage capability of quasicrystals. The main reason seems to lay in the impossibility of loading hydrogen in the Al-based icosahedral phases, which were the first to be discovered and investigated. On the other side, another family of quasicrystals, namely the Ti-based ones, has proven to be excellent for H-storage [64, 65] mainly because of the favorable interstitial site geometry and of the high chemical affinity between the early transition metals, main components of these materials (Ti and Zr in particular), and hydrogen.

Among the useful informations which are needed for the interpretation of our mechanical spectroscopy results, are the *chemistry* of the interstitial sites surrounding a dissolved hydrogen atom and the *geometry* of the site itself. As regards the first problem, almost nothing is known with certainty for the quasicrystalline state of the Zr-Cu-Ni-Al alloy investigated in this work. On the other side, for the Ti-Zr-Ni icosahedral quasicrystals, selected extended X-ray absorption fine structure (EXAFS) [66] and nuclear magnetic resonance (NMR) [67] studies have shown that hydrogen prefers to stay near Zr or Ti atoms. In particular it was shown in Ref. [66], that upon hydrogenation the Ti-Ti, Ni-Ni and Ti-Ni distances remained almost unchanged, while the Zr-Zr and Ti-Zr ones were considerably affected. This observation led the authors to conclude that hydrogen normally sits in an environment surrounded mainly by Zr and partly by Ti atoms. We think that similar considerations should hold also for the metastable quasicrystalline state in $Zr_{69,5}Cu_{12}Ni_{11}Al_{7,5}$, particularly because of the chemical affinity of Zr for hydrogen, by far the highest if compared to all the other elements in this alloy [68].

Concerning the geometry of the interstitial sites in quasicrystals, we start from considering what are thought to be the main building blocks of such structures, that is the Bergman or the Mackay clusters, schematically represented in Fig. (4.22) [65, 69, 70]: the first one consists of an inner regular icosahedron with metal atoms at the center and at its vertices, surrounded by a second shell, always in the form of an icosahedron, with atoms placed at the vertices and at the face centers; the second configuration has the same core as in the Bergman cluster, but the outer icosahedral shell has metal atoms at the vertices and at the edge centers. The main feature of such elementar blocks of the icosahedral quasicrystals consists in the abundance of interstitial tetrahedral sites which can possibly be occupied by hydrogen. Just by looking at the structure of these basic units, and considering that not all of the available

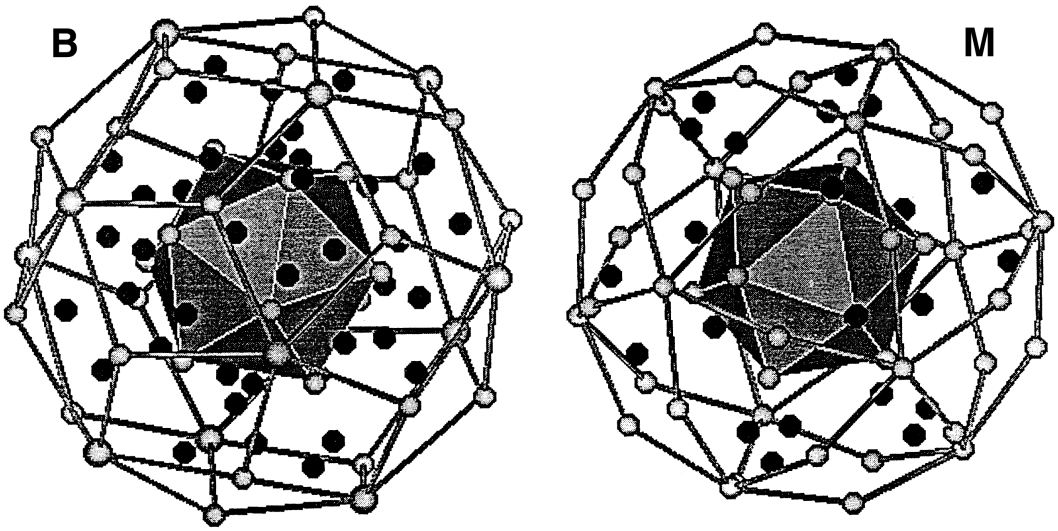

Figure 4.22: *The Bergman (B) and Mackay (M) clusters: metal atoms are grey and all possible tetrahedral interstitials are black. The inner icosahedral shell is shaded and can accommodate up to 4 additional H atoms [64].*

sites can be simultaneously occupied due to the Switendick criterion, it turns out that the Bergman (Mackay) cluster can accommodate up to 48 (28) hydrogen atoms [64]. Since a Bergman (Mackay) cluster contains 45 (55) metal atoms, the theoretical H concentration that can be reached in such structure is 1,07 (0,509) H/M. Even though the experimental evidence has shown that such values are an underestimation of the actual H storage capability of quasicrystals (up to 1,9 and 1,6 H/M have been reported for Zr-Cu-Ni-Al [42] and Ti-Zr-Ni [65] respectively), the importance of these theoretical calculation lies in the possibility of distinguishing between different clusters according to the maximum amount of hydrogen that can be absorbed by the material under investigation. In fact, quasicrystals thought to be based on the Mackay unit have proven to be worse than quasicrystals based on the Bergman cluster, as concerns the maximum H storage capability [64].

The main conclusion of these observations is that hydrogen, in Ti- or Zr-based quasicrystals, sits in tetrahedral sites surrounded by the early transition metals. Our following question concerns the structure of the metastable icosahedral phase in $Zr_{69,5}Cu_{12}Ni_{11}Al_{7,5}$.

Bergman or Mackay?

At present there is no direct experimental evidence which can support a particular structural model for the Zr-based quasicrystals considered in this work. Apart from the high H storage capability of this material which, if we con-

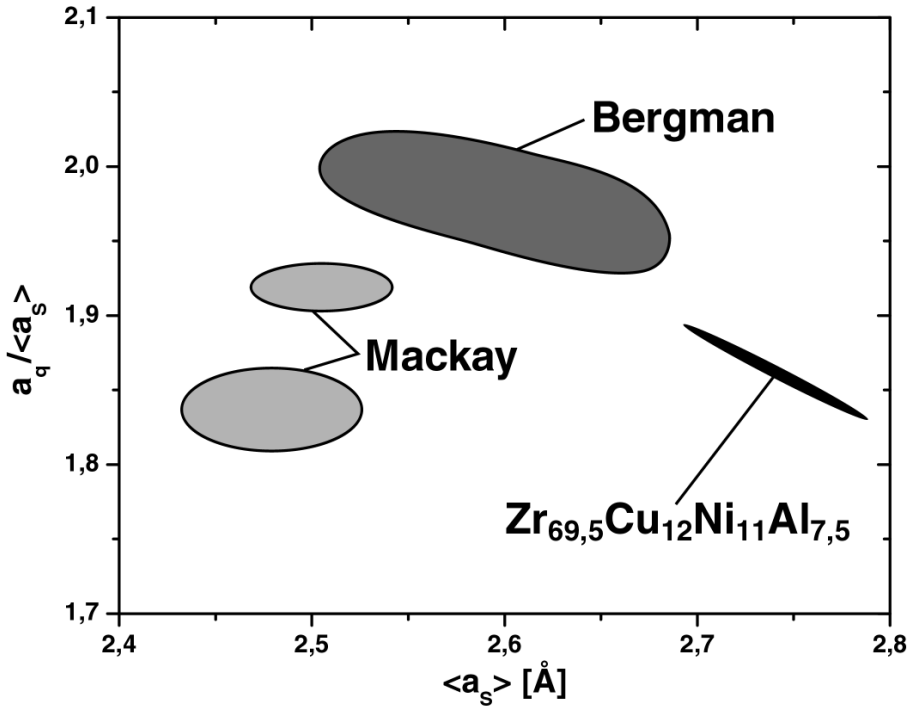

Figure 4.23: *Classification scheme for quasicrystals based on the average atomic separation* $\langle a_S \rangle$ *[72].*

sider the affirmations of the preceding paragraph, suggest a predominance of the Bergman cluster, we found useful a classification scheme based on intrinsic properties of the quasicrystals like the quasilattice parameter a_q, defined after Bancel *et al.* [71] as the position of a particular X-ray diffraction peak of a quasicrystalline structure, and the average atomic separation $\langle a_S \rangle$ [72]. In particular, from the knowledge of the density ρ of the quasicrystal, we can calculate $\langle a_S \rangle = (\langle A_w \rangle / \rho N_V)^{1/3}$, where $\langle A_w \rangle$ is the weighted atomic mass of the alloy and N_V is the Avogadro's number. By plotting the quantity $a_q / \langle a_S \rangle$ against the average atomic separation itself for a large number of quasicrystalline systems, Kim *et al.* were able to show that there exist definite ranges which delimit the alloys based on the Bergman unit from the ones based on the Mackay cluster [72]. In Fig. (4.23) we report these findings and we add our estimate as regards $Zr_{69,5}Cu_{12}Ni_{11}Al_{7,5}$, for which the quasilattice constant is $a_q = 5,06$ Å [12]; our results are affected by a poor precision in the determination of the density, which we carried out through Archimedes weighing¶ with

¶The precision which can normally be obtained with this method is high, but in our case the influence of surface tension upon immersion in water of our too light melt spun samples, has caused an excessive scattering in the measured weight.

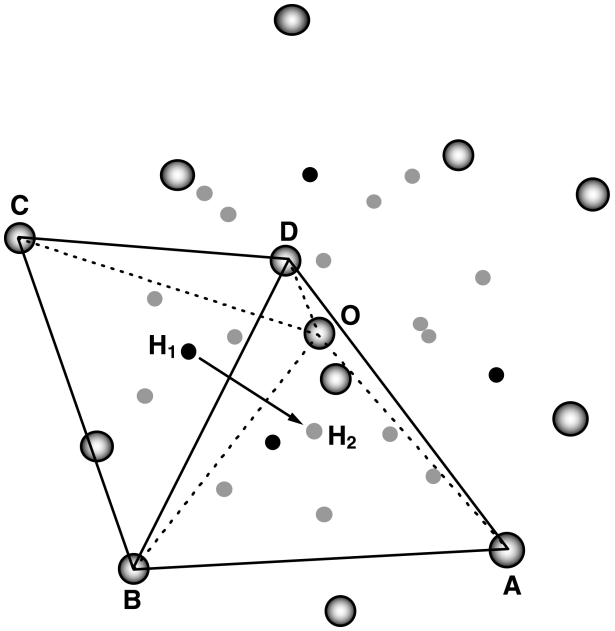

Figure 4.24: *A regular icosahedron with 12 metal atoms at its vertices and 1 at its center (big circles). The small circles represent the centers of the 20 possible tetrahedral sites for interstitial hydrogen; of these only the 4 black ones can be simultaneously occupied. Emphasized is a possible H-reorientation jump between adjacent sites ($H_1 \leftrightarrow H_2$). Eventual blocking effects are here not considered.*

the result $\rho = 6,45 \pm 0,3\ \mathrm{g\,cm^{-3}}$, and this is the reason why we choose to draw a range instead of a single point. From the plot no definitive conclusion can be taken since no clear tendency towards a particular structure can be discerned.

Since the uncertainty in the determination of the structure is still quite big, we prefer in the following to concentrate only on the inner icosahedral shell, which is common to both Mackay and Bergman clusters, in order to show what is our perception of a possible reorientation relaxation mechanism due to hydrogen in a quasicrystalline phase.

Qualitative H-reorientation relaxation model

In Fig. (4.24) we have drawn a regular icosahedron with metal atoms at its center (denoted with the letter O) and at its vertices (denoted A, B, ...). The possible interstitial sites for hydrogen are 20 and are all tetrahedra, each one formed by the central atom and three other atoms delimiting a face of the icosahedron; the position of hydrogen in such sites is indicated by the small circles, among which the 4 black ones represent a possible combination of interstitial sites which can be simultaneously occupied by hydrogen. From the knowledge of the space coordinates of the metal atoms and of the interstitial positions [73, 64], we can calculate the main distances characterizing the structure. In particular, by writing each length in units of the quasilattice parameter, we obtain: $OA = 0,5$; $AB = 0,526$; $OH_1 = 0,298$; $BH_1 = 0,319$; $H_1H_2 = 0,213$. Let's concentrate first of all on the center-vertex distance OA and the vertex-vertex distance AB. In a *regular* tetrahedron we would have $OA = AB$ and

the center of the figure would be equidistant from all the 4 vertices: the insertion of a hydrogen atom would cause, in such interstitial position, an isotropic variation of the metal-metal distances and a reorientation relaxation would be in this case impossible. On the other side, in the regular icosahedron shown in Fig. (4.24), the tetrahedral sites are *irregular*, as expressed by the condition $OA \neq AB = BD = DA$, so that a hydrogen interstitial lies closer to the central rather than to the outer metal atoms ($OH_1 < BH_1$). In this situation the distortion field caused by hydrogen has trigonal symmetry and a relaxation caused by the elastic dipole reorientation is in principle possible, assuming that the icosahedral quasicrystal without the presence of point defects has a symmetry system higher than trigonal.[‖] In order to emphasize the hydrogen hopping process, we have drawn in Fig. (4.24) two neighboring tetrahedral sites and the possible reorientation jump from position H_1 to H_2. In this schematic model the possible blocking effects due to the saturation of the available interstitial sites is not taken into account and its consideration is not the scope of this work. More important for our purposes is the fact that, until now, we have referred to the ideal situation of a regular geometry for the icosahedral structure and a single type of metal atoms. In the case of an alloy, it is natural to expect a greater variety of distorted tetrahedral sites, and consequently a broadening of the spectrum of site and activation energies for the H hopping processes.

We have seen that, at least qualitatively, the occurring of anelastic relaxation due to hydrogen is plausible in icosahedral quasicrystals. Similarly to the amorphous case, the shift of the relaxation peak in the low and intermediate ranges of H concentration (Figs. (4.17) and (4.18)) may be explained by the filling of the site energy distribution obeying a Fermi-Dirac statistics (cf. section 2.6). In the light of these considerations we find interesting the discussion of the mechanical spectroscopy results in the high H concentration range, that is $c_H > 0,1$ H/M.

Damping at high hydrogen concentration

Referring to Fig. (4.19), we have seen how the peaks shift to higher temperatures for increasing H content, which is at a first look somewhat surprising. This anomalous effect can be explained if we think that there are two mechanisms regulating the dependence of the activation energy for the H reorientation relaxation on c_H: on one side, we know that hydrogen occupies places with increasing equilibrium site energy, starting with the most favorable ones. Following the arguments of paragraph 2.6 and 4.3.4, this is the

[‖]The last affirmation seems plausible, since it has been demonstrated that icosahedral quasicrystals are elastically isotropic materials [74].

reason why the activation energy decreases when c_H increases. On the other side, we have seen how, in the case of amorphous structures, there is a clear tendency of the activation energy to increase when the average Zr-Zr distances grow. These two processes act together and the actual shift of our damping peaks is the result of a combination between these opposing tendencies. Now, starting from $c_H \gtrsim 0,1$ H/M, the quasilattice parameter in quasicrystalline $Zr_{69,5}Cu_{12}Ni_{11}Al_{7,5}$ grows with the H content [75], meaning that the Zr-Zr distances also increase. Therefore, we suppose that in the "high" H concentration range the tendency towards higher activation energies due to the dilatation of the Zr-Zr distances is, in our samples, stronger than the competing process relative to the occupation by hydrogen of unfavorable interstitial sites.

Among the consequences of the existence of a damping mechanism due to hydrogen in quasicrystals, is the possibility of comparing the spectra obtained for the amorphous and the icosahedral phases. This is the problem addressed in the next paragraph.

4.4.2 Glassy and quasicrystalline states: similar SRO?

The most interesting feature of the damping spectra observed in quasicrystalline $Zr_{69,5}Cu_{12}Ni_{11}Al_{7,5}$ is their broad outline, if compared to a pure Debye relaxation, and their asymmetric shape with a long tail on the low temperature side. Such characteristics are extremely similar to the ones found in the precursor amorphous state of this alloy; a direct comparison of the results between these two phases is shown in Fig. (4.25), where an inverse temperature scale has been chosen, in order to emphasize the asymmetry of the spectra. Moreover, the calculation of the average activation energy gave very similar results for both phases (about 0,48 eV at a concentration of $3 \cdot 10^{-3}$ and $8 \cdot 10^{-3}$ H/M for the amorphous and quasicrystalline state, respectively), again indicating that a comparable relaxation mechanism is involved. By using MHS for comparing the relaxation parameters given by the peak temperatures and peak heights, the similarity between these different states of the alloy is even clearer. It appears in fact from Fig. (4.26), which represents a collection of data taken from several samples, that the temperature shift upon hydrogenation is the same, inside the experimental errors, for the glassy and for the quasicrystalline phase. The high concentration range, as discussed in the last paragraph for the quasicrystalline phase, apparently dominated by the H-induced expansion of the quasilattice, could not be included in this comparison because there were no data on amorphous samples in this range.

All the aforementioned observations point in the direction of an internal friction mechanism governed by local jumps of hydrogen between neighboring tetrahedral sites, indicating therefore that a polytetrahedral short range

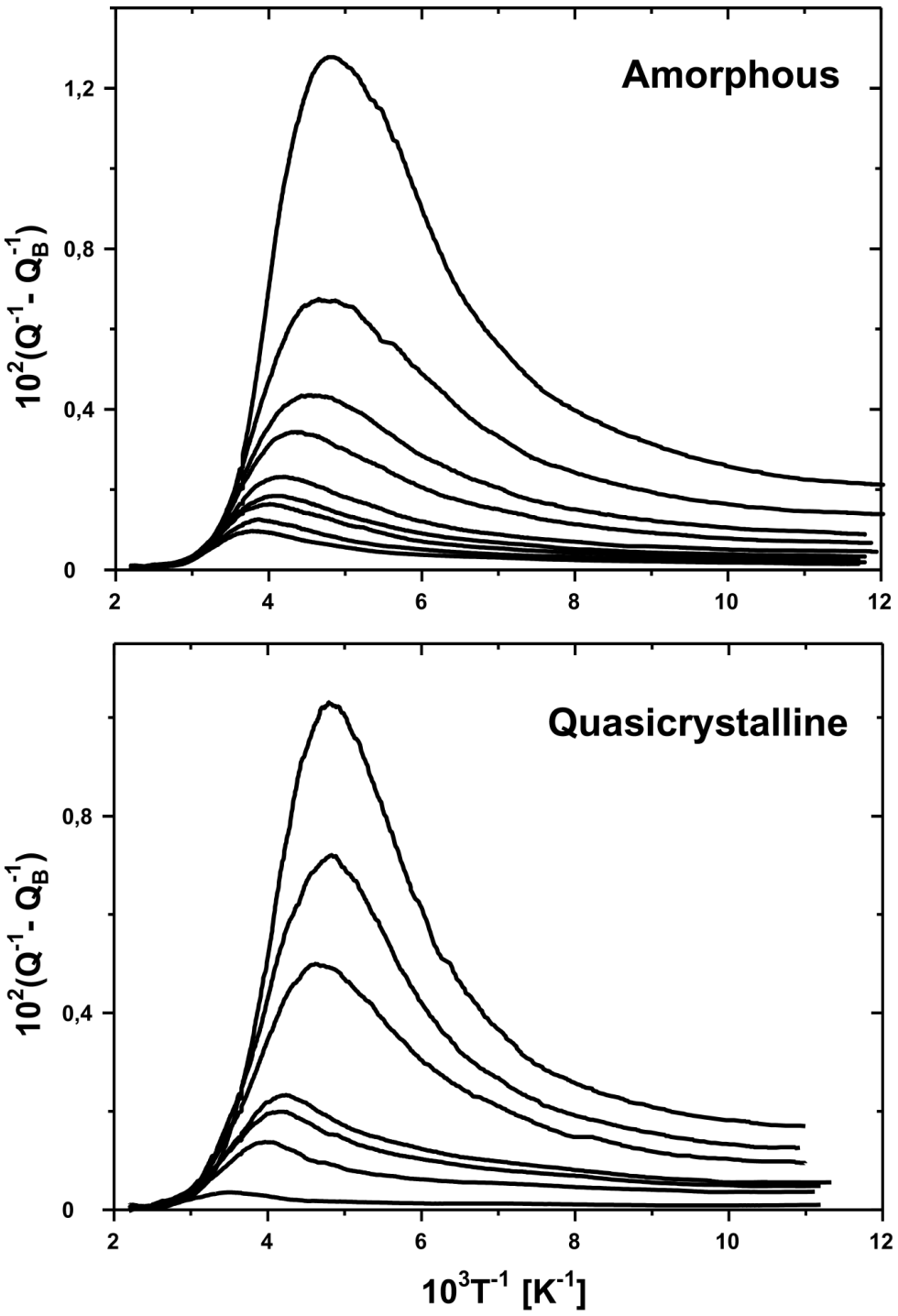

Figure 4.25: *H-induced internal friction, after a linear background subtraction, for increasing c_H in the glassy and quasicrystalline states of $Zr_{69,5}Cu_{12}Ni_{11}Al_{7,5}$; H-charging times: between 33 and 196 h (1 bar, 453 K) in the glass, between 17 and 280 h (1 bar, 453 K) in the quasicrystals; heating rate 2 K/min; $f_r \backsimeq$ 1,1 kHz.*

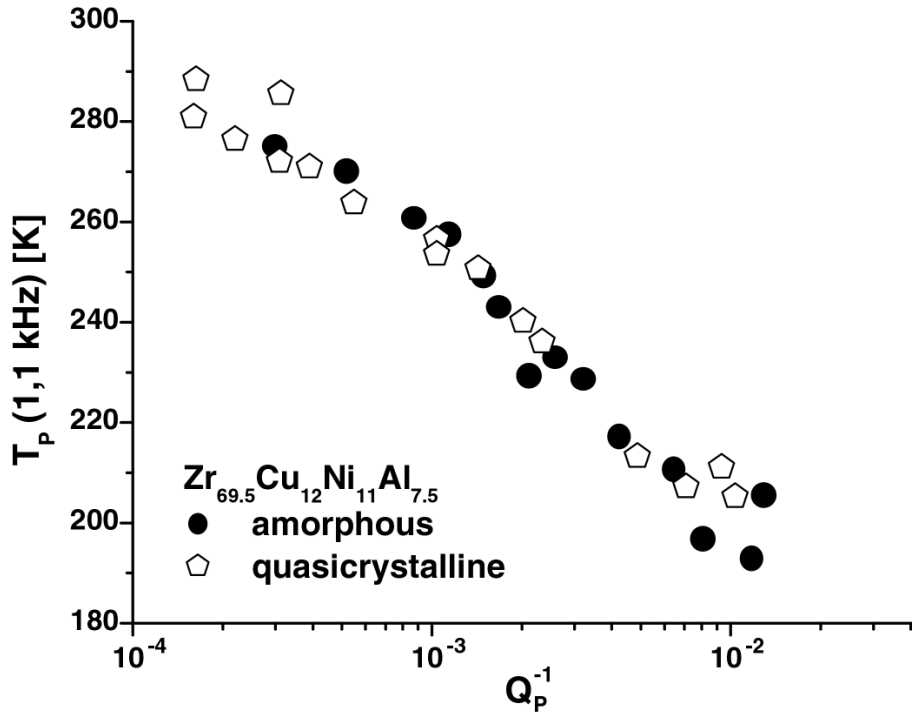

Figure 4.26: *Comparative MHS results for the amorphous and icosahedral phases of a Zr-Cu-Ni-Al system.*

order dominates these structures. This conclusion is only partly surprising since, for example, measurements of the interfacial energy between the undercooled liquid and the icosahedral phase of $Zr_{69,5}Cu_{12}Ni_{11}Al_{7,5}$ gave a result of 13 $\mathrm{mJ\,m^{-2}}$, which is about ten times smaller than between the crystalline state and its melt [13]. Moreover, it was already postulated that icosahedral SRO should be present in the amorphous phase [5] and, vice versa, that the icosahedral phase is dominated by local tetrahedral order, as it was shown in the preceding paragraphs in connection with the description of the Bergman and Mackay clusters.

Even though there is a noteworthy similarity among the internal friction spectra in the structures we analyzed, such curves are nevertheless not completely equal, especially in the higher hydrogen concentration ranges. In fact, for $c_H \simeq 0,1$ H/M, we measured somewhat broader damping curves in the amorphous samples than in the quasicrystalline ones, as shown in Fig. (4.27). The reason for this lies probably in the different distributions of activation energies for H hopping, which seems to be narrower in the icosahedral phase than in the completely amorphous one. Considering that even in a monatomic Bergman type cluster there are at least four different types of tetrahedral sites (one in

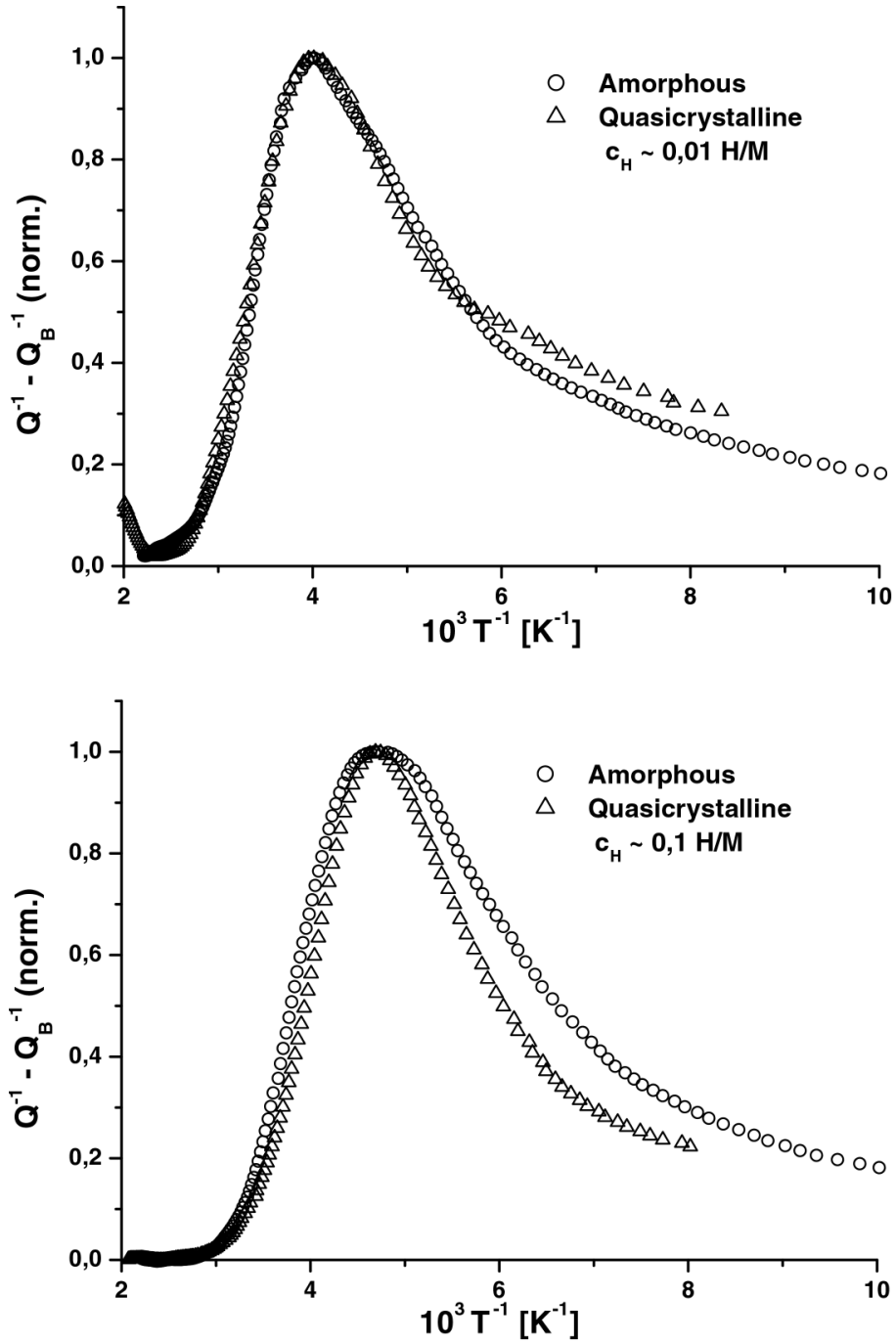

Figure 4.27: *Normalized damping spectra for glassy and quasicrystalline* $Zr_{69,5}Cu_{12}Ni_{11}Al_{7,5}$ *in two H concentration ranges; for a better comparison the temperature scale has been adjusted to compensate for the shift due to the different measuring frequency between the samples.*

the inner icosahedral shell and the others between the inner and the outer shells), and that there must exist an additional differentiation of the interstitial sites due to the presence of four atomic species, we expect, as pointed out previously, a rather broad spectrum of activation energies in quasicrystalline $Zr_{69,5}Cu_{12}Ni_{11}Al_{7,5}$. The point is, that we also expect an even *broader* distribution in the respective amorphous structure, due to the presence of a greater variety of sites, and this is indeed confirmed by our measurements, at least for relatively high hydrogen concentrations. On the other side, we notice from the first plot in Fig. (4.27) that the internal friction spectra are characterized, when the H concentration lays about $c_H \simeq 10^{-2}$ H/M, by the same full width at half maximum, again indicating the high similarity of SRO between these structures.

Discussion

One of the questions posed at the beginning of this work regarded the structural reasons for the destabilization of an undercooled melt. A very different SRO between the amorphous and the respective crystalline equilibrium phase is one of the main conditions which favors a deep undercooling and, therefore, the production of bulk metallic glasses. This is the reason why the damping spectra of our amorphous alloys are different from the ones measured in their crystallized states (as it will be shown in a following paragraph). But what is the role of the metastable phases which are normally built during the devitrification sequence? The formation of an icosahedral quasicrystalline state in $Zr_{69,5}Cu_{12}Ni_{11}Al_{7,5}$ gave us the opportunity of analyzing the SRO of this structure and comparing it with the glassy one. From our results it clearly emerges that, at least from the geometrical point of view, the icosahedral SRO is dominating in the amorphous phase. Consequently, the quasicrystalline state seems the best candidate for the initial destabilization of the undercooled melt. In the meantime, a considerable number of bulk amorphous alloys has proven to start the devitrification sequence through the formation of quasicrystals [13, 14, 76]. It seems that the geometrical SRO of the bulk glasses favors the nucleation of a quasicrystalline phase, degradating therefore the stability of the undercooled melt. An important role is assumed then by the chemistry of the alloy: if the chemical composition of the glass is considerably different from the range of existence of the respective icosahedral phase, then the nucleation of the quasiperiodic structure can be hindered. This could be a possible explanation of the different stability against crystallization observed in different bulk glasses.

4.5 MHS of crystalline samples

In the previous section we mentioned that the H-induced internal friction in crystallized Zr-based alloys differs significantly from the one observed in the respective amorphous and quasicrystalline phases. This can be seen for example in Figs. (4.28) and (4.29), where the developing of the spectra with increasing hydrogen concentration ($0,002 < c_H < 0,05$ H/M) is presented for two different materials. These hydrogen induced damping effects are much broader on the temperature scale than those measured in the precursor glasses (see Fig. (4.6)) and are characterized by two or three different peaks. For the interpretation of these results, we must pay attention to two different aspects: the grain size of the polycrystalline samples and their crystalline structure. We start from considering what kind of crystalline phase is built upon devitrification of our Zr-based glasses. It turns out that these alloys mainly crystallize in the tetragonal $CuZr_2$ system, where Ni or Al atoms occupy some of the sites normally taken by Cu [77, 78]. By giving a look to the unit cell of this structure, which is schematically drawn in Fig. (4.30), it was concluded that, at least at low hydrogen concentrations, the H atoms should occupy either the octahedral (Zr_5Cu) or the tetrahedral (Zr_3Cu) sites [79]. Among these, only the tetrahedral ones have the necessary symmetry requirements for the occurring of a Snoek type relaxation, but the distance between two such neighboring sites, as calculated following a hard spheres model, is only 0,29 Å (compared to the hole radii of 0,46 Å and 0,48 Å for the octahedral and tetrahedral sites, respectively), which is much too short to account for the activation energy of 0,50 eV measured for the peaks located at about 280 K in such systems [80].

In fact, similarly to the known behavior in bcc metals (cf. paragraph 2.6), one may even expect a delocalization of H within these groups of 1 octahedral plus 4 tetrahedral sites. The only other possible short range mechanism that can explain the internal friction observed at this temperature is a Zener type reorientation of H-H pairs between the octahedral sites [63]. This situation concerning the short-range reorientation, and the underlying configuration of interstitial sites, is completely different from a polytetrahedral structure and underlines again the big difference in local atomic structure between the amorphous and quasicrystalline phases on the one, and the crystalline equilibrium phase on the other side.

Concerning the broad peaks observed at high temperatures, the mechanism is of different nature and originates basically from an intercrystalline diffusion of hydrogen. Such process is induced by the elastic anisotropy of the grains in the polycrystalline specimen: due to such anisotropy, zones of compression and dilatation are created on the scale of the grain size when an external mechanical stress is applied to the specimen. Hydrogen tends then to diffuse

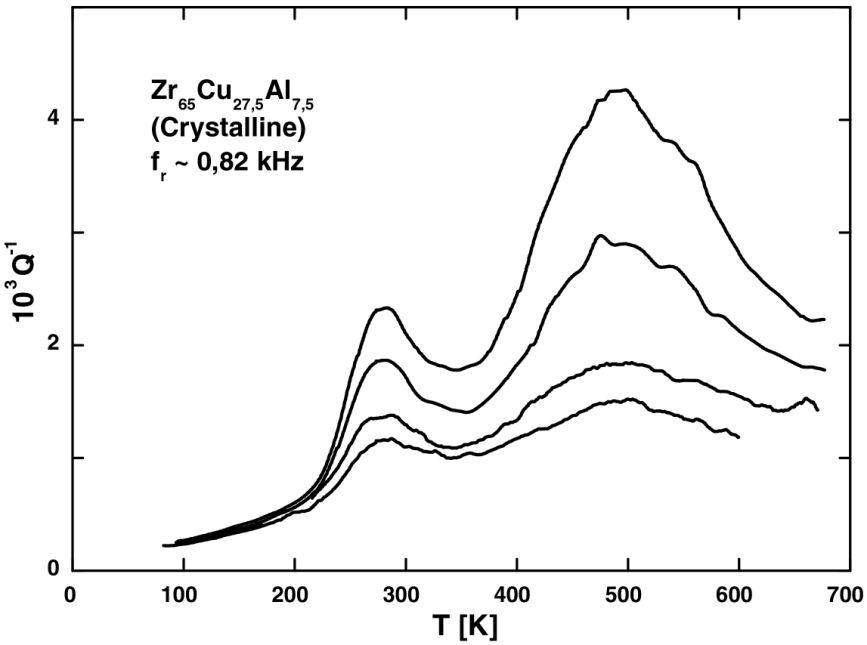

Figure 4.28: *Damping spectra in a crystallized Zr-Cu-Al alloy; H-charging times: 19, 61, 88, 130 h (1 bar, 473 K); heating rate 2 K/min.*

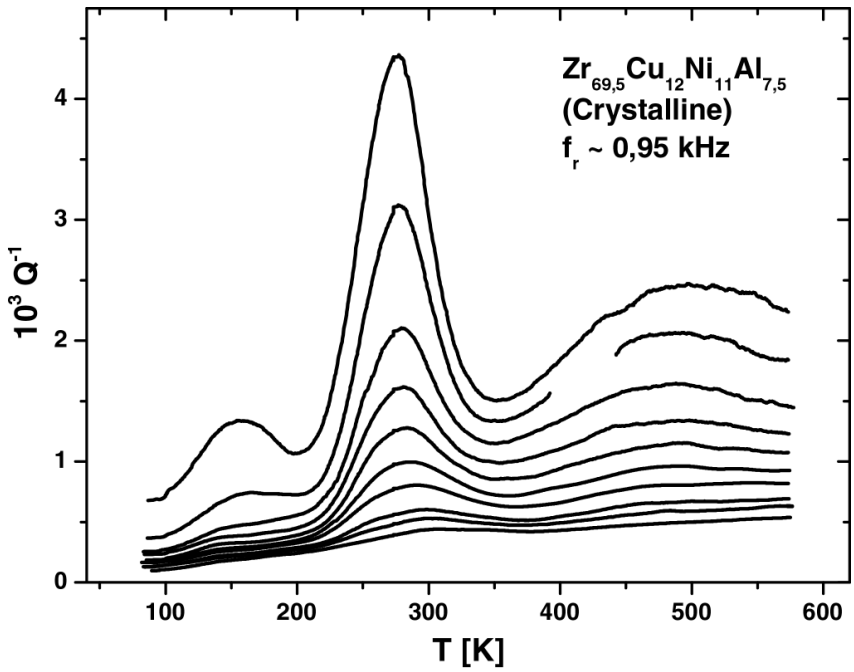

Figure 4.29: *Damping spectra in a crystallized Zr-Cu-Ni-Al alloy; H-charging times: 18, 36, 48, 67, 99, 141, 207, 248, 355, 660 h (1 bar, 453-473 K); heating rate 2 K/min.*

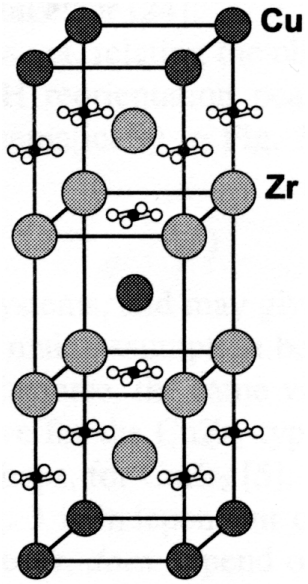

Figure 4.30: *Unit cell of* $CuZr_2$ *with the positions of the* Zr_5Cu *octahedral and the* Zr_3Cu *tetrahedral sites, indicated, respectively, by the small black and by the small white circles [63].*

from the compressed to the dilated parts, generating a medium-range** Gorsky-type relaxation. The nature of this internal friction mechanism has induced its discoverer to call it *intercrystalline Gorsky effect* [80]. One of the starting points which led to the investigation of this new mechanical loss source, was the observation of the position's dependence of the high temperature peaks on the grain size of the specimens. In particular, it was shown that for bigger and bigger dimensions of the grains, the damping peaks shifted to higher and higher temperatures [81]. An emblematic example concerns the comparison of the spectra for crystalline $CuZr_2$ on one side and $Zr_{65}Cu_{27,5}Al_{7,5}$ on the other side: in Fig. (4.31) we can see two bright field TEM pictures clearly indicating the different dimensions of the grains. At the same time, while in the ternary alloy the high temperature peak is situated at about 500 K (Fig. (4.28)), for the binary $CuZr_2$ compound the peak lies above 700 K [63, 81].

A first quantitative treatment, both of the relaxation time and of the relaxation strength, was given by Sinning [80] for this new intercrystalline Gorsky effect. However, because this medium range diffusion mechanism in its present state of description (exclusively in polycrystals) is completely distinct from the glassy state and from the questions of SRO discussed mainly in this work, a detailed consideration is beyond our aims. Only the kinetic aspect will be addressed briefly, since a comparison between the relaxation time τ_{IG} for the Gorsky mechanism and the respective quantity τ_R concerning a short range re-

**The well known Gorsky effect takes place because of atomic long range diffusion on the scale of the sample's thickness. Here we deal with a phenomenon which happens on the scale of the grain size and from this comes the word "medium-range".

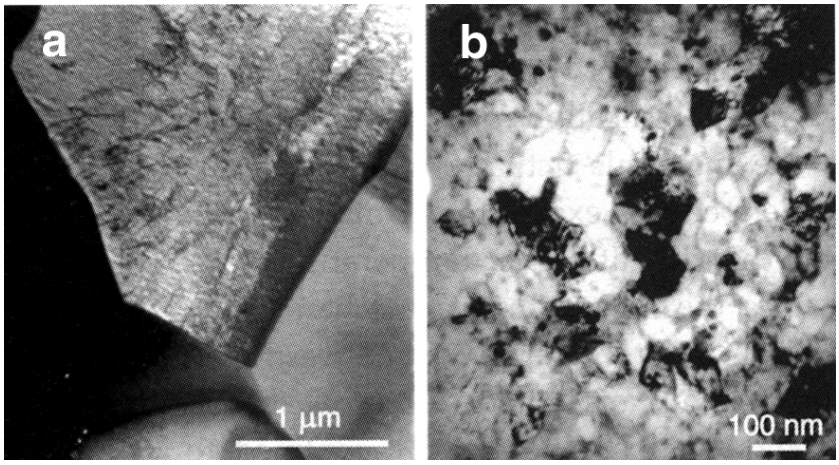

Figure 4.31: *Bright field TEM images for crystallized* $CuZr_2$ *(a) and* $Zr_{65}Cu_{27,5}Al_{7,5}$ *(b).*

orientation mechanism allows for a very clear distinction between both types of processes. We consider here only the case in which the short-range and long-range mechanisms are both governed by the same diffusion coefficient D, which is obvious for the $CuZr_2$ structure as discussed above, but may not be valid in general. In this case the two relaxation times can be written as

$$\tau_{IG} = \frac{d^2}{3\pi^2 D} \qquad \text{and} \qquad \tau_R = \frac{a^2}{\beta D}\,, \tag{4.16}$$

where d is the grain size and a the lattice constant. The factor β depends on the crystallographic details of the short range reorientation. The relaxation times are thermally activated and obey an Arrhenius relationship, with an activation energy E_a which is the same as for diffusion, but with pre-exponential factors which differ according to the ratio $(d/a)^2$ (if we suppose, in contrast, that both peaks e.g. in Fig. (4.28) are determined by short-range hydrogen hopping, then the pre-exponential factors should be the same in both cases, while the activation energy should change considerably). By taking $d \simeq 30$ nm as a typical grain size for polycrystalline Zr-Cu-Al(-Ni) and $a = 0,322$ nm for $CuZr_2$ [82], it turns out from Eq. (4.16) that the pre-exponential factors for short and medium-range mechanisms should differ by approximately four orders of magnitude.[††] This statement has been indeed experimentally verified in the case of $Zr_{65}Cu_{17,5}Ni_{10}Al_{7,5}$, which also crystallizes mainly in the tetragonal $CuZr_2$ phase; here an activation energy $E_a = 0,50 \pm 0,03$ ($E_a = 0,52 \pm 0,06$) eV and a pre-exponential factor $\tau_0 = 10^{-13,5\pm0,6}$ ($\tau_0 = 10^{-9,4\pm0,6}$) s was

[††]We did not consider the factor $\beta/3\pi^2$ in the calculation because it is of the order of unity.

measured for the low (high) temperature peaks, respectively [80]. This result confirms the existence of the intercrystalline Gorsky effect, but leaves open some questions, like the one concerning its relaxation strength in relation to that of the short-range process, manifestly different for alloys with similar grain sizes but different chemical compositions, as shown for example in Figs. (4.28) and (4.29).

Before concluding this paragraph we want to discuss briefly the internal friction peak occurring at 150 K in the case of $Zr_{69,5}Cu_{12}Ni_{11}Al_{7,5}$ as seen in Fig. (4.29). Such effect is typical of this composition and was not found in the other crystallized Zr-based alloys investigated in this work. A quantitative description of this effect is not our aim, but at least qualitatively it seems that the peak can be linked to the presence of the $NiZr_2$ phase. In fact, among the alloys crystallized starting from different Zr-based bulk glasses, $Zr_{69,5}Cu_{12}Ni_{11}Al_{7,5}$ was the only one which contained a significative amount of the aforementioned phase [83]. Moreover, it is known that a hydrogen damping peak appears in the same temperature range in crystalline $NiZr_2$ [15, 16, 33].

Chapter 5

Conclusions

In this work the vibrating reed technique has been used for the investigation of the anelastic properties of several Zr-Ti-Cu-Ni-Be and Zr-Cu-Al(-Ni) alloys, previously prepared in their amorphous or (quasi)crystalline phases and successively hydrogenated. Our results have shown interesting aspects concerning, on one side, the methodology of Mechanical Hydrogen Spectroscopy (MHS) and, on the other side, the microstructure and atomic short-range order of the different materials investigated.

One of the questions for which we intended to give an answer, was whether MHS could be applied with success to our Zr-based bulk glasses: in particular, we wanted to check the theoretical predictions concerning the calculation of the activation energy E_a for H-hopping in a model amorphous structure [1] with our experimental results. Of interest was not only the comparison of the theoretical and experimental value of $\langle E_a \rangle$ in different H concentration ranges, but also the whole activation energy spectrum, whose spread is responsible for the broad outline of the measured internal friction peaks.

Through the model proposed by Richards and used in this work, it was possible to calculate a priori a theoretical Gaussian distribution $P_{th}(E_a)$ for hydrogen hopping in an amorphous structure. Moreover, the H concentration dependence of $\langle E_a \rangle$ could be computed, for different ratios of hydrogen-metal atoms interaction forces a_E and a_S in the equilibrium site and saddle point positions respectively, by assuming a tetrahedral site occupancy and a Gaussian radial distribution function in the metallic glass. The results have shown that, by taking $a_S/a_E = 1,5$ there is a good agreement between the theory and the experiment as far as the dependence of E_a on c_H is concerned, in particular at low hydrogen concentrations. The numerical value of 1,5 was already postulated qualitatively by Sinning [19]: now such prevision is supported on a more quantitative base.

Another interesting point is the dependence of the slope of the $\langle E_a \rangle (c_H)$ function on the amount of Zr contained in the different alloys. The experimental

observations tell us that for lower and lower Zr content, the average activation energy decreases faster and faster when the amount of dissolved hydrogen increases. This effect can be explained by considering that hydrogen occupies the available interstitial sites following a Fermi-Dirac statistic, with different densities of the preferred Zr-surrounded sites at different Zr contents.

MHS has been also a useful tool to emphasize the difference in the SRO of the Zr atoms between the Inoue and Johnson-type alloys: at least for that part of the partial radial distribution function which is scanned by MHS at low hydrogen concentrations, a larger average Zr-Zr nearest neighbors distance was found in the Zr poorer, rather than in the Zr-richer, alloys.

Finally, answering the first question we posed in the Introduction of this work, we can say that MHS can be applied with success in Zr-based bulk glasses and that the link between the accessible experimental parameters and the SRO of the materials, as expressed by Richards' model, seems convincing, especially in the hydrogen concentration range $c_H \leq 10^{-2}$ H/M.

Concerning our second aim, that is the investigation of the icosahedral quasicrystalline phase produced upon annealing from amorphous $Zr_{69,5}Cu_{12}Ni_{11}Al_{7,5}$, we can summarize as follows. First of all, we have proven for the first time that a hydrogen induced reorientation relaxation is possible in such structures [35]; in the meantime, another group has obtained independently similar results on a Ti-Zr-Ni alloy, by using a different technique [36]. We also proposed a qualitative model according to which the internal friction, measured at room temperature and below, can be attributed to classical H-hopping between adjacent tetrahedral sites. Secondly, we compared the damping spectra originating from the glassy and the quasicrystalline states: from the similarities of such curves in all the investigated H-concentration ranges, we concluded that a similar polytetrahedral SRO dominates both these phases. This interpretation has important consequences as far as the problem of the stability of the undercooled melts is concerned. At least from the geometrical point of view, the formation of metastable quasicrystalline states from a Zr-based glass seems more favorable than the equilibrium crystalline phases. This has been indeed observed experimentally in different types of Inoue and Johnson glasses [13, 14]. One of the possibilities for the suppression of the nucleation of ordered states from the melt could be then to choose an alloy whose chemistry is as far away as possible from a favorable quasicrystalline, as well as crystalline, composition.

The last point discussed was the behavior of the H-induced internal friction in the crystallized Zr-based alloys. The experiments have shown a very different shape of the spectra in comparison to the amorphous and quasicrystalline phases, strengthening the hypothesis of a very different SRO among these structures. The mechanisms of the mechanical relaxation of hydrogen in the

crystalline phases, built upon devitrification of our alloys, are of different nature with respect to the ones in the other phases. In particular, for the peaks at room temperature the most probable explanation is as yet a Zener-type reorientation of H-H pairs in the $CuZr_2$-type phase. The broad spectra measured at higher temperatures derive, on the other side, from an intercrystalline diffusion of hydrogen produced by elastic mismatch strains between adjacent grains, also called intercrystalline Gorsky effect [80]: an important condition for the occurring of such phenomenon is the elastic anisotropy of the grains themselves. The obvious missing of a damping effect based on this mechanism in the poly-quasicrystalline samples is in fact explained with the elastic isotropy of this kind of structure.

Some future work which can originate from our investigations is planned on the following topics: the measurement of the H-induced damping in stable quasicrystalline alloys, in particular belonging to the Ti-Zr-Ni family, with the aim of a deeper understanding of the anelastic relaxation in the icosahedral phase, for wich a theory is still lacking; a systematic study of the intercrystalline Gorsky mechanism on different polycrystalline samples, including a better understanding of its relaxation strength.

Bibliography

[1] P. M. Richards *Phys. Rev. B*, vol. 27, no. 4, p. 2059, 1983.

[2] A. Inoue, T. Zhang, and T. Masumoto *Mat. Trans. JIM*, vol. 31, p. 425, 1990.

[3] A. Peker and W. L. Johnson *Appl. Phys. Lett.*, vol. 63, p. 2342, 1993.

[4] A. Inoue, *Bulk Amorphous Alloys: Preparation and Fundamental Characteristics*, vol. 4 of *Materials Science Foundations*. Trans Tech Publications, 1998.

[5] J. H. Harris, W. A. Curtin, and M. A. Tenhover *Phys. Rev. B*, vol. 36, no. 11, p. 5784, 1987.

[6] T. Mütschele and R. Kirchheim *Scripta Met.*, vol. 21, p. 1101, 1987.

[7] R. Kirchheim *Acta Mat.*, vol. 29, p. 835 and 845, 1981.

[8] R. Kirchheim *Progr. Mat. Sci.*, vol. 32, p. 261, 1988.

[9] A. Inoue *Mat. Trans. JIM*, vol. 36, p. 866, 1995.

[10] A. Inoue *Acta Mater.*, vol. 48, p. 279, 2000.

[11] E. Matsubara and Y. Waseda *Mat. Trans. JIM*, vol. 36, p. 883, 1995.

[12] U. Köster, J. Meinhardt, S. Roos, and H. Liebertz *Appl. Phys. Lett.*, vol. 69, no. 2, p. 179, 1996.

[13] U. Köster, J. Meinhardt, S. Roos, and R. Busch *Mat. Sci. Eng. A*, vol. 226-228, p. 995, 1997.

[14] N. Wanderka, M. P. Macht, M. Seidel, S. Mechler, K. Stahl, and J. Z. Jiang *Appl. Phys. Lett.*, vol. 77, no. 24, p. 3935, 2000.

[15] H.-R. Sinning, *Anelastische Relaxation von Wasserstoff in intermetallischen Strukturen*. Verlag Mainz, Aachen, 1994. Habilitation thesis.

[16] H.-R. Sinning *Defect and Diffusion Forum*, vol. 123-124, p. 1, 1995.

[17] H.-R. Sinning *J. Alloys Compd.*, vol. 211/212, p. 216, 1994.

[18] F. Winter, S. Adam, and H.-R. Sinning *J. de Physique IV, Colloque C8*, p. 55, 1996.

[19] H.-R. Sinning *Phys. Rev. B*, vol. 46, p. 5989, 1992.

[20] A. S. Nowick and B. S. Berry, *Anelastic Relaxation in Crystalline Solids*. Academic Press, 1972.

[21] R. de Batist, *Internal Friction of Structural Defects in Crystalline Solids*. North-Holland, 1972.

[22] J. R. Macdonald *J. Chem. Phys.*, vol. 36, p. 345, 1962.

[23] C. Zener, *Elasticity and Anelasticity of Metals*. Univ. of Chicago Press, 1948.

[24] B. S. Berry, in *Metallic Glasses*. J. J. Gilman and H. J. Leamy (eds.), p. 161. American Society for Metals, 1978.

[25] J. L. Snoek *Physica (Utrecht)*, vol. 6, p. 591, 1939.

[26] H. Wipf and B. Kappesser *J. Phys.: Condensed Matter*, vol. 8, p. 7233, 1996.

[27] L. E. Hazelton and W. L. Johnson *J. Non-Cryst. Solids*, vol. 61-62, p. 667, 1984.

[28] R. Kirchheim, F. Sommer, and G. Schluckbier *Acta Mat.*, vol. 30, p. 1059, 1981.

[29] A. C. Switendick *Z. Phys. Chem. Neue Folge*, vol. 117, p. 89, 1979.

[30] H.-R. Sinning *phys. stat. sol. (a)*, vol. 140, p. 97, 1993.

[31] U. Stolz *J. Phys. F: Metal Phys.*, vol. 17, p. 1833, 1987.

[32] B. S. Berry and W. C. Pritchet *Z. Phys. Chemie Neue Folge*, vol. 163, p. 381, 1989.

[33] H.-R. Sinning *phys. stat. sol. (a)*, vol. 131, p. 445, 1992.

[34] H.-R. Sinning *J. Phys.: Condensed Matter*, vol. 3, p. 2005, 1991.

[35] R. Scarfone and H.-R. Sinning *J. Alloys Compd.*, vol. 310, p. 229, 2000.

[36] K. Foster, R. G. Leisure, J. B. Shaklee, J. Y. Kim, and K. F. Kelton *Phys. Rev. B*, vol. 61, no. 1, p. 241, 2000.

[37] M. Weller, M. Feuerbacher, J. Diehl, and K. Urban *J. de Physique IV*, vol. C8, p. 239, 1996.

[38] B. Damson, M. Weller, M. Feuerbacher, B. Grushko, and K. Urban *J. Alloys Compd.*, vol. 310, p. 184, 2000.

[39] G. Hupe Entwurfarbeit, Institut für Messtechnik and Institut für Werkstoffe, Technische Universität Braunschweig, 1984.

[40] R. Busch, S. Schneider, A. Peker, and W. L. Johnson *Appl. Phys. Lett.*, vol. 67, no. 11, p. 1544, 1995.

[41] J. Eckert, N. Mattern, M. Zinkevitch, and M. Seidel *Mat. Trans. JIM*, vol. 39, no. 6, p. 623, 1998.

[42] B. I. Wehner, J. Meinhardt, U. Köster, H. Alves, N. Eliaz, and D. Eliezer *Mat. Sci. Eng. A*, vol. 226-228, p. 1008, 1997.

[43] M. M. Nicolaus. Dr.-ing. thesis, Technische Universität Braunschweig, 1992.

[44] C. Nagel, K. Rätzke, E. Schmidtke, F. Faupel, and W. Ulfert *Phys. Rev. B*, vol. 60, no. 13, p. 9212, 1999.

[45] C. Nagel, K. Rätzke, E. Schmidtke, J. Wolff, U. Geyer, and F. Faupel *Phys. Rev. B*, vol. 57, no. 17, p. 10224, 1998.

[46] L. Q. Xing, C. Bertrand, J.-P. Dallas, and M. Cornet *Mat. Sci. Eng. A*, vol. A241, p. 216, 1998.

[47] T. A. Waniuk, R. Busch, A. Mashur, and W. L. Johnson *Acta Mater.*, vol. 15, p. 5229, 1998.

[48] W. L. Johnson *Mat. Sci. Forum*, vol. 225-227, p. 35, 1996.

[49] R. Busch, Y. J. Kim, and W. L. Johnson *J. Appl. Phys.*, vol. 77, no. 8, p. 4039, 1995.

[50] K. Ohsaka, S. K. Chung, W. K. Rhim, A. Peker, D. Scruggs, and W. L. Johnson *Appl. Phys. Lett.*, vol. 70, no. 6, p. 726, 1997.

[51] H.-R. Sinning *J. Alloys Compd.*, vol. 310, p. 224, 2000.

[52] B. S. Berry and W. C. Pritchet, *Hydrogen in disordered and amorphous solids*, p. 215. Plenum Publishing Corporation, 1986.

[53] J. Völkl and G. Alefeld, in *Hydrogen in metals I*, vol. 28 of *Topics in applied physics*, ch. 12, p. 321. Springer-Verlag, 1978.

[54] H.-R. Sinning, G. Steckler, and R. Scarfone *Defect and diffusion forum*, vol. 167-168, p. 1, 1999.

[55] M. Steyer, H.-U. Krebs, and H. C. Freyhardt *Z. Phys. B*, vol. 66, p. 317, 1987.

[56] W.-H. Wang, Q. Wei, and S. Friedrich *Phys. Rev. B*, vol. 57, no. 14, p. 8211, 1998.

[57] V. F. Petrunin, S. K. Dolukhanyan, M. G. Zemlyanov, S. V. Marchenko, and P. P. Parshin *Sov. Phys. Solid State*, vol. 23, no. 7, p. 1126, 1981.

[58] G. L. Miller, *Metallurgy of the rarer metals - Zirconium*, vol. 2, p. 275. Butterworths Scientific Publications, 2nd ed., 1957.

[59] D. L. Douglass, *The metallurgy of Zirconium*, p. 82. International Atomic Energy Agency, 1971.

[60] J. G. Couch, O. K. Harling, and L. C. Clune *Phys. Rev. B*, vol. 4, no. 8, p. 2675, 1971.

[61] H. Okumura, A. P. Tsai, A. Inoue, and T. Masumoto *Mat. Sci. Eng. A*, vol. 181-182, p. 781, 1994.

[62] M. Feuerbacher, M. Weller, J. Diehl, and K. Urban *Phil. Mag. Lett.*, vol. 74, p. 81, 1996.

[63] H.-R. Sinning and R. Scarfone, *Proc. Int. Conf. on Imperfections Interaction and Anelasticity Phenomena in Solids (IIAPS 10), Tula (Russia).* 13-15 Nov. 2001. To be published in Bull. Russian Acad. Sci., Physics.

[64] A. M. Viano. PhD thesis, Washington University, St. Louis, 1996.

[65] A. M. Viano, R. M. Stroud, P. C. Gibbons, A. F. McDowell, M. S. Conradi, and K. F. Kelton *Phys. Rev. B*, vol. 51, no. 17, p. 12026, 1995.

[66] A. Sadoc, J. Y. Kim, and K. F. Kelton *Phil. Mag. A*, vol. 79, no. 11, p. 2763, 1999.

[67] K. R. Faust, D. W. Pfitsch, N. A. Stojanovich, A. F. McDowell, N. L. Adolphi, E. H. Majzoub, J. Y. Kim, P. C. Gibbons, and K. F. Kelton *Phys. Rev. B*, vol. 62, no. 17, p. 11444, 2000.

[68] E. Fromm and E. Gebhardt, *Gase und Kohlenstoff in Metallen*. Springer, 1976.

[69] M. Boulard and M. de Boissieu, in *Physical properties of quasicrystals*, vol. 126 of *Solid-state sciences*, ch. 4, p. 107. Springer, 1999.

[70] P. C. Gibbons and K. F. Kelton, in *Physical properties of quasicrystals*, vol. 126 of *Solid-state sciences*, ch. 12, p. 416. Springer, 1999.

[71] P. A. Bancel, P. A. Heiney, P. W. Stephens, A. I. Goldman, and P. M. Horn *Phys. Rev. Lett.*, vol. 54, no. 22, p. 2422, 1985.

[72] W. J. Kim, P. C. Gibbons, and K. F. Kelton *Phil. Mag. A*, vol. 78, no. 5, p. 1111, 1998.

[73] A. Shastri, "private communications.".

[74] P. S. Spoor, J. D. Maynard, and A. R. Kortan *Phys. Rev. Lett.*, vol. 75, no. 19, p. 3462, 1995.

[75] U. Köster, D. Zander, and Triwikantoro *Mat. Sci. Forum*, vol. 343-346, p. 202, 2000.

[76] M. W. Chen, T. Zhang, A. Inoue, A. Sakai, and T. Sakurai *Appl. Phys. Lett.*, vol. 75, no. 12, p. 1697, 1999.

[77] J. Eckert, N. Mattern, M. Zinkevitch, and M. Seidel *Mat. Trans. JIM*, vol. 39, no. 6, p. 623, 1998.

[78] A. Inoue, D. Kawase, A. P. Tsai, T. Zhang, and T. Masumoto *Mat. Sci. Eng. A*, vol. 178, p. 255, 1994.

[79] H.-R. Sinning, R. Scarfone, and G. Steckler *J. Alloys Compd.*, vol. 310, p. 219, 2000.

[80] H.-R. Sinning *Phys. Rev. Lett.*, vol. 85, no. 15, p. 3201, 2000.

[81] H.-R. Sinning, G. Steckler, and R. Scarfone *Adv. Eng. Mater.*, vol. 9, no. 3, p. 706, 2001.

[82] P. Villars, *Pearson's Handbook Desk Edition, Crystallographic Data for Intermetallic Phases*, vol. 2, p. 1604. Materials Park, Ohio: ASM International, 1997.

[83] V. V. Molokanov, M. I. Petrzhik, T. N. Mikhailova, T. A. Sviridova, and N. P. Djakonova *J. Non-Cryst. Solids*, vol. 250-252, p. 560, 1999.